Imperial College London
Department of Physics

Engineering and Characterisation of Quantum non-Gaussian States

Catherine N. Hughes

Thesis submitted in partial fulfilment of the
requirements for the degree of
Doctor of Philosophy in Physics
of
Imperial College London

December 2015

Abstract

This thesis presents an investigation into the generation and characterisation of non-Gaussian states in continuous variable quantum optics. Beginning by placing the study of continuous variables within the context of quantum information processing more generally, we then motivate the need for non-Gaussianity within quantum computing protocols. The focus then narrows to the consideration of two particular sets of non-Gaussian states: orthogonal superposition states and the cubic resource state. The superposition of two orthogonal states has been shown to enhance certain continuous variable quantum information processing protocols that rely on entanglement, and within this section two distinct methods for generating such states are considered. While one of these methods provides a specific example, the other introduces a general orthogonaliser that relies solely on knowledge of the expectation value for the chosen orthogonalising operator in order to produce the superposition. The second case for non-Gaussian state generation employs current results demonstrating the production of a weak approximation of the cubic resource state in order to illustrate the use of such single-mode states to generate multimode states with similar features. These states are implemented as ancillas for a deterministic non-Gaussian gate operation on a system of choice. We show that generating multimode states through this distribution scheme allows an enhancement of the output state to better approximate the nonlinear features. Finally, we consider methods of characterising non-Gaussian states. In particular, we introduce a witness for pure states existing outside of the Gaussian convex hull. Such states exclude Gaussian pure states as well as non-Gaussian states generated from mixtures of squeezed and coherent states, and therefore consist of non-Gaussian states generated from non-Gaussian operations. We present a detection-independent bound for such states based on the generalised quasiprobability distribution.

Declaration of Originality

This thesis presents my own work, and was composed entirely by myself. Any information from the work of others has been appropriately acknowledged and referenced.

Catherine Hughes

Copyright Declaration

"It's not an End, but an And."
– PJS

Acknowledgements

For taking me on as a student, for giving me the opportunities to learn not only physics, but skills from website development to proposal writing, and for the freedom to see other parts of the world, I would like to first thank my supervisor, Myungshik Kim. Your experience and your generosity have helped me to become a better physicist and a more well-rounded individual, and for that I am very grateful. I am also deeply indebted to my collaborators, Marco Genoni, Tommaso Tufarelli, and Doug Plato, who provided mentorship from the very beginning and have each been instrumental in their own way to my development.

My gratitude toward all members of the controlled quantum dynamics theory group cannot be overstated. In particular I thank Mercedes Gimeno-Segovia for inspiring me to work harder and Howard Dale for inspiring me to take a snack break. In all seriousness, though, your friendship and support has been a priceless part of this experience. I also thank Kyle McEnery, Vignesh Venkataraman and Chuanqi Wan for making Team MSK really feel like a team.

I would also like to thank my parents, my brother Neil, and my sister Genevieve for listening to me when I needed to talk and for always encouraging me through the high points as well as the low.

A special thank you to SJ for showing me the importance of hard work even when the road is long, and especially to LHJ for the motivation to never stop trying to improve myself.

Finally, to Raul: it is impossible to describe the amount of gratitude I feel toward you for so many different reasons. Muito, muito obrigadinha.

Contents

List of Figures

Introduction

The field of quantum optics can trace its roots back to Planck's groundbreaking work on blackbody radiation in 1899. His work led to the understanding that light propagating in a vacuum is quantised in energy and momentum, leading to the description of light quanta, or photons. Einstein's work on the photoelectric effect provided further evidence of this quantisation, and additional work of his in which he derived Planck's radiation law using a formalism based on probabilities of absorption, spontaneous emission, and stimulated emission of electromagnetic radiation [1] instigated further advancements. The notion of stimulated emission in particular led to the development of the laser, first demonstrated in 1960 by Maiman [2]. With the expansion of laser science, the need for a mathematical formalism to describe the devices became apparent. As a result, following the work of Dirac in quantum field theory [3], Glauber, Sudarshan, and Mandel extended this aspect of quantum theory to better understand the electromagnetic field, and in particular to improve our knowledge of photodection and the statistics of light [4–6]. From this work came the notion of coherent states [4] and new realisations that variations exist between laser light, thermal light, and more exotic forms like squeezed light, to the extent that it is insufficient to try to describe such states of light using the classical wave description of the electromagnetic field. This led to a proliferation of results in the field of quantum optics: noting that the coherent state exhibits Poissonian number statistics [4], it then became clear that via certain non-linear interactions, the state could be changed such that it yielded super- or sub-Poissonian statistics [7] (as is the case for squeezed states). Beyond this, experimental techniques such as parametric down-conversion [8] allowed for the generation of twin beams of photons with shared characteristics.

Quantum optics was proliferating as a field of study alongside quantum theory in general, and as a result it also encountered the exponential growth of research efforts in applying quantum mechanics to information processing. Quantum mechanics is typically heralded as a facilitator for less noisy, more secure communication and information transfer. Indeed, using single photons to transmit confidential information over distances of kilometers has already been demonstrated [9–11]. The application

of quantum theory to information processing quickly evolved into a field on its own: quantum information. Much of the work in quantum optics is closely related to that of quantum information and quantum computation. Initial approaches to quantum information processing were focused on the quantum analogue of the classical bit – the qubit [12, 13]. These qubits are discrete, two-level systems employed as the main logical units for quantum processing tasks. The frequently-stated goal of quantum information and computation is the development of a so-called quantum computer. However, it is more nuanced to say that the goal is universal quantum computation – the ability to effect any unitary transformation over a finite number of variables to any degree of precision [14] through the repeated application of local operations affecting only a few variables at a time.

While this terminology and mode of problem-solving is suitable for discrete variable (dv) systems, since they are the natural analogue for the bipartite system of bits used in classical computing, many operations and systems in quantum optics are defined on an infinite-dimensional Hilbert space. These continuous variable (cv) systems differ in many ways from the discrete variable case. To begin with, defining an arbitrary unitary transformation over even one continuous variable requires infinite parameters, and as a result cannot typically be approximated by a finite number of continuous operations. For example, it is not possible to produce an arbitrary unitary transformation through the application of beamsplitters, phase-shifters, squeezers and other nonlinear devices to the quantum state. This should not, however, be taken as a reason to abandon the continuous variable regime. Indeed, if we group our transformations into various subclasses – one example could correspond to Hamiltonians that are polynomial functions of the operators $\hat{x}$ and $\hat{p}$ – it is possible to define a notion of universal quantum computation over such a subset. In general, a set of continuous quantum operations is said to be universal for a specific set of transformations if one can approximate to arbitrary accuracy any transformation in the set through a finite number of applications of the operations [15].

In order to achieve universal quantum computation over continuous variables, the ability to engineer suitable quantum states and operations is critical. With a well-developed catalogue of states and operations, we greatly reduce the number of constraints on the type of information processing protocols we wish to implement. In the continuous variable regime, in fact, a number of aspects of implementing quantum information protocols, particularly in the preparation, unitary manipulation, and measurement of entangled quantum states, can be achieved in a straightforward manner. For instance, homodyne detection [16] coupled with feed-forward techniques allow us to measure a quadrature with near-unit efficiency or to displace an optical mode in

phase space. Meanwhile, continuous variable entanglement may be efficiently produced using linear optics and squeezed light generated via a nonlinear optical interaction [17]. Continuous variable quantum states and operations are often divided into those with Gaussian Wigner functions and those without. The vast majority of states and operations typically considered within the cv regime are Gaussian; in fact, Gaussian states and operations are those described by interaction Hamiltonians at most quadratic in the annihilation and creation operators of the optical modes, and as a result are linear in their input-output relations [15]. While these states have been proven to be quite accessible and actually form the basis of a number of quantum processing tasks including quantum teleportation [18], cryptography [19], and cloning [20–24], it has been shown that non-Gaussian operations are required for long-distance communication protocols based on entanglement distillation [25, 26] and swapping [27], quantum memory [28], and high-fidelity quantum teleportation [29].

Achieving this range of quantum information processing tasks has motivated, and is motivated by, the expansion of the types of quantum states we can generate experimentally. From the basic states – single photons [30], entangled photon pairs [8], squeezed states [31], and quadrature entangled states [32] – to more exotic states like optical qubits [33], displaced Fock states [34], photon-added states [35, 36], as well as superposition states like the so-called Schrödinger cat state [37], work in this field is strongly driven to broaden the range of states we know how to generate. The goal, in fact, is to be able to generate any arbitrary quantum state. This aim is the motivation for the original work presented in Chapters 2 and 3.

Even in the most ideal situation where we are able to generate a completely arbitrary quantum state, it will always be necessary to have protocols for characterising the output of a given experiment. For example, the classification of classical vs. non-classical states has long been a focus of research within quantum optics and quantum information, with the most common viewpoint being that classical states have a density matrix distribution that is described by a probability density function [4, 5]. Some argue that this does not fully solve the issue, as such states – including the aforementioned coherent state – do not necessarily form a mutually orthogonal set. Further difficulties come with trying to classify non-Gaussian states. Noting that non-Gaussianity does not necessarily follow from, or imply, non-classicality (a classical non-Gaussian state may be prepared by, for example, phase-diffusion of coherent states or photon subtraction on thermal states [38]), the presence of both non-Gaussianity and non-classicality does allow an improvement in performance for certain processing tasks[39]. The vast majority of the effort to classify quantum states has focused on non-classicality. Methods falling under this category include looking at the negativity

of the Wigner [40, 41] and Glauber-Sudarshan P [6, 42–44] functions, as well as examining the distinguishability of the given state from a known state with negative Wigner function [45]. Several such comparative approaches have been taken, looking at either the Hilbert-Schmidt distance as a measure of similarity between the given (pure) state and the whole set of coherent states (taken to be the most classical set of pure states) [46], or comparing the Hilbert-Schmidt scalar products rather than distance and using the Fock states as the reference set [47]. Gaussian states with a regular P representation have also been used as a comparison set [48]. Other methods that employ a comparison between the measured state and some reference include the Bures distance [49, 50] and relative entropy [51–55]. Additional work has looked at entanglement potential [56], Klyshko criteria [57], and conditions based on the quadrature moments of the given state [58, 59].

From the approaches to classifying non-classicality of a quantum state, it is only the Wigner function negativity that also directly tests whether the state is non-Gaussian. Direct efforts to classify non-Gaussianity in states have primarily focused on bounding a specific set of quantum non-Gaussian states, which will be described in more detail in Chapter 4. Generally speaking, quantum non-Gaussian states are those which require higher-order nonlinearities to be produced experimentally, unlike, for example, some non-Gaussian states which are simply mixtures of squeezed and displaced states. Significantly less work has been done to classify such states, despite the fact that witnesses for such strong nonlinearities in quantum systems are valuable for heralding the creation of more complex quantum states, such as the cubic state discussed in Chapter 3. Efforts to classify quantum non-Gaussian states include a criterion based on direct measurements of the probabilities of finding the n^{th} Fock state in the analysed state [60], and bounds based on the Wigner function which require knowledge of the mean photon number of the state [61]. Work presented in Chapter 4 builds on this second case, employing generalised quasiprobability distributions to determine a bound on quantum non-Gaussianity for states in a noisy channel.

Publications

Sections of this thesis are based on material published in the following:

- [62] A. S. Coelho, L. S. Constanzo, A. Zavatta, C. Hughes, M. S. Kim, M. Bellini. Universal state orthogonalizer and qubit generator. *arXiv:1407.6644v1* (2014). Accepted for publication in Phys. Rev. Lett. (2016).

- [63] C. Hughes, M. G. Genoni, T. Tufarelli, M. G. A. Paris, and M. S. Kim. Quantum non-Gaussianity witnesses in phase space. Phys. Rev. A **90**, 013810 (2014).

Chapter 1

Background

1.1 Quantum Information Processing

Quantum information processing seeks to exploit the fundamental properties of quantum systems as a resource for a different and ideally more efficient treatment of information. In general, the implementation of a quantum processing protocol requires the preparation of the resources through the encoding of information onto the desired quantum state, followed by an operation on the prepared state or set of states, and finally measurement of the output. Typical resource states for such protocols include single-photon states [30], squeezed states [31], and the more exotic Schrödinger cat states [37]. In the operation stage, several things can happen. In some cases the experimental evolution is not controlled and rather the decoherence of the state as it couples to the environment is observed. In other cases, the operation is completely controlled in order to effect a specific and dedicated quantum protocol upon a system. Following the operation, a measurement is performed in order to characterise the state as well as being a further method for engineering the desired output, as in the case of a fully controlled information processing protocol.

The initial foray into the study of quantum mechanics through its application to information protocols was in the area of discrete variables (dv). These systems have finite Hilbert spaces and are the most natural extension from classical information theory and computation; the notion of quantum bits, or qubits, emerges nicely from classical bits, while classical operations can similarly be mapped to their quantum counterparts. In the dv domain, information is contained in a superposition of two orthogonal pure quantum states as

$$|\phi\rangle = \alpha|0\rangle + \beta|1\rangle, \tag{1.1}$$

where $|\alpha|^2 + |\beta|^2 = 1$. This definition implies that a single physical object is carrying the information, and indeed, in the case of quantum optics, such a qubit is associated with single-photon states. Information is encoded in this superposition using the properties of the modes, for example through the polarisation of the photon. Such a superposition has also been extended to three or four states, called a qutrit and qutrat, respectively [64]. These dv systems are based on the preparation of states in the Fock basis, and the use of photon-counting measurements. However, as we consider Fock states with higher photon numbers, these practices become increasingly challenging experimentally. In fact, for states with large photon numbers or quantum information processing with multiple input states, an alternative approach to discrete variables becomes advantageous. As a result, we have the field of continuous variable (cv) information processing. Just as the dv regime employs Fock states and photon counting, cv encoding uses the states produced by laser light and typically employs homodyne measurements [16] to acquire information about the field quadratures of the state from the amplitude and phase properties of the light. These states occupy an infinite-dimensional Hilbert space and are often expressed in the basis of the measured quadratures, either position eigenbasis x or, equivalently, momentum eigenbasis p [64]. In the cv case, quantum information is defined as a continuous superposition of eigenstates

$$|\phi\rangle = \int \langle x|\phi\rangle |x\rangle dx, \tag{1.2}$$

where $\langle x|\phi\rangle$ is the wave function in the basis of continuous variable x [65]. The ability to describe a quantum system in terms of these orthogonal quadrature variables leads to some novel techniques for thinking about quantum states and quantum information protocols. For example, we can express the properties of these states using a phase-space representation, defining the axes in terms of the quadratures. These so-called quasiprobability distributions are discussed in more detail in Sec.1.2.2.

This chapter will continue with a more rigorous discussion of the formalism of continuous variable systems, including the presentation of the aforementioned quasiprobability distributions. We then present a broader context for the original work presented in this thesis by outlining the various uses of resource states in quantum information processing, as well as outlining the types of states that can currently be generated.

1.2 Continuous variable systems

Continuous variable states are valuable tools for accessing quantum information protocols within quantum optics in part because they are unconditional [15]. That is,

cv resources like entangled states can be generated through the nonlinear interaction of a laser with a crystal in a deterministic fashion. While this approach may need to be supplemented by linear-optical interactions, it is still easier than producing dv quantum states, which require particular coincidence measurement results in order to rule out undesired contributions from, typically, vacuum terms. This is not to say that this unconditionalness does not have a price; in this case, the quality of entanglement in the prepared states suffers. It is possible to prepare highly entangled cv states using, for example, the two-mode squeezed state, but the maximally entangled state requires infinite squeezing [66]. As a result, entanglement and any protocol based on entanglement within the cv regime are always imperfect. This is not a problem in general, however, and implementations of protocols that do not rely on entanglement do not suffer from this particular issue. We now present the formalism for describing cv quantum states, and will follow up with further discussion on the use of such states in Sec.1.5.

1.2.1 Preliminary notions

A cv system of n bosonic modes has a Hilbert space $\mathcal{H} = \bigotimes_{k=1}^{n} \mathcal{F}_k$ described by the tensor product of n infinite-dimensional Fock spaces $\mathcal{F}_k$. Each mode is defined by mode operators $\hat{a}_k$, $k = 1, ..., n$, which obey the bosonic commutation relations $[\hat{a}_k, \hat{a}_l^\dagger] = \delta_{kl}$. These operators are also referred to as annihilation and creation operators due to how they act on number states by either annihilating or creating a photon in the mode:

$$\hat{a}|n\rangle = \sqrt{n}|n-1\rangle \qquad\qquad \hat{a}^\dagger|n\rangle = \sqrt{n+1}|n+1\rangle. \tag{1.3}$$

Fock spaces $\mathcal{F}_k$ are spanned by the eigenstates of the number operator $\hat{n}_k = \hat{a}_k^\dagger \hat{a}_k$. Expressed in these dimensionless variables, the Hamiltonian for the quantum harmonic oscillator of a single mode k is written $\hat{H}_k = \hbar\omega_k(\hat{n}_k + \frac{1}{2})$ for a given mode frequency ω_k. The bosonic operators may also be expressed in terms of the standard quadrature operators $\hat{x}$ and $\hat{p}$

$$\hat{a}_k = \frac{1}{\sqrt{2\hbar\omega_k}}(\omega_k \hat{x}_k + i\hat{p}_k) \qquad\qquad \hat{a}_k^\dagger = \frac{1}{\sqrt{2\hbar\omega_k}}(\omega_k \hat{x}_k - i\hat{p}_k), \tag{1.4}$$

or conversely,

$$\hat{x}_k = \sqrt{\frac{\hbar}{2\omega_k}}(\hat{a}_k + \hat{a}_k^\dagger) \qquad\qquad \hat{p}_k = -i\sqrt{\frac{\hbar\omega_k}{2}}(\hat{a}_k - \hat{a}_k^\dagger). \tag{1.5}$$

This relation allows the familiar Hamiltonian for the harmonic oscillator to be rewritten as:

$$\hat{H}_k = \frac{1}{2}(\hat{p}_k^2 + \omega_k^2 \hat{x}_k^2). \tag{1.6}$$

The position and momentum operators satisfy the canonical commutation relation $[\hat{x}_k, \hat{p}_l] = i\hbar\delta_{kl}$. Noting the relationship between the bosonic operators and the operators $\hat{x}$ and $\hat{p}$, we define the dimensionless conjugate variables

$$\hat{X}_k \equiv \sqrt{\frac{\omega_k}{\hbar}}\hat{x}_k = \Re\ \hat{a}_k, \qquad\qquad \hat{P}_k \equiv \frac{1}{\sqrt{\hbar\omega_k}}\hat{p}_k = \Im\ \hat{a}_k. \tag{1.7}$$

These operators represent the amplitude and phase quadratures of a single mode k and satisfy the commutation relation $[\hat{X}_k, \hat{P}_l] = i\delta_{kl}$. In the classical sense, these operators correspond to the real and imaginary parts of the harmonic oscillator's complex amplitude. Henceforth we refer to these dimensionless operators as the position and momentum operators directly, and will use $(\hat{x}, \hat{p})$ to refer to them. Unless otherwise specified, we will also drop the mode label k. These operators have corresponding quadrature eigenstates

$$\hat{x}|x\rangle = x|x\rangle \qquad\qquad \hat{p}|p\rangle = p|p\rangle. \tag{1.8}$$

Although they are unphysical themselves, the quadrature eigenstates can be formally defined (indirectly) through the wavefunction $\psi(x) = \langle x|\psi\rangle$. Just as the position and momentum operators have eigenstates $|x\rangle$ and $|p\rangle$, the coherent state $|\beta\rangle$ is the eigenstate of the bosonic mode operator $\hat{a}$:

$$\hat{a}|\beta\rangle = \beta|\beta\rangle. \tag{1.9}$$

The description of coherent states is derived from the analysis of a single-mode oscillator with amplitude β satisfying the eigenvector equation Eq. (1.9) [4]. In general a coherent state may be defined in terms of an infinite expansion of number states, in the form

$$|\beta\rangle = e^{-\frac{1}{2}|\beta|^2} \sum_n \frac{\beta^n}{\sqrt{n!}}|n\rangle. \tag{1.10}$$

These states are overcomplete, and have an average occupation number for the n^{th} state defined by a Poisson distribution with mean value $|\beta|^2$. Coherent states can be alternatively expressed as an operator acting on the ground state $|0\rangle$ of the oscillator. This operator, denoted $\hat{D}(\beta)$, $\beta \in \mathbb{C}$, acts by displacing operators $\hat{a}$ and $\hat{a}^\dagger$ according

to

$$\hat{D}^\dagger(\beta)\hat{a}\hat{D}(\beta) = \hat{a} + \beta\mathbb{1} \qquad \hat{D}^\dagger(\beta)\hat{a}^\dagger\hat{D}(\beta) = \hat{a}^\dagger + \beta^*\mathbb{1}. \tag{1.11}$$

When acting on the vacuum, the result is the familiar coherent state $\hat{D}(\beta)|0\rangle = |\beta\rangle$. The displacement operator is a linear, unitary operator with the explicit form

$$\hat{D}(\beta) = e^{\beta\hat{a}^\dagger - \beta^*\hat{a}}. \tag{1.12}$$

1.2.2 Quasiprobability distributions

Phase-space distributions of quantum states resemble classical probability distributions and allow for the calculation of measurable quantities, namely mean values and variances, in a similar way to classical distributions. Such quantum 'quasiprobability' distributions differ from classical probability distributions by also allowing negative values. In this section we present these distributions in the standard formalism of states and operators, as well as in a formalism using symplectic matrices. The former is the form used throughout this thesis to describe such distributions, but we also provide the second description in order to better define Gaussian states, and to highlight the covariance matrix, which is relevant for the analysis of the state in Chap. 3.

1.2.2.1 State representation

Quasiprobability distributions were first proposed by Wigner in 1932 [67]. He defined the Wigner function of the state ρ in the position basis as

$$W(x,p) = \frac{2}{\pi}\int dy\ e^{4iyp}\langle x-y|\rho|x+y\rangle. \tag{1.13}$$

Throughout this thesis, unless otherwise specified, integration is over the entire space of the integration variable. The standard description of generalised quasiprobability distributions is in terms of the Weyl characteristic function [68]. A quantum state ρ has an s-parametrised characteristic function

$$C_s(\beta) = \mathrm{Tr}[\hat{D}(\beta)\rho]e^{\frac{s}{2}|\beta|^2}, \tag{1.14}$$

where $-1 \leq s \leq 1$. The corresponding generalised quasiprobability distribution is expressed as the symplectic Fourier transform of such a distribution [69]:

$$Q_s(\alpha) = \frac{1}{\pi^2}\int d^2\beta\ C_s(\beta)e^{(\alpha\beta^* - \alpha^*\beta)}. \tag{1.15}$$

$Q_s(\alpha)$ satisfies the standard normalisation condition for probability distributions, namely $\int Q_s(\alpha)d^2\alpha = 1$ for any s, but it may not necessarily be positive semi-definite. Three distinct values of s correspond to different orderings of the operators in the characteristic function. The Wigner function of Eq. (1.13) corresponds to symmetric ordering $s = 0$. For $s = 1$, $Q_1(\alpha)$ is the quasiprobability distribution for normally ordered operators and is called the Glauber-Sudarshan P function [4, 5], $P(\alpha)$. This function is related to the density matrix of the state through

$$\rho = \int P(\alpha)|\alpha\rangle\langle\alpha|d^2\alpha, \tag{1.16}$$

and, when positive, is considered a standard probability function. It should be noted that the P function is not necessarily a well-behaved and positive function, and the absence of such characteristics is considered to be a sign of nonclassicality for a state [70]. Finally, $s = -1$ corresponds to antinormally ordered operators, and is referred to as the Q function [71]. This distribution is positive at every point in phase space, and may be written as the overlap between ρ and a coherent state:

$$Q(\alpha) = \frac{1}{\pi}\langle\alpha|\rho|\alpha\rangle. \tag{1.17}$$

Although these quasiprobability distributions are only well-behaved for certain values of the parameter s, for $s < -1$ the distribution will be positive definite, while for $s < 0$ it will always be regular and therefore may be expressed in terms of continuous functions [72, 73]. For $s > 0$ the distributions may be expressed in term of δ functions and their derivatives [74].

1.2.2.2 Matrix representation

While the description of quasiprobability distributions in the previous section follows directly from the form used since the beginning of this work, it is pertinent to include that Gaussian states in particular may be described using symplectic matrices [75]. The convenience of this symplectic formalism for Gaussian states will be illustrated in this section, and the covariance matrix, which will be used in later chapters, will be introduced. It is important to note that for non-Gaussian states, knowledge of the mean and covariance is not sufficient. Taking the canonical commutation relation $[\hat{x}_k, \hat{p}_l] = i\delta_{kl}$, we define the vector of operators $\hat{\mathbf{R}} = (\hat{x}_1, \hat{p}_1, ..., \hat{x}_n, \hat{p}_n)^T$. This is then used to re-express the commutation relation as

$$[\hat{R}_k, \hat{R}_l] = i\Omega_{kl} \tag{1.18}$$

where $\Omega_{kl} \equiv [\mathbf{\Omega}]_{kl}$ are the elements of the symplectic matrix

$$\mathbf{\Omega} = \bigoplus_{k=1}^{n} \omega, \qquad \omega = \begin{pmatrix} 0 & 1 \\ -1 & 0 \end{pmatrix}. \tag{1.19}$$

The matrix $\mathbf{\Omega}$ satisfies the condition $\mathbf{\Omega}^{\mathrm{T}} = -\mathbf{\Omega} = \mathbf{\Omega}^{-1}$. The general n-mode vector $\mathbf{\Lambda} = (a_1, b_1, ..., a_n, b_n)^{\mathrm{T}} \in \mathbb{R}^{2n}$, corresponds to the coherent state of Eq.(1.10) with a_i and b_i providing the real and imaginary parts of the coherent state parameter for mode i. The displacement operation used to generate such a state is written

$$D(\mathbf{\Lambda}) = e^{-i\mathbf{\Lambda}^{\mathrm{T}}\mathbf{\Omega}\hat{\mathbf{R}}}. \tag{1.20}$$

We can then express the s-parametrised characteristic function in terms of these new parameters:

$$C_s[\rho](\mathbf{\Lambda}) = \mathrm{Tr}[\rho D(\mathbf{\Lambda})] e^{\frac{1}{2}s|\mathbf{\Lambda}|^2}. \tag{1.21}$$

As in the previous case, taking the Fourier transform of the characteristic function results in the general s-parametrised quasiprobability distribution

$$Q_s[\rho](\mathbf{Y}) = \frac{1}{(2\pi^2)^n} \int d^{2n}\mathbf{\Lambda}\ e^{i\mathbf{\Lambda}^{\mathrm{T}}\mathbf{\Omega}\mathbf{Y}} C_s[\rho](\mathbf{\Lambda}). \tag{1.22}$$

where we introduce vector $\mathbf{Y} = (y_1, z_1, ..., y_n, z_n)^{\mathrm{T}}$. Using this formulation, it is also possible to define the covariance matrix σ of the state described by the moments of vector $\hat{\mathbf{R}}$. A given entry (k, l) is defined:

$$\sigma_{kl} \equiv [\sigma]_{kl} = \frac{1}{2}\langle \hat{R}_k \hat{R}_l + \hat{R}_l \hat{R}_k \rangle - \langle \hat{R}_k \rangle \langle \hat{R}_l \rangle. \tag{1.23}$$

In general, $\langle \hat{O} \rangle = \mathrm{Tr}[\rho \hat{O}]$ is the expectation value of operator $\hat{O}$. Typically the vector of expectation values $\langle \hat{\mathbf{R}} \rangle \equiv \mathrm{Tr}[\rho \hat{\mathbf{R}}]$ is called the first-moments vector, with the individual entries being labelled the first moments for a given mode. From this description it is straightforward to see that the diagonal elements $k = l$ of the matrix are the variances for the individual modes, while off-diagonal entries describe covariance either of $\hat{x}$ and $\hat{p}$ in the same mode, or between two modes.

1.3 Gaussian states and operations

While the focus of this thesis is on non-Gaussian states, it is important to provide an overview on Gaussian states and operations as well. This is because such operations dominate the field of cv quantum optics, and therefore remain relevant for the

techniques of non-Gaussian state generation and characterisation presented in later chapters.

1.3.1 Gaussian states

Gaussian states are defined as states with a Gaussian characteristic function [76], and may be completely characterised by the first and second moments of the quadrature operators [77] – that is, they may be completely described through the covariance matrix and the first moments vector. This allows us, using the second formulation of Sec. 1.2.2 , to write the characteristic function for a Gaussian state $\rho_{\mathcal{G}}$ as:

$$C_s[\rho_{\mathcal{G}}](\mathbf{\Lambda}) = e^{-\frac{1}{2}\mathbf{\Lambda}^{\mathrm{T}}\mathbf{\Omega}\sigma\mathbf{\Omega}^{\mathrm{T}}\mathbf{\Lambda} - i\mathbf{\Lambda}^{\mathrm{T}}\mathbf{\Omega}\langle\hat{\mathbf{R}}\rangle}\ e^{\frac{1}{2}s|\mathbf{\Lambda}|^2} \tag{1.24}$$

These states describe a class of optical quantum states that are useful for quantum communication and computation, as well as being experimentally accessible. In fact, some classes of Gaussian states are available on-demand and unconditionally [15]. We take the Fourier transform of the characteristic equation with $s = 0$ in order to find a general expression for the Wigner function:

$$Q_0[\rho_{\mathcal{G}}](\mathbf{Y}) = \frac{1}{(2\pi^2)^n}\int d^{2n}\mathbf{\Lambda}\ e^{i\mathbf{\Lambda}^{\mathrm{T}}\mathbf{\Omega}\mathbf{Y}} C_s[\rho_{\mathcal{G}}](\mathbf{\Lambda}). \tag{1.25}$$

Using the identity

$$\int_{\mathbb{R}^n} d^{2n}\mathbf{\Lambda}\ e^{-\frac{1}{2}\mathbf{\Lambda}^{\mathrm{T}}\mathbf{Q}\mathbf{\Lambda} + i\mathbf{\Lambda}^{\mathrm{T}}\mathbf{Y}} = \frac{(2\pi)^n e^{-\frac{1}{2}\mathbf{Y}^{\mathrm{T}}\mathbf{Q}^{-1}\mathbf{Y}}}{\sqrt{\det[\mathbf{Q}]}}, \tag{1.26}$$

for the real, positive-definite symmetric $2n \times 2n$ matrix $\mathbf{Q}$, we can express the Wigner function as the Gaussian:

$$Q_0[\rho_{\mathcal{G}}](\mathbf{Y}) = \frac{e^{-\frac{1}{2}(\mathbf{Y}-\langle\hat{\mathbf{R}}\rangle)^{\mathrm{T}}\sigma^{-1}(\mathbf{Y}-\langle\hat{\mathbf{R}}\rangle)}}{\pi^n\sqrt{\det[\sigma]}}. \tag{1.27}$$

1.3.2 Gaussian operations

Gaussian operations are those which preserve the Gaussian character of the state. An evolution satisfying this condition may be described by linear transformations of the position and momentum operators which preserve the commutation relations. Such operations are called symplectic transformations [75]. To see this in more detail, we examine the equations of motion for a Hamiltonian $\hat{H}$ of a classical system of particles

described by coordinate vector $\hat{\mathbf{R}}$,

$$\dot{R}_k = \Omega_{kl} \frac{\partial H}{\partial R_l}, \tag{1.28}$$

where $\dot{R}_k$ denotes the time derivative of the k^{th} element of vector $\hat{\mathbf{R}}$, and $\mathbf{\Omega}$ is, as defined in Eq.(1.19), a symplectic matrix. It is possible to understand the purpose of the symplectic matrix by looking at a generic coordinate transformation $\mathbf{R} \to \mathbf{R}' \equiv \mathbf{F}\mathbf{R}$. The equations of motion are thereby transformed as

$$\dot{R}'_k = F_{ks}\Omega_{st}F_{lt} \frac{\partial H}{\partial R'_l}, \tag{1.29}$$

and remain invariant if and only if:

$$\mathbf{F}\mathbf{\Omega}\mathbf{F}^{\mathrm{T}} = \mathbf{\Omega}. \tag{1.30}$$

This last expression is called the symplectic condition, and it characterises the canonical transformations of coordinates for a system. From the quantum mechanics perspective, if the mode transformation $\hat{\mathbf{R}}' = \mathbf{F}\hat{\mathbf{R}}$ does not change the canonical commutation relations, the system kinematics are also left invariant. In this case, $\mathbf{F}$ satisfies the symplectic condition. As a result, $\mathbf{F}^{\mathrm{T}} = \mathbf{F}^{-1} = \mathbf{\Omega}\mathbf{F}^{\mathrm{T}}\mathbf{\Omega}^{-1}$ also holds [75].

If we return to discussions of Hamiltonians in terms of bosonic field operators, Gaussianity of the state is preserved if the evolution of the state can be described by a Hamiltonian that consists of linear and bilinear combinations of the annihilation and creation operators [76]. A number of such Hamiltonians are experimentally realisable in quantum optics [78, 79], optomechanics [80, 81], micromechanics [82], and cold gas systems [83–88]. For the purpose of this work, our discussion is based on the quantum optical implementation of such transformations; this is more commonly referred to as linear optical quantum information processing due to the linear evolution of the modes. We write the general Hamiltonian describing such a Gaussian evolution as [75]

$$\hat{H} = \sum_{k=1}^{n} g_k^{(1)} \hat{a}_k^\dagger + \sum_{k \geq l=1}^{n} g_{kl}^{(2)} \hat{a}_k^\dagger \hat{a}_l + \sum_{k,l=1}^{n} g_{kl}^{(3)} \hat{a}_k^\dagger \hat{a}_l^\dagger + h.c. \tag{1.31}$$

The three terms in this Hamiltonian generate the types of unitary evolutions that form the building blocks for the work undertaken in this thesis.

1.3.2.1 Displacement operator

We begin with the first term of Eq.(1.31), describing the linear evolution

$$\hat{H}_1 = \sum_{k=1}^{n} g_k^{(1)} \hat{a}_k^\dagger + h.c. \tag{1.32}$$

The unitary transformations generated by this Hamiltonian are precisely the displacement operations of Eqs.(1.12) and (1.20). This operation is named such due to its action on the first-moments vector $\hat{\mathbf{R}}$, in the formalism of Eq.(1.20):

$$D^\dagger(\mathbf{\Lambda})\hat{\mathbf{R}}D(\mathbf{\Lambda}) = \hat{\mathbf{R}} + \mathbf{\Lambda}. \tag{1.33}$$

It follows that the displacement operation has no effect on the covariance matrix, which may be observed by comparing the effect of the displacement operation in Eq.(1.33) to the expression for the covariance matrix in Eq.(1.23), noting that Λ is a vector of scalars and the covariance matrix is defined element-wise.

1.3.2.2 Phase shift and two-mode mixing

The second term of Eq.(1.31),

$$\hat{H}_2 = \sum_{k \geq l=1}^{n} g_{kl}^{(2)} \hat{a}_k^\dagger \hat{a}_l + h.c. \tag{1.34}$$

describes two distinct physical processes, depending on whether the modes are the same or different. In the case where $k = l$, the k^{th} subsystem is undergoing free evolution. During free evolution a field will pick up an overall phase that, for a single mode, has no physical meaning and disappears with normalisation. However, in the case where the field interacts with another field, such as in the study of interference phenomena with beams of light and the interferometric scheme used to implement homodyne detection [16], the relative phases between modes will have a nontrivial effect. The phase shift operation is written

$$\hat{U}(\theta) = e^{-i\theta \hat{a}_k^\dagger \hat{a}_k}, \tag{1.35}$$

and acts by rotating the mode operator $\hat{a}_k$:

$$\hat{U}^\dagger(\theta)\hat{a}_k\hat{U}(\theta) = e^{-i\theta}\hat{a}_k. \tag{1.36}$$

The corresponding symplectic matrix form is the more recognisable way of writing the phase rotation operator (as it acts on quadratures $\hat{x}$ and $\hat{p}$):

$$\mathbf{U}(\theta) = \begin{pmatrix} \cos\theta & \sin\theta \\ -\sin\theta & \cos\theta \end{pmatrix}. \tag{1.37}$$

The second case, where $k \neq l$ in Eq.(1.34), is referred to as two-mode mixing as it describes the linear mixing of operators from two different modes. Within the context of quantum optics (and therefore this work) two-mode mixing is commonly referred to as beamsplitting. A beamsplitter is a linear optical medium, such as a dielectric plate, where such an interaction occurs. In the two-mode case, which is the one used throughout this work, the beamsplitter operator may be written as

$$\hat{B}(\zeta) = e^{\zeta \hat{a}_1^\dagger \hat{a}_2 - \zeta^* \hat{a}_1 \hat{a}_2^\dagger}, \tag{1.38}$$

where the coupling coefficient $\zeta = \frac{\theta}{2} e^{i\phi} \in \mathbb{C}$ is proportional to the length of time the interaction occurs as well as the linear susceptibility of the medium. The coupling coefficient can be expressed in terms of the transmissivity $t = \cos\frac{\theta}{2}$ or reflectivity $r = \sin\frac{\theta}{2}$ of the optical medium, where $t^2 + r^2 = 1$. The beamsplitter transforms the bosonic field modes as

$$\hat{B}^\dagger(\zeta)\hat{a}_1\hat{B}(\zeta) = \cos\frac{\theta}{2}\hat{a}_1 + e^{i\phi}\sin\frac{\theta}{2}\hat{a}_2, \tag{1.39}$$

$$\hat{B}^\dagger(\zeta)\hat{a}_2\hat{B}(\zeta) = \cos\frac{\theta}{2}\hat{a}_2 + e^{-i\phi}\sin\frac{\theta}{2}\hat{a}_1, \tag{1.40}$$

while the symplectic matrix for the operation reads [89]

$$\mathbf{B}(\theta) = \begin{pmatrix} \cos\frac{\theta}{2}\mathbb{1} & \sin\frac{\theta}{2}\mathbf{U}(\phi) \\ -\sin\frac{\theta}{2}\mathbf{U}^{\mathrm{T}}(\phi) & \cos\frac{\theta}{2}\mathbb{1} \end{pmatrix}. \tag{1.41}$$

Here, $\mathbf{U}(\phi)$ is the rotation matrix of Eq.(1.37).

1.3.2.3 Squeezing

The final term of Eq.(1.31),

$$\hat{H}_3 = \sum_{k,l=1}^{n} g_{kl}^{(3)} \hat{a}_k^\dagger \hat{a}_l^\dagger + h.c., \tag{1.42}$$

describes Gaussian evolution, and in particular $\chi^{(2)}$ interactions [31] whereby two photons are generated with energy and momentum both conserved, as well as in processes

involving parametric amplification [90, 91]. The emission of two photons into the same mode is called phase matching, and is described by this Hamiltonian when $k = l$. This transformation is referred to as single-mode squeezing due to its effect on the quadrature operators. The single-mode squeezing operator is written

$$\hat{S}_k(\xi) = e^{\frac{1}{2}[\xi(\hat{a}_k^\dagger)^2 - \xi^*(\hat{a}_k)^2]}, \tag{1.43}$$

with the corresponding effects on the mode operators:

$$\hat{S}_k^\dagger(\xi)\hat{a}_k\hat{S}_k(\xi) = \cosh r\ \hat{a}_k + e^{i\psi}\sinh r\ \hat{a}_k^\dagger, \tag{1.44}$$

$$\hat{S}_k^\dagger(\xi)\hat{a}_k^\dagger\hat{S}_k(\xi) = \cosh r\ \hat{a}_k^\dagger + e^{-i\psi}\sinh r\ \hat{a}_k. \tag{1.45}$$

Here, $\xi = re^{i\psi}$ is the squeezing parameter, with $r,\ \psi \in \mathbb{R}$. We note that squeezing is a Gaussian operation that linearly transforms the bosonic mode operators, despite being described by a Hamiltonian nonlinear in those operators. The symplectic transformation describing single-mode squeezing follows from the mode transformations and the definition of the quadrature operators:

$$\mathbf{S}_k(\xi) = \cosh r\mathbb{1} + \sinh r\mathcal{R}, \qquad \mathcal{R}(\psi) = \begin{pmatrix} \cos\psi & \sin\psi \\ \sin\psi & -\cos\psi \end{pmatrix}. \tag{1.46}$$

Taking $k \neq l$ in Eq.(1.42) corresponds to two-mode squeezing transformations. This operation still describes $\chi^{(2)}$ nonlinear interactions, however in this case the two photons are emitted in different modes. In this case, the squeezing operator is typically written

$$\hat{S}_{kl}(\xi) = e^{\xi\hat{a}_k^\dagger\hat{a}_l^\dagger - \xi^*\hat{a}_k\hat{a}_l}. \tag{1.47}$$

The symplectic form of the two-mode squeezing transformation is

$$\mathbf{S}_{kl} = \begin{pmatrix} \cosh r\mathbb{1} & \mathcal{R}(\xi) \\ \mathcal{R}(\xi) & \cosh r\mathbb{1} \end{pmatrix}, \tag{1.48}$$

where $\mathcal{R}(\xi)$ is defined as in Eq.(1.46).

1.4 Non-Gaussian states

Until this point we have reviewed the framework of continuous variable quantum mechanics within the context of Gaussian states and operations. While it has been shown that linear optics is sufficient for efficient quantum information processing with pho-

tons [92], in order to achieve a scheme for universal quantum computation nonlinear optics is necessary. In this context, we use the terms linear and nonlinear to describe the way in which the bosonic mode operators are transformed. For example, Gaussian operations are by definition linear. However, Gaussian states, which are defined by the form of their Wigner function, are not necessarily themselves linear in the bosonic operators (see for example squeezed states in Sec.1.3.2.3).

The need for non-Gaussianity in cv quantum optics is similarly motivated by the requirements of universal quantum computing. In other words, since any circuit with Gaussian inputs and operations may be efficiently simulated on a classical computer [93], universal quantum computing in the cv regime requires non-Gaussianity. Research in this area is directed by three further results [94]:

1. universal cv quantum computation is achievable with linear optics, homodyne measurement with feed-forward, and photon counting,

2. the photon-counting measurement necessarily involves an optical nonlinearity,

3. nonlinear quantum resources can be prepared off-line, allowing linear optical cv quantum computation to succeed deterministically.

It is therefore natural that research in the field of non-Gaussian states and operations, including the work contained here, follows the scheme of homodyne measurement, photon counting, and off-line resource preparation laid out above.

While it is straightforward to see why the ability to generate non-Gaussian states and operations is essential, actually producing such states is challenging. Much of the formalism presented above remains relevant for discussions of non-Gaussian states, and as a result is important for the analysis contained in later chapters. In the final sections of this chapter we motivate the study of non-Gaussian states by considering their use in common quantum information protocols. We provide a more complete overview of the classes of non-Gaussian states related to the original work presented in this thesis in Chapters 2 and 3. Similarly, a broader examination of methods used to classify such states is given before the specific analysis presented in Chapter 4.

1.5 Non-Gaussian enhancement of cv resources & protocols

In this section, we will examine a number of uses of continuous variable states as resources for quantum information processing protocols. Entanglement [77] has proven to be the key resource for most quantum protocols just as it has come to be known

as the hallmark for the inherent 'quantumness' of a system. Entanglement occurs between two or more quantum systems, and is a product of an interaction that produces some correlations between the two systems. As a result of the quantum nature of the systems, even if the two systems are later separated by a large distance, the correlations remain provided there has not been excessive decoherence of either system. Furthermore, if one is to measure a local observable on one of the systems and cause the state to collapse into an eigenstate of the observable, it is the case that the second system, despite the spatial separation, will be modified. This is what Einstein referred to as 'spooky action at a distance' [95].

1.5.1 Entanglement

In order to properly understand how entanglement works in a quantum system, we first look at what it means for two quantum subsystems to be correlated. This is of interest because, generally, if the observables associated with the different systems are correlated, and these correlations cannot be reproduced purely classically, we say the joint system contains quantum correlations. As a result, the joint system is also inseparable or unfactorisable in some way. Checking such correlations is straightforward when the whole system is a globally pure quantum state: for example, it is sufficient to verify that a Bell-CHSH inequality [96, 97] is violated [98]. Indeed, this is not the only such test for pure states. Where it becomes more challenging to determine correlations is when we are dealing with systems of mixed states. In general, a mixed state may be prepared in infinitely many ways and due to this we cannot extract all of its information since we cannot reconstruct the method used to prepare it. This is discussed in more detail at the end of this section.

To begin, consider entanglement between pure states. Define a pure two-mode quantum state $|\psi\rangle$ defined on the Hilbert space product $\mathcal{H} = \mathcal{H}_1 \otimes \mathcal{H}_2$. This state is separable if it can be written as a product of states on each of the Hilbert spaces, i.e. if there exists $|\phi\rangle_1 \in \mathcal{H}_1$ and $|\chi\rangle_2 \in \mathcal{H}_2$ such that

$$|\psi\rangle = |\phi\rangle_1 \otimes |\chi\rangle_2. \tag{1.49}$$

In order to fully qualify the entanglement of such a system, we diverge briefly to discuss the primary method for characterising such states. The intent is to give a more complete picture of the sort of operations required to produce such states, and hence motivate the work presented later in this thesis. To begin, let us write the pure

quantum state in its unique Schmidt decomposition [99]

$$|\psi\rangle = \sum_{k=1}^{d} \lambda_k |u_k, v_k\rangle, \tag{1.50}$$

where

$$\lambda_k \geq 0, \ \sum_{k=1}^{d} \lambda_k^2 = 1. \tag{1.51}$$

Here, d is called the Schmidt number and gives the number of non-zero terms in the expansion of Eq.(1.50). The $\{\lambda_k\}$ are positive numbers called the Schmidt coefficients, while the local bases $\{|u_k\rangle\} \in \mathcal{H}_1$ and $\{|v_k\rangle\} \in \mathcal{H}_2$ are the Schmidt bases [77]. With this formalism, we can write the so-called reduced density matrices of our pure state $|\psi\rangle$:

$$\varrho_1 = \sum_{k=1}^{d} \lambda_k^2 |u_k\rangle\langle u_k|, \quad \varrho_2 = \sum_{k=1}^{d} \lambda_k^2 |v_k\rangle\langle v_k|. \tag{1.52}$$

Now, suppose we vary the parameter d in order to see how the separability of the state changes. We observe right away that for $d = 1$, we can write our reduced density matrices as pure states of the form we use in Eq.(1.49)

$$\varrho_1 = |\phi\rangle\langle\phi| \qquad \varrho_2 = |\chi\rangle\langle\chi|, \tag{1.53}$$

and as a consequence our composite system is separable and therefore not entangled. We then formulate an entanglement criterion for pure quantum states [77]:

$$|\psi\rangle \text{ is entangled} \Leftrightarrow \ d > 1. \tag{1.54}$$

Within this formalism we can also define the canonical measure of bipartite entanglement of a pure state system, the von Neumann entropy $E_V(|\psi\rangle)$ [100]:

$$E_V(|\psi\rangle) = -\sum_{k=1}^{d} \lambda_k^2 \log \lambda_k^2. \tag{1.55}$$

Since this measure is not basis-dependent, it is invariant under local unitary operations

$$E_V\left((\hat{U}_1 \otimes \hat{U}_2)|\psi\rangle\right) = E_V\left(|\psi\rangle\right). \tag{1.56}$$

It can be shown [101] that $E_V(|\psi\rangle)$ cannot increase under Local Operations and Clas-

sical Communication (LOCC). This result is fundamental, and shows generally that entanglement cannot be created using exclusively LOCC [52, 102].

Meanwhile, in the mixed state case, we first note that we can decompose a mixed state ϱ into a convex combination of pure states $|\psi_k\rangle$:

$$\varrho = \sum_k p_k |\psi_k\rangle\langle\psi_k|, \tag{1.57}$$

where p_k is the weighting of the elements of the superposition. If we take as an example pure states that are superpositions of Fock states with different weights, it quickly becomes clear from this decomposition why the preparation of mixed states is not unique, since we can choose different sets of pure states with different weights to give the same outcome. Due to this ambiguity, it is impossible to know without further information whether these correlations are the result of quantum (entanglement) or classical (LOCC) correlations. It is possible to also have a defined notion of entanglement in mixed state quantum systems. Specifically, we say that a mixed quantum state for a bipartite system of Hilbert spaces $\mathcal{H} = \mathcal{H}_1 \otimes \mathcal{H}_2$ is separable if and only if there exist coefficients $\{p_k | p_k \geq 0, \sum_k p_k = 1\}$ and states $\{\sigma_k\} \in \mathcal{H}_1$, $\{\tau_k\} \in \mathcal{H}_2$, such that

$$\varrho = \sum_k p_k (\sigma_k \otimes \tau_k). \tag{1.58}$$

Otherwise, ϱ is an entangled state [77]. Note that this expression can also apply for pure states, specifically in the case when $k = 1$, meaning that the only separable pure states are product states. For mixed states, in comparison, in general any convex combination of separable states will be separable. In effect, we should note that the criterion of Eq.(1.58) is impractical because it would require us to find the appropriate decomposition. For this reason, we turn to a number of other criteria to detect entanglement in mixed quantum states. These include checking the positivity in the partial transpose, also called the Peres-Horodecki condition [103, 104], and other entanglement witnesses [105–107]. Entanglement witnesses that are practical experimentally have also been demonstrated [108–111].

For mixed states, further entanglement measures also exist, and are reviewed extensively in [112, 113]. These include entanglement of formation, entanglement cost, and distillable entanglement [112], the relative entropy of entanglement [114], negativities [115, 116], and squashed entanglement [117]. The usefulness of entanglement as a resource for quantum information protocols is highlighted in the next two sections, which discuss the specific application of entanglement in teleportation and cloning. In particular, these examples are used to emphasise the fact that research into non-

Gaussianity in the cv regime is highly motivated by enhancements provided to certain computational tasks.

1.5.2 Quantum teleportation

Quantum teleportation describes the process by which quantum information is transmitted without physically moving the quantum state between two locations, and is the most common example of using entanglement as a resource for quantum information processing. First described in [118], quantum teleportation employs long-range correlations between entangled quantum states along with classical communication to show how an unknown quantum state may be disassembled in one location and reconstructed in another. This ability relies on the preparation of an entangled (in this case called EPR-correlated after the work of [95]) state – let us call it ρ_{ab} with subsystems a and b. One of the entangled subsystems, say a, is then used for a joint measurement with the unknown state. The result of this joint measurement is sent using classical communication to the holder of the other entangled subsystem b, and the classical information along with the subsystem b of the entangled pair can be used to fully reconstruct the initial unknown state.

As with much of the field of quantum information processing, initial focus on teleportation relied on discrete variable states [118–124]. However, continuous variable teleportation was shown to be possible [18, 125] and also demonstrated experimentally and unconditionally for the first time in [126]. This result uses Gaussian quantum states – in particular squeezed states – in order to achieve the entanglement necessary for the protocol to work. The ability to unconditionally perform quantum teleportation is meaningful in several ways [126]. To begin, the tools used for this particular implementation apply to other protocols in quantum computing, notably error correction for continuous variables using linear optics [127] and superdense coding of optical information [128]. Furthermore, as stated previously, it is possible to describe finite-dimensional systems within the framework of continuous variables, and as a result it is possible to take advantage of cv optics in the consideration of dv states. Finally, the limiting components to many cv schemes are the need for nonlinear operations – a need which, in this case, has been eliminated [125]. This reference achieved quantum teleportation using Gaussian states with an input-output fidelity of 0.58 ± 0.02 [126], while classical communication can achieve at best a fidelity of 0.5 [129]. So far, we have seen that a standard quantum information task that uses entanglement as a resource can be achieved better-than-classically using Gaussian states. Our goal, however, is to motivate the need for non-Gaussian states, so we ask the question: is there any benefit to employing non-Gaussian states or operations in order to improve the outcomes of

a quantum teleportation protocol?

The answer is yes. The imperfect input-output fidelity in the teleportation schemes described above is due in part to decoherence of the quantum state in the communication channel, but also because of the difficulty in unconditionally producing perfectly entangled states [130]. There have been a number of schemes focused on trying to improve the quality of the entanglement of the state using operations and measurements of redundant variables [130], filtering [131] as well as through quantum privacy amplification [132]. However, it is through the use of non-Gaussian operations – specifically conditional photon subtraction [29] – that one sees a significant improvement in the fidelity of the teleported state. In particular, it was shown that in theory the attainable fidelity using a squeezed vacuum state with squeezing parameter $r = \tanh^{-1}(0.8178)$ as the entangled state in a quantum teleportation protocol is 0.6463, whereas by performing the non-Gaussian operation of photon subtraction, the fidelity can be improved to 0.7444 [29]. Methods for improving the quality of quantum teleportation using non-Gaussian photon subtraction have also been examined in [133, 134]. It is important to note that these results use the ideal case of photon-counting measurements, which require highly efficient detectors that are still generally unavailable. Despite this, it is possible to introduce sufficient non-Gaussianity into a quantum state using an approximative form of photon subtraction with beamsplitting and on-off detection to witness improvements in the quantum teleportation protocols.

As these methods for improving teleportation primarily involve enhancing the entanglement of the quantum state, it is important to note the result of [135]. Here, it was shown that it is possible to have quantum states that are too entangled to be useful as a computational resource, and that in fact most quantum states are too highly entangled to provide a universal quantum computation speedup. This does not preclude the previous results, however, instead illustrating that boundless enhancement of entanglement in a system is not the correct route for improving quantum information processing tasks.

1.5.3 Quantum cloning

Another example motivating the use of non-Gaussianity in cv quantum information is quantum cloning, which is the procedure describing the copying of a quantum state. Ideally, this process is characterised by the transformation

$$|s\rangle_a|Q\rangle_x \to |s\rangle_a|s\rangle_b|Q'\rangle_x, \tag{1.59}$$

where $|s\rangle$ is the state we wish to copy and $|Q\rangle$ is the state of our copying device. The goal of such a cloning protocol is to exactly reproduce the input state of mode a in the state of mode b, and as a result, a unitary transformation must be found to map the left side of Eq.(1.59) to the right. For an arbitrary initial state, however, it has been shown that such a procedure is impossible [136]. This result is known as the No-Cloning Theorem and applies to both the pure states used in the original result as well as mixed states [137], but it does not preclude generating states that are near-, albeit less than, perfect copies of the initial state. Testing the bounds on such quantum copying is motivated by applications in quantum computing and quantum cryptography [138]. Specifically, it is pertinent to understanding the limits on the operations we can perform on quantum information. Furthermore, such imperfect copying still allows us to restrict our cloning ability to a desired subset of states, thereby acquiring the information we want. Similar to quantum teleportation, quantum cloning in an imperfect sense relies on an understanding of entanglement. The cloning operation induces a high level of entanglement between the input state and the output 'copy' state. This has the potential to be problematic because it means that operations performed on the copy will have a significant impact on the state, and vice versa. In effect, this defeats the original purpose of producing the copy since ideally we wish to be able to perform independent operations on the two near-identical states.

It has been shown that the quality of the copy is dependent on the dimensions of the Hilbert space as well as the distribution of states chosen from that space. In the case of a uniform distribution chosen from the dv Hilbert space for qubits, the best fidelity of any pure input state with its copy was found to be $\frac{5}{6}$ [20], which can be compared to the fidelity of the same distribution over the set of all coherent states of $\frac{2}{3}$ [22]. As in the case of teleportation, cloning in the cv regime is also considered. For Gaussian states, it is found that for coherent states chosen from finite Gaussian distributions one can optimise the cloning device to achieve a maximum fidelity of 0.6125 [139], just short of the optimum cloning limit for Gaussian states. For coherent states on a line, a different cloning limit is found of $\frac{4}{9}(\sqrt{10}-1)$ [139]. Further work on cloning using coherent states can be found in [140]. If we move to look at quantum cloning by means of non-Gaussian states, for certain measures (in particular the case of single clones) non-Gaussian operations can enhance the fidelity to above the $\frac{2}{3}$ Gaussian limit. Meanwhile in the case of generating multiple cloned states at once, Gaussian operations are already optimal [141].

1.6 Final Remarks

In this chapter we have presented the formalism underlying quantum information in the continuous variable regime. The types of states and operations introduced here are combined to generate an array of quantum states for use in quantum information processing tasks, a number of which we have also outlined here. In particular, our goal has been to motivate the work of this thesis; that is, to introduce the importance in considering the cv regime for implementing quantum computing tasks, emphasising the need for non-Gaussian operations. Indeed, while we discussed the benefits of such operations for quantum teleportation and quantum cloning protocols, Gaussian states have also been used for dense coding protocols [128, 142, 143], while non-Gaussian states have been used to improve storage of entanglement in quantum memories [144] aside from their necessity in the construction of an optical quantum computer [145, 146].

In the remainder of this work we discuss the generation of two classes of non-Gaussian states in full detail, as well as presenting a method for characterising a subset of non-Gaussian states. A more thorough overview of the literature on these topics is presented at the beginning of each chapter.

Chapter 2

Generating non-Gaussian states 1: superposing orthogonal states

2.1 The qubit orthogonaliser

In this chapter we introduce the first of two approaches for constructing certain non-Gaussian states. While these by no means encompass all efforts for generating such states, they highlight two distinct areas of research in quantum state generation: superposition of orthogonal states and nonlinear resource state creation. We are already capable of producing experimentally the two-mode squeezed vacuum [147], single- and double-photon Fock state [30, 148], as well as variations of the squeezed Schrödinger cat state [25, 149]. The motivation behind quantum state engineering is to remove the limitation of the quantum state we are working with, allowing us to focus on implementing protocols and processing tasks. In the following sections we describe the engineering of a superposition of orthogonal states using two distinct methods.

The ability to produce precise superpositions of quantum states in a general fashion is motivated by the use of such states in quantum information processing tasks. This property was initially observed in [150], where it was found that more information could be encoded in antiparallel pairs of spins than in parallel pairs. Specifically, if we consider a two-qubit state $|\psi, \psi_\perp\rangle$ where $\langle\psi|\psi_\perp\rangle = 0$, we can estimate $|\psi\rangle$ with a fidelity of $\frac{1}{2}(1 + \frac{1}{\sqrt{3}})$ [150, 151]. For an identical qubit pair $|\psi, \psi\rangle$, the fidelity of the optimal measurement only reaches $\frac{3}{4}$. As we have discussed previously, it is possible to encode such information in a cv state, and the outcome for encoding a randomly chosen position in phase space into a pair of phase-conjugate coherent states $|\alpha, \alpha^*\rangle$ is shown to have a higher optimal fidelity as compared to encoding the same information into a near-identical pair [152]. The advantages gained by using orthogonal pairs of states have also demonstrated an advantage when it comes to cloning coherent states:

it is possible to create approximately identical clones of a coherent state $|\alpha\rangle$ with a higher fidelity from the state $|\alpha, \alpha^*\rangle$ than from $|\alpha, \alpha\rangle$ [153]. These phase-conjugate states are not orthogonal, so the natural extension was to investigate whether clones of a cv qubit $|\psi\rangle$ could be produced from the orthogonal pair $|\psi, \psi_\perp\rangle$ with a higher fidelity than from the identical pair $|\psi, \psi\rangle$. It was demonstrated in [154] that this is, in fact, the case. A probabilistic scheme for such optimal cloning of a pair of photons with orthogonal polarisations is presented in [155], while the tradeoff between deterministic and probabilistic cloning has also been investigated [156].

Superpositions of a state with one of its orthogonal states has also allowed for an experimental realisation of an optical approximation to the universal NOT gate [157]. In order to effect such a gate, one needs an antiunitary operation Θ to operate on a general qubit as

$$\Theta(\alpha|0\rangle + \beta|1\rangle) = \beta^*|0\rangle - \alpha^*|1\rangle. \tag{2.1}$$

The issue is that such an operation does not exist in the universal sense. In particular, since this operation is not completely positive it cannot be applied to a subset of, for example, a multi-mode system without changing the rest of the system. It is therefore not possible to use such an operation as a gate operating on only one part of a system. We see that for a general state, it is in fact impossible to find a universal NOT operation. It is possible, however, to find such an operation for a subclass of quantum states – in fact, an operation that orthogonalises a state is a gate with these properties [158, 159]. This is not the same as a universal orthogonaliser that only acts on a subsystem in general, as it requires the full system of quantum states to be constrained prior to determining the orthogonalising operation. Such a quantum NOT gate based on orthogonalising the input state was realised experimentally in [157]. The search for efficient and effective orthogonalising operations is hence heavily motivated by the implementation of such a logical gate.

The first method, described in Sec. 2.2, employs conditional photon subtraction on a two-mode squeezed state, coupled with specific choices of measurement to produce the orthogonal superposition. The approach is purely theoretical, but through a comparison of exact results with those anticipated in more experimentally realistic situations, it is shown that the desired effect may still be achieved. In the second approach, outlined in Sec. 2.3, we provide a general method of creating an orthogonal state, or superposition of orthogonal states, that is state-independent and can be achieved with any operator provided the expectation value of that operator can be computed for the chosen input state. Both of the following examples of orthogonalisation procedure are original work.

2.2 Orthogonalisation by photon subtraction

In this first method, we show how photon subtraction from a two-mode squeezed state results in a superposition of a coherent state and an orthogonal state. Photon subtraction from a quantum state is achieved via the photon annihilation operator $\hat{a}$, the action of which lowers the occupation number of a Fock state by one quantum. It is not possible to directly implement this operator on a quantum state because the operator is not Hermitian and therefore not observable. We instead turn to other techniques to experimentally create the photon-subtracted state. Specifically, photon subtraction can be implemented through a well-tuned beamsplitter interaction accompanied with single-photon detection [70]. This operation, first demonstrated in [149] with a photon-subtracted squeezed state, has become commonplace in quantum optics.

In this section, we consider the use of photon subtraction on a two-mode squeezed state to generate a superposition of a coherent state and an orthogonal state. We begin with an introduction to idealised photon subtraction in Sec. 2.2.1, followed by the more realistic case of photon subtraction using a beamsplitter and single-photon detection. We show that both of these methods allow us to engineer a superposition state that is dependent on the measurement of one of the modes of the two-mode squeezed state. The outcome of such a measurement is illustrated for the cases of homodyne (Sec. 2.2.3) and heterodyne (Sec. 2.2.4) detection. Finally, in Sec. 2.2.5, we consider the case of performing photon subtraction with a beamsplitter when a photon-counting measurement is not possible.

2.2.1 Ideal photon subtraction

In this first section we present the idealised form of photon subtraction, and illustrate its use as an orthogonaliser when applied to a specific choice of initial state. The initial state used in this procedure is the two-mode squeezed (tms) vacuum state, which may be produced experimentally through parametric down-conversion [35]. This state is the result of applying the squeezing operator,

$$\hat{S}_{12}(r) = e^{-r\hat{a}_1^\dagger \hat{a}_2^\dagger + r\hat{a}_1\hat{a}_2}, \tag{2.2}$$

to the two-mode vacuum $|0\rangle_1|0\rangle_2$. Here, $\hat{a}_1$ ($\hat{a}_1^\dagger$) and $\hat{a}_2$ ($\hat{a}_2^\dagger$) are the annihilation (creation) operators on modes 1 and 2, respectively, and r is the squeezing parameter, which we take to be real for the purpose of this work. The tms operation of Eq.(2.2) can be factorised using the Baker-Campbell-Hausdorff technique [160] and written as a product of exponentials with terms $\hat{a}_1^\dagger\hat{a}_2^\dagger$, $\hat{a}_1\hat{a}_2$, and $\hat{a}_1^\dagger\hat{a}_2 + \hat{a}_1\hat{a}_2^\dagger$, allowing it to be

written in the useful form [76]:

$$\hat{S}_{12}(r) = \frac{1}{\cosh r} e^{-\hat{a}_1^\dagger \hat{a}_2^\dagger \tanh r} e^{-(\hat{a}_1^\dagger \hat{a}_2 + \hat{a}_1 \hat{a}_2^\dagger) \ln \cosh r} e^{-\hat{a}_1 \hat{a}_2 \tanh r}. \tag{2.3}$$

Applying this operation to the vacuum allows for a straightforward simplification, giving the final form of the tms vacuum as:

$$\hat{S}_{12}(r)|0\rangle_1|0\rangle_2 = \frac{1}{\cosh r} e^{-\hat{a}_1^\dagger \hat{a}_2^\dagger \tanh r}|0\rangle_1|0\rangle_2. \tag{2.4}$$

Working with this simplified form, we now consider the effect of photon subtraction. In particular, we look at mode-independent, or conditional, photon subtraction wherein the photon is removed from either mode 1 or 2, without preference. This is achieved through application of the operation

$$\hat{a}_1 + \lambda \hat{a}_2, \tag{2.5}$$

where λ is a tuneable real parameter that we take to be 1 in this ideal case. We start by examining the effect of the first term, which subtracts a photon from mode 1:

$$\hat{a}_1 \hat{S}_{12}(r)|0\rangle_1|0\rangle_2 = \frac{\hat{a}_1}{\cosh r} e^{-\hat{a}_1^\dagger \hat{a}_2^\dagger \tanh r}|0\rangle_1|0\rangle_2. \tag{2.6}$$

Inserting the identity to the left of $\hat{a}_1$ by writing it as

$$\mathbb{1} = e^{-\hat{a}_1^\dagger \hat{a}_2^\dagger \tanh r} e^{\hat{a}_1^\dagger \hat{a}_2^\dagger \tanh r}, \tag{2.7}$$

we can rewrite Eq.(2.6) as

$$\begin{aligned} \frac{\hat{a}_1}{\cosh r} e^{-\hat{a}_1^\dagger \hat{a}_2^\dagger \tanh r}|0\rangle_1|0\rangle_2 &= \frac{1}{\cosh r} e^{-\hat{a}_1^\dagger \hat{a}_2^\dagger \tanh r}(\hat{a}_1 - \hat{a}_2^\dagger \tanh r)|0\rangle_1|0\rangle_2 \\ &= \frac{-\hat{a}_2^\dagger \tanh r}{\cosh r} e^{-\hat{a}_1^\dagger \hat{a}_2^\dagger \tanh r}|0\rangle_1|0\rangle_2. \end{aligned} \tag{2.8}$$

Here, we note that a variation of the Baker-Campbell-Hausdorff formula [160] is used to show that

$$e^{\hat{a}_1^\dagger \hat{a}_2^\dagger \tanh r} \hat{a}_1 e^{-\hat{a}_1^\dagger \hat{a}_2^\dagger \tanh r} = \hat{a}_1 - \hat{a}_2^\dagger \tanh r. \tag{2.9}$$

We then combine the result of Eq.(2.8) with the full conditional subtraction operation, yielding

$$\frac{(\hat{a}_1 + \hat{a}_2)}{\cosh r} e^{-\hat{a}_1^\dagger \hat{a}_2^\dagger \tanh r}|0\rangle_1|0\rangle_2 = \frac{\hat{a}_2 - \hat{a}_2^\dagger \tanh r}{\cosh r} e^{-\hat{a}_1^\dagger \hat{a}_2^\dagger \tanh r}|0\rangle_1|0\rangle_2. \tag{2.10}$$

It is interesting to note that we can achieve the superposition of two very distinct operations, namely annihilation and creation, just by subtracting a photon. Furthermore, such a superposition has been shown to achieve orthogonalisation of any pure continuous variable input field [161]. The state of Eq.(2.10) is orthogonal to the original squeezed state, and we note that the orthogonalising operation $(\hat{a}_2 - \hat{a}_2^\dagger \tanh r)$ commutes with all operations on mode 1. Therefore, through a choice of measurement on the mode 1, we can further manipulate the output state. Since such a measurement will commute with the orthogonalising operation, we can study the effect of the measurement without accounting for the orthogonaliser. The final state will be the orthogonal superposition of the state we engineer through our choice of measurement.

2.2.2 Photon subtraction with a beamsplitter

We now contrast the idealised case of photon subtraction with a more experimentally feasible method. In the context of experiment, photon annihilation is achieved through the use of high-transmissivity beampslitters and single-photon measurement [70]. The experimental setup for such an operation is shown in Fig.2.1. As above, the initial

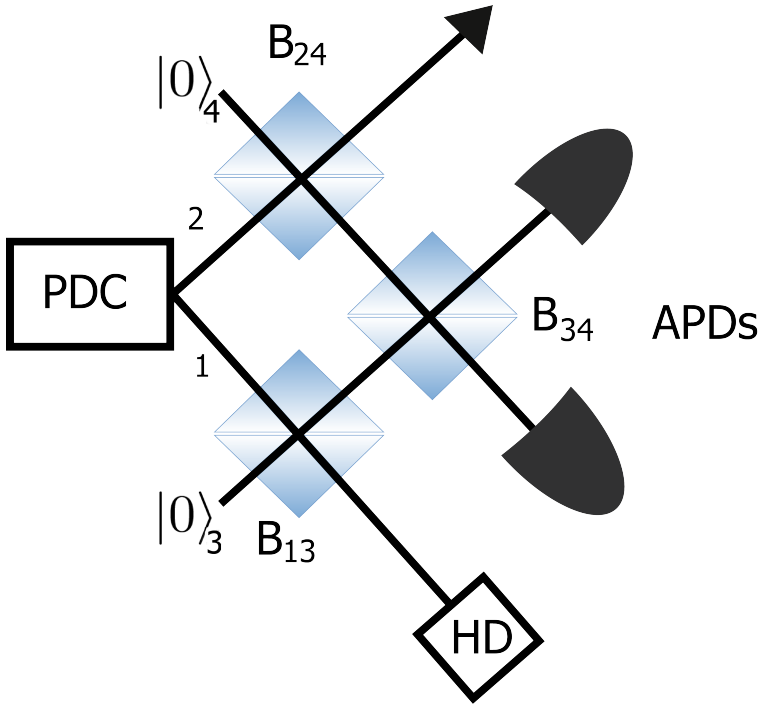

Figure 2.1: Optical setup. A two-mode squeezed vacuum state is produced by parametric down-conversion (PDC) and conditional photon subtraction is implemented through beamsplitters $\hat{B}_{13}$ and $\hat{B}_{24}$. A choice of homodyne or heterodyne detection (HD) is performed on mode 1, along with detection using avalanche photodiodes (APD) on modes 3 and 4 following mixing on a third unbalanced beamsplitter $\hat{B}_{34}$.

state is the tms vacuum state. Beamsplitters $\hat{B}_{13}$ and $\hat{B}_{24}$ are tuned to have high transmissivity, thereby approximating the operation of Eq.(2.5) when the second input is the vacuum. The third beamsplitter, $\hat{B}_{34}$, can be tuned as desired and serves to erase the photon pathway. We write the beamsplitter operation as

$$\hat{B}_{ij}(\theta) = e^{\frac{\theta}{2}(\hat{a}_i^\dagger \hat{a}_j + \hat{a}_i \hat{a}_j^\dagger)}. \tag{2.11}$$

The parameter θ determines the value of reflectivity $r = \sin\frac{\theta}{2}$ and transmissivity $t = \cos\frac{\theta}{2}$. We rewrite Eq.(2.11) using the same Baker-Campbell-Hausdorff technique [160] we used for the squeezing operator:

$$\hat{B}_{ij}(\theta) = e^{-\tan\frac{\theta}{2}\hat{a}_i\hat{a}_j^\dagger} t^{\hat{a}_i^\dagger\hat{a}_i - \hat{a}_j^\dagger\hat{a}_j} e^{\tan\frac{\theta}{2}\hat{a}_i^\dagger\hat{a}_j}. \tag{2.12}$$

The first two beamsplitters $\hat{B}_{13}$ and $\hat{B}_{24}$ are taken to have equal transmissivities (we set both equal to t and let $\theta_{13} = \theta_{24} = \theta$) that are both close to 1. Subtracting a photon from either mode 1 or mode 2 corresponds to adding a photon to mode 3 or 4, respectively. As an ideal measurement this is projecting the state onto $|0\rangle_3|1\rangle_4$ or $|1\rangle_3|0\rangle_4$. Without loss of generality we choose the latter and compute:

$$|\Psi\rangle_{12}^{\text{out}} =_3 \langle 1|_4\langle 0|\hat{B}_{34}\hat{B}_{24}\hat{B}_{13}\hat{S}_{12}|0\rangle_1|0\rangle_2|0\rangle_3|0\rangle_4 \tag{2.13}$$

yielding the state

$$|\Psi\rangle_{12}^{\text{out}} = -(\tan\frac{\theta_{34}}{2}\hat{a}_2 + \hat{a}_1)\tan\frac{\theta}{2}\frac{t_{34}t^{\hat{a}_2^\dagger\hat{a}_2}t^{\hat{a}_1^\dagger\hat{a}_1}}{\cosh r}e^{-\hat{a}_1^\dagger\hat{a}_2^\dagger\tanh r}|0\rangle_1|0\rangle_2. \tag{2.14}$$

Above we have once again made use of Eq.(2.9). Making the assumption that the transmissivity of the first two beamsplitters is close to 1, as is described in [70] as the condition for getting photon subtraction, we can then let $t^{\hat{a}_1^\dagger\hat{a}_1} \approx 1$ and $t^{\hat{a}_2^\dagger\hat{a}_2} \approx 1$. Concluding from Eq.(2.8) that $\hat{a}_1\hat{S}_{12}|00\rangle_{12} = -\hat{a}_2^\dagger \tanh r \hat{S}_{12}|00\rangle_{12}$, we make the substitution $\hat{a}_1 \to -(\tanh r)\hat{a}_2^\dagger$ and get:

$$|\Psi\rangle_{12}^{\text{out}} = -(\tan\frac{\theta_{34}}{2}\hat{a}_2 - \tanh r\hat{a}_2^\dagger)\tan\frac{\theta}{2}\frac{t_{34}}{\cosh r}e^{-\hat{a}_1^\dagger\hat{a}_2^\dagger\tanh r}|0\rangle_1|0\rangle_2. \tag{2.15}$$

We notice immediately that, under the high-transmissivity approximation, any action of the beamsplitters on the initial two-mode squeezed state consists solely of operators acting on mode 2. Hence, any measurement of mode 1 can be computed as acting exclusively on the squeezed state as it will commute with the product of beamsplitter operators. This is the same result as the one we found when considering the ideal case

in the previous section.

Now that we have shown that photon subtraction with a beamsplitter is a good approximation for idealised photon subtraction, we consider the types of state we can engineer in mode 2 based on different types of detection in mode 1.

2.2.3 Homodyne detection

It is possible to control the output state in Fig.2.1 through changing the type of measurement made on mode 1. The first type of measurement we consider is homodyne detection. Homodyne detection is a method that allows one to perform phase-sensitive measurements of the electric field using standard detectors [16, 156, 162–164]. It provides a means of measuring the amplitude of the phase component of a light mode, and thereby determining the marginal distribution. By finding a range of these marginal distributions, the full quantum state can be reconstructed by reversing the integration of these distributions in order to reconstruct the Wigner function [164]. This reversal is possible because integration is a linear process. In terms of a projective measurement, homodyne detection is equivalent to projecting the state on the position eigenstate [160]

$$|x\rangle_1 = \frac{1}{\pi^{1/4}} e^{-\frac{1}{2}x^2} e^{\sqrt{2}x\hat{a}_1^\dagger - \frac{1}{2}(\hat{a}_1^\dagger)^2}|0\rangle_1, \tag{2.16}$$

where $\hat{x}|x\rangle = x|x\rangle$. We note that since this measurement acts exclusively on mode 1, and since the photon subtraction operation can be written as a superposition of photon subtraction and addition acting exclusively on mode 2, we ignore the photon subtraction operation for the next few sections in order to better illustrate the effect of the measurement. Applying the homodyne detection projector to the tms state gives

$${}_1\langle x|\hat{S}_{12}|0\rangle_1|0\rangle_2 = \frac{1}{\cosh r\ \pi^{1/4}} e^{-\frac{1}{2}x^2} e^{-\sqrt{2}x\hat{a}_2^\dagger \tanh r} e^{(\hat{a}_2^\dagger)^2 \tanh^2 r}|0\rangle_2. \tag{2.17}$$

This result can be directly compared to the action of a displacement operator $\hat{D}(\alpha)$, $\alpha \in \mathbb{R}$, followed by a single-mode squeezing operation $\hat{S}(s)$:

$$\hat{S}(s)\hat{D}(\alpha)|0\rangle = \frac{1}{\cosh s} e^{-e^{-2s}(\alpha \tanh s + \alpha^2)} e^{\alpha\hat{a}^\dagger(\cosh s - \sinh s \tanh s)} e^{-\frac{1}{2}(\hat{a}^\dagger)^2 \tanh s}|0\rangle. \tag{2.18}$$

Up to an overall phase and with suitable choices of squeezing parameter s and coherent state parameter α, this squeezed displaced state emulates exactly the state produced by homodyne detection. With the addition of the photon subtraction operation described in Sec. 2.2.1, we achieve a superposition of this squeezed displaced state with one of its orthogonal states.

2.2.4 Heterodyne detection

Just as we can employ homodyne detection to engineer a squeezed displaced single-mode state from the two-mode initial state, heterodyne measurement of one mode can be used to displace the state in the other mode. Optical heterodyne detection uses a local oscillator mode-matched to the signal beam and detected on a photodiode. The output photocurrent is proportional to the square of total electric field amplitude [164]. This type of measurement is also referred to as coherent detection, and corresponds to projecting the system onto a coherent state $|\gamma\rangle$, where γ is a complex number. The result of projecting mode 1 of the tms state is

$$\langle\gamma|_1\hat{S}_{12}|0\rangle_1|0\rangle_2 = \frac{e^{-\frac{1}{2}|\gamma|^2}}{\cosh r}e^{-\gamma^*\hat{a}_2^\dagger\tanh r}|0\rangle_2. \tag{2.19}$$

Multiplying this result by $\mathbb{1} = e^{\frac{1}{2}|\gamma|^2\tanh^2 r}e^{-\frac{1}{2}|\gamma|^2\tanh^2 r}$ and rearranging, we see that with this particular choice of measurement on mode 1, we have produced a displaced state in mode 2:

$$\frac{e^{-\frac{1}{2}|\gamma|^2}}{\cosh r}e^{-\gamma^*\hat{a}_2^\dagger\tanh r}|0\rangle_2 = \frac{e^{-\frac{1}{2}|\gamma|^2(1-\tanh^2 r)}}{\cosh r}|-\gamma^*\tanh r\rangle_2. \tag{2.20}$$

We have thus shown that, using heterodyne detection on one of the modes, the setup of Fig.2.1 allows us to engineer a displaced state without interfering with the orthogonalising operation produced by the photon subtraction, as illustrated by Eq.(2.10).

2.2.5 Beyond single-photon detection

We now re-examine the single-photon detection that allowed us to achieve photon subtraction using beamsplitters. Up until this point our work has hinged upon the assumption that we detect a single photon in either mode 3 or 4 of Fig.2.1, at which point we know whether we have subtracted a photon from mode 1 or 2. The conventional Avalanche Photodiode (APD) detector [165], on the other hand, is saturated at the single-photon level. Such detectors act as on-off switches, where a signal indicates one or more photons has been measured, without any knowledge of the precise number. We say the detector measures either the state $|0\rangle\langle 0|$ or $\mathbb{1} - |0\rangle\langle 0|$. If we define the state where only mode 1 has been measured as ρ_{234}, then the measurement can be viewed as the operation:

$$\mathrm{Tr}_{34}[(\mathbb{1} - |0\rangle\langle 0|)_3 \otimes |0\rangle_4\langle 0|\rho_{234}] \tag{2.21}$$

which becomes

$$\mathrm{Tr}_3[{}_4\langle 0|\rho_{234}|0\rangle_4] - {}_3\langle 0|{}_4\langle 0|\rho_{234}|0\rangle_4|0\rangle_3. \tag{2.22}$$

We now employ techniques described in the previous sections to engineer a tuneable superposition state. The operations produced by this setup simulate those discussed in the ideal case for photon subtraction discussion in Sec. 2.2.1. We specifically look at the final output following heterodyne detection, thereby considering a superposition of a coherent state and an orthogonal state. The beamsplitters that mix modes 1 and 2 with modes 3 and 4, respectively, have high transmissivity to provide good approximations to the annihilation operation $(\hat{a}_1 + \hat{a}_2)$. The third beamsplitter mixes modes 3 and 4. This addition allows a weighting on the annihilation operations equivalent to performing $(t\hat{a}_1 + \sqrt{1-t^2}\hat{a}_2)$ in Sec. 2.2.1. Adjusting the transmissivity for this beamsplitter shifts the final state from a coherent state with a positive Wigner function (for high t) to a non-classical state with a Wigner function that goes negative for some values of its parameters. We wish to express this result in terms of the Wigner function. To do so, we find that expressing the states in the form of coherent states greatly simplifies the calculation. We begin by multiplying the two-mode squeezed vacuum state by the identity operators $\mathbb{1}_1$ and $\mathbb{1}_2$ expressed in their coherent state form

$$\mathbb{1}_1 = \frac{1}{\pi}\int d^2\alpha |\alpha\rangle_1\langle\alpha| \tag{2.23}$$

where α is a complex number. We use α for mode 1 and β for mode 2. Since a density matrix for a pure state, which we will call ρ_{12}, can be written in the form $|\psi\rangle_{12}\langle\psi|$, we consider only the effect on the state $|\psi\rangle_{12} = \hat{S}_{12}|0\rangle_1|0\rangle_2$. Once we need to treat the state as a density matrix in order to compute the Wigner function we will take the outer product. Multiplying the state $|\psi\rangle_{12}$ by the identities, we get

$$|\psi'\rangle_{12} = \mathbb{1}_1\mathbb{1}_2|\psi\rangle_{12} = \frac{1}{\pi^2\cosh r}\int d^2\alpha d^2\beta e^{-\frac{1}{2}(|\alpha|^2+|\beta|^2)-\alpha^*\beta^*\tanh r}|\alpha\rangle_1|\beta\rangle_2. \tag{2.24}$$

Note that the action of the beamsplitter operator on the coherent state of mode 1 and the ground state of mode 3 is simply $B_{13}|\alpha\rangle_1|0\rangle_3 = |t_{13}\alpha\rangle_1|r_{13}\alpha\rangle_3$ where $t_{13} = \cos\frac{\theta_{13}}{2}$ and $r_{13} = \sin\frac{\theta_{13}}{2}$ are the transmissivity and reflectivity of the beamsplitter mixing modes 1 and 3. Applying beamsplitters $\hat{B}_{13}$ and $\hat{B}_{24}$ we get

$$\hat{B}_{13}\hat{B}_{24}|\psi'\rangle_{12}|0\rangle_3|0\rangle_4 = \int d^2\alpha d^2\beta F(\alpha,\beta,s)|t_{13}\alpha\rangle_1|t_{24}\beta\rangle_2|r_{13}\alpha\rangle_3|r_{24}\beta\rangle_4. \tag{2.25}$$

Here $F(\alpha,\beta,s) = \frac{1}{\pi^2\cosh s}e^{-\frac{1}{2}(|\alpha|^2+|\beta|^2)-\alpha^*\beta^*\tanh s}$. Applying a final beamsplitter with

transmissivity and reflectivity given by t and r to modes 3 and 4, gives

$$\hat{B}_{34}|r_{13}\alpha\rangle_3|r_{24}\beta\rangle_4 = |r_{13}t\alpha + r_{24}r\beta\rangle_3|r_{24}t\beta - r_{13}r\alpha\rangle_4. \tag{2.26}$$

We now consider measurements on modes 1, 3, and 4. Heterodyne detection is performed on mode 1: we project the state onto a coherent state $|\gamma\rangle_1$, giving the factor

$$\langle\gamma|t_{13}\alpha\rangle = e^{-\frac{|\gamma|^2}{2}-\frac{t_{13}^2|\alpha|^2}{2}+t_{13}\gamma^*\alpha}. \tag{2.27}$$

Following this measurement we post-select on detecting photons at the detector for mode 3, with no incidence counts detected in mode 4. This is described by the measurement operator $(\mathbb{1}-|0\rangle\langle 0|)_3 \otimes |0\rangle_4\langle 0|$. Applying this measurement and putting everything together we get an expression for the final state in mode 2:

$$\begin{aligned}\rho_b = \int d^2\alpha d^2\beta\ |F(\alpha,\beta,s)|^2 e^{-|\gamma|^2-t_{13}^2|\alpha|^2+t_{13}(\gamma^*\alpha+\gamma\alpha^*)} \\ \times\, e^{-|r_{13}\alpha t+r_{24}\beta r|^2} e^{-|r_{24}\beta t-r_{13}\alpha r|^2}\left(e^{|r_{13}t\alpha+r_{24}r\beta|^2}-1\right)|t_{24}\beta\rangle_2\langle t_{24}\beta|\end{aligned} \tag{2.28}$$

Now that we have the density matrix for the output mode 2 we examine the Wigner function form. Reiterating that the object of this work is to engineer a quantum state that is a superposition of orthogonal states in the analysis of the ideal case for photon subtraction in Sec. 2.2.1, the operation $(\hat{a}_1+\hat{a}_2)$ was shown in Eq.(2.10) to be equivalent to $(\hat{a}_2-\hat{a}_2^\dagger\tanh s)$. Comparing this to the experimental setup of Fig.2.1, we see that the weighting of the two operators can be tuned according to the transmissivity of the third beamsplitter $\hat{B}_{34}$. By tuning this superposition, we can shift the weight of the terms in the superposition. In the case of the orthogonaliser acting on a coherent state, this amounts to shifting the weighting of the superposition from the Gaussian coherent state to a non-Gaussian displaced single-photon state. This tuning appears in the operator expression from Eq.(2.10) as

$$(r\hat{a}_2 - t\hat{a}_2^\dagger\tanh s). \tag{2.29}$$

We therefore expect for low transmissivity to recover a Gaussian state, while for higher transmissivity the state becomes increasingly non-Gaussian.

These expectations meet the reality of the beamsplitter setup. The transmissivities of the first two beamsplitters are chosen so they closely mimic the effect of the annihilation operator – that is $t_{13}=t_{24}=\frac{9}{10}$. The squeezing parameter s as well as the choice of coherent state used for heterodyne detection γ are both assigned values

of $\frac{3}{2}$. These values are chosen to be greater than 1 so their effect is more observable. Plots are produced for three values of transmissivity t, and where x and y are used to denote the position and momentum quadratures. Fig 2.2 is a plot for a low value of $t = \frac{1}{10}$, which approximately gives the Wigner function for a coherent state. As t is increased so the superposition is balanced, we get the result of Fig. 2.3. Finally, for large t, taken to be $\frac{9}{10}$, we arrive at a function skewed in favour of the orthogonal state, as illustrated in Fig. 2.4.

It is clear from the plots that for low transmissivity the Wigner function is a Gaussian distribution while for increasing transmissivity it becomes non-Gaussian. This matches the prediction from the ideal case illustrated by Eq.(2.29).

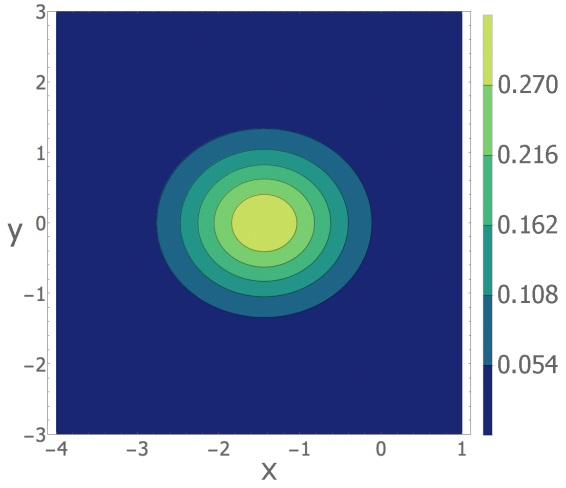

Figure 2.2: Wigner function for the superposition of a coherent state with one of its orthogonal states, $|\alpha\rangle + |\alpha_\perp\rangle$, where the tuneable photon subtraction parameter is taken to be $t = \frac{1}{10}$. In this case, we see that we recover an approximately coherent state as the final state. Here, x and y denote the position and momentum quadratures.

2.2.6 Preliminary conclusions

Here we have presented a method for generating a superposition of orthogonal states using conditional photon subtraction. Further engineering of the final state is shown to be possible based on the type of measurement used on one of the modes. Specifically, we have shown that conditional photon subtraction on a two-mode squeezed state can be expressed as a superposition of the photon annihilation and photon creation operations acting on one of the modes, and, as a result, we can engineer the output state by performing different measurements on the other mode. We considered two types of detection, homodyne and heterodyne, which generated respectively a squeezed displaced state and a coherent state. We finally looked at tuning the superposition of

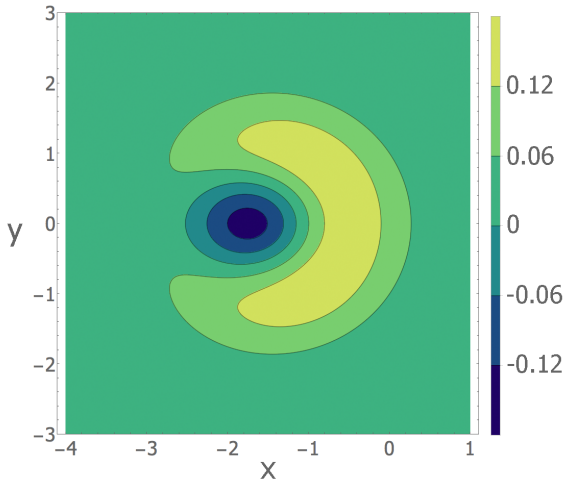

Figure 2.3: Wigner function for the superposition of a coherent state with one of its orthogonal states, $|\alpha\rangle + |\alpha_\perp\rangle$, where the tuneable photon subtraction parameter is taken to be $t = \frac{1}{\sqrt{2}}$. In this case, we have generated an equal superposition of the two orthogonal states. Here, x and y denote the position and momentum quadratures.

a coherent state and an orthogonal state by adjusting beamsplitter $\hat{B}_{34}$ of Fig.2.1.

2.3 Orthogonalisation of arbitrary input fields

The second scheme presents a general method for producing a superposition of orthogonal states and is pending publication as [62]. This work describes a theoretical proposal which is original work, while the experimental work was performed by collaborators. Within quantum mechanics, two states $|\psi\rangle$ and $|\psi_\perp\rangle$ are said to be orthogonal when their inner product, or overlap, is zero: $\langle\psi|\psi_\perp\rangle = 0$. These two states are thereby maximally discernible [67, 166]. In the classical discrete variable domain, as in the case of the classical binary system, states denoted 0 and 1 are orthogonal and it is possible to move from one to the other via the NOT operation [159]. Within quantum mechanics, an exact form of this operation – orthogonalisation without knowledge of the initial state – is impossible [159]. Quantum theory further restricts our ability to perfectly and deterministically clone or amplify a state [136, 167] without prior information. This difficulty is magnified when we move into the continuous variable regime and use general quantum states in infinite-dimensional Hilbert spaces. In this case, a given state has an infinite number of orthogonal states. It has been proposed that a perfect orthogonalisation procedure for infinite-dimensional states is realisable given some limited preliminary information [168]. In the following sections we present a method to realise continuous variable quantum state orthogonalisation. This method is general, and includes experimental demonstrations. In addition to allowing for the

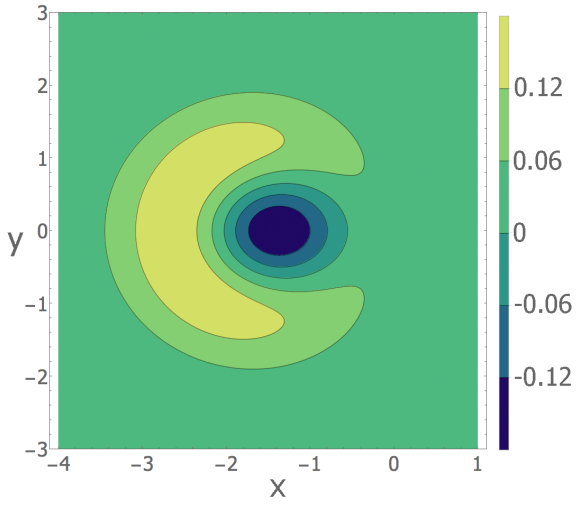

Figure 2.4: Wigner function for the superposition of a coherent state with one of its orthogonal states, $|\alpha\rangle + |\alpha_\perp\rangle$, where the tuneable photon subtraction parameter is taken to be $t = \frac{9}{10}$. In this case, we see that we recover a nonclassical final state. Here, x and y denote the position and momentum quadratures.

generation of an orthogonal state, this method can also be trivially adjusted to generate a superposition of the orthogonal states.

2.3.1 General orthogonaliser

The construction of the generalised orthogonalisation procedure is centred on the operation rather than the input state. While some information about the input state is necessary to achieve full orthogonalisation, there is no theoretical restriction on the type of state that can be orthogonalised. We construct the orthogonalising operator $\hat{O}_C$ from an arbitrary operator $\hat{C}$ and its mean value $\langle\hat{C}\rangle$ on the input state $|\psi\rangle$:

$$\hat{O}_c = \hat{C} - \langle\hat{C}\rangle\mathbb{1}, \tag{2.30}$$

where $\mathbb{1}$ is the identity operator. We define the generic normalised quantum state $|\psi\rangle$ and one of its orthogonal states $|\psi_\perp\rangle$, and we observe directly that since

$$\langle\psi|\hat{O}_C|\psi\rangle = \langle\psi|\hat{C}|\psi\rangle - \langle\psi|\langle\hat{C}\rangle|\psi\rangle \tag{2.31}$$

$$= 0, \tag{2.32}$$

applying $\hat{O}_C$ to the input state yields $\hat{O}_c|\psi\rangle = |\psi_\perp\rangle$. The choice of operator $\hat{C}$ is only limited by the fact that it must not be the case that the input states $|\psi\rangle$ are among its eigenstates as, in that case, the success probability drops to zero. This

type of orthogonaliser for states in a two-dimensional Hilbert space was demonstrated recently [157]. This operation is not limited to production of an orthogonal state, but may be trivially extended to produce a superposition of the input state and an orthogonal state much like the results presented in the Sec.2.2. The superposition state is achieved by realising the same operation $\hat{O}_C$ but with a linear shift from the mean value. Specifically, for any complex number c, the (un-normalised) superposition

$$c|\psi\rangle + |\psi_\perp\rangle = (c\hat{\mathbb{1}} + \hat{O}_C)|\psi\rangle \tag{2.33}$$

$$= [\hat{C} + (c - \langle\hat{C}\rangle)\hat{\mathbb{1}}]|\psi\rangle \tag{2.34}$$

is realised by applying the same operation of Eq.(2.30) to the input state, but with an appropriate change in the weight of the identity operator. Therefore, once the orthogonaliser is in operation, any quantum superposition of $|\psi\rangle$ and $|\psi_\perp\rangle$ can also be straightforwardly realised. The generality of these procedures – any operator can be used to implement the orthogonaliser, and the schemes may be applied to any input state (either classical or non-classical, and of any dimensionality) – makes them a particularly novel and significant step forward in the field of quantum state engineering.

Before going into more detail on the nature of experimentally generating such a superposition, a number of limitations should be noted. Ideally, it would be possible to design a specific setup to generate the orthogonal state (or superposition) using a full tomographic reconstruction of the given input state. However, as state tomography necessitates the measurement of observable probabilities for a large number of experimental settings and therefore requires many identical copies of the initial input state in order to make an accurate estimation of the state, such a strategy becomes very inefficient and is far from universal. Moreover, it would be necessary to design specific experimental schemes for each input state, which in general may be far from trivial. While having infinite identical copies of the input state may be ideal in order to measure the mean value of operator $\hat{C}$, it is possible to perform the measurement with a finite N copies and still find a measure of accuracy. With N copies, the estimation of the mean value is accurate by $\Delta C/\sqrt{N}$, where ΔC is the standard deviation of the measurement outcomes for the expectation value of the operator $\hat{C}$. In this way, such an approach becomes much more resource-efficient than another based on full state reconstruction, although we do not claim that this scheme requires the fewest resources. Furthermore, the scheme described here requires only a single universal parameter (the mean value $\langle\hat{C}\rangle$) in order to orthogonalise arbitrary states and produce arbitrary quantum superpositions.

With this general discussion presented, we now go into detail for two specific cases.

In particular, we look at two different choices of operator $\hat{C}$, substituting it with the creation operator $\hat{a}^\dagger$ and the number operator $\hat{n}$, and consider the effect of using these operators as orthogonalisers on representative cases of highly non-classical states: an even cat state $|\alpha\rangle + |-\alpha\rangle$ with $|\alpha| = 0.9$, and a squeezed vacuum state $\hat{S}(\xi)|0\rangle$ with $\xi = 0.8$, whose Wigner functions are shown in Figs 2.5(a) and 2.5(b).

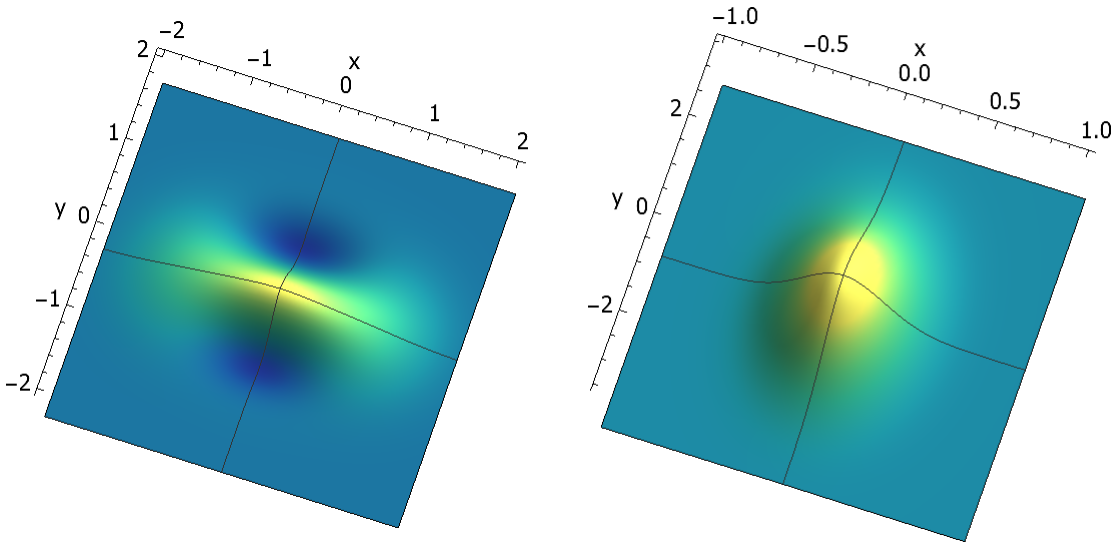

(a) (b)

Figure 2.5: Wigner functions for (a) the Schrödinger cat state $|\alpha\rangle + |-\alpha\rangle$ for $|\alpha| = 0.9$ and (b) the squeezed vacuum state $\hat{S}(\xi)|0\rangle$ for $\xi = 0.8$. Darker (blue) colours represent regions of negative probability while lighter (yellow) colours represent regions of higher probability. Here, x and y denote the position and momentum quadratures.

2.3.2 Case 1: $\hat{a}^\dagger$ as orthogonaliser

The first case we consider is when $\hat{C} = \hat{a}^\dagger$, the bosonic creation operator, which has no eigenstates and can thus be safely applied independently of the arbitrary state at the input. It is sufficient to know the mean value $\langle \hat{a}^\dagger \rangle$ on the particular input state in order to construct the orthogonalising operator $\hat{O}_{a^\dagger} \equiv \hat{a}^\dagger - \langle \hat{a}^\dagger \rangle \hat{\mathbb{1}}$. This operation is conditionally realised experimentally in [62] via stimulated parametric down-conversion (PDC) in a nonlinear crystal seeded by the optical input state in the signal mode [35, 36, 70]. Mixing of the herald idler PDC mode with a coherent light field on an unbalanced beamsplitter, which, as mentioned before in the discussion on conditional photon subtraction, erases the information on the origin of the click in the heralding single-photon detector at one of its outputs, allows for the coherent superposition of the orthogonal operation and the identity. Different superpositions of the creation

operator and the identity can be controlled through the relative phase of the input and coherent state, as well as the reflectivity of the beamsplitter upon which the two states impinge. A simplified scheme of the experimental setup is shown in Fig.2.6a.

The techniques used to produce this orthogonal superposition experimentally are similar to those for quantum state engineering up to two photons [169] and for the generation of optical CV qubits from superpositions of squeezed vacuum and squeezing single-photon state [33]. All three methods employ parametric down conversion coupled with homodyne detection of the signal mode, while the idler mode is mixed with a weak coherent state prior to performing single photon counting detection. In these cases, the single photon detection is used to herald the homodyne detector.

We now consider the operation of this particular orthogonaliser on several different states. The concept is tested on the coherent state $|\alpha\rangle$. In this case, the orthogonaliser operator based on photon creation becomes

$$\hat{O}_{a^\dagger}(\alpha) = \hat{a}^\dagger - \alpha^* \hat{\mathbb{1}}, \tag{2.35}$$

which, when applied to the original coherent state, results in the clearly orthogonal displaced Fock state $\hat{D}(\alpha)|1\rangle$.

While the coherent state is a simple case whereby the effect of the orthogonalisation is visible without extensive processing, it must be emphasised that this procedure is general, and that the orthogonaliser constructed from a particular operator is capable of orthogonalising any state. To highlight this, we now consider two highly non-classical inputs – the cat state $|\alpha\rangle + |-\alpha\rangle$ and the squeezed vacuum $\hat{S}(\xi)|0\rangle$. To best illustrate the orthogonalisation of the input states, we construct the Wigner functions of the original states as well as the states following application of the operator $\hat{O}_{a^\dagger}$. An additional feature of this procedure is that a set of orthogonal states may be constructed by repeated application of the operator $\hat{O}_{a^\dagger} \equiv (\hat{a}^\dagger - \alpha^* \mathbb{1})$ to $|\alpha\rangle$. Noting only that $\langle\alpha|\hat{O}_{a^\dagger} = 0\mathbb{1}$, it is evident that $\langle\alpha|\hat{O}_{a^\dagger}|\alpha\rangle = 0$. Furthermore, the result will be the same for $\hat{O}_{a^\dagger}\hat{O}_{a^\dagger}|\alpha\rangle$, and on to states of form $\hat{O}^n_{a^\dagger}$ for $n \in \mathbb{Z}^+$. Thus with this operation we can construct a set of states orthogonal to the coherent state.

We now consider the theoretical implementation of the scheme in Fig. 2.6a. This generates the operation of $\hat{O}_{a^\dagger}$, approximating it with some tuning through the operation $\hat{B}_{bc}(|1\rangle_b\hat{a}^\dagger + |0\rangle_b\mathbb{1})|\beta\rangle_c$. Here, $\hat{B}_{bc}$ is the beamsplitter operator, which acts on coherent states mixed with the vacuum as $\hat{B}_{bc}|0\rangle_b|\beta\rangle_c = |-r\beta\rangle_b|t\beta\rangle_c$. Note that $\hat{a}$ and $\hat{a}^\dagger$ are not operating on any of the modes present in this expression. The final step in this method is to project the expression onto $|1\rangle_b|0\rangle_c$, yielding

$$t\hat{a}^\dagger - r\beta\mathbb{1}, \tag{2.36}$$

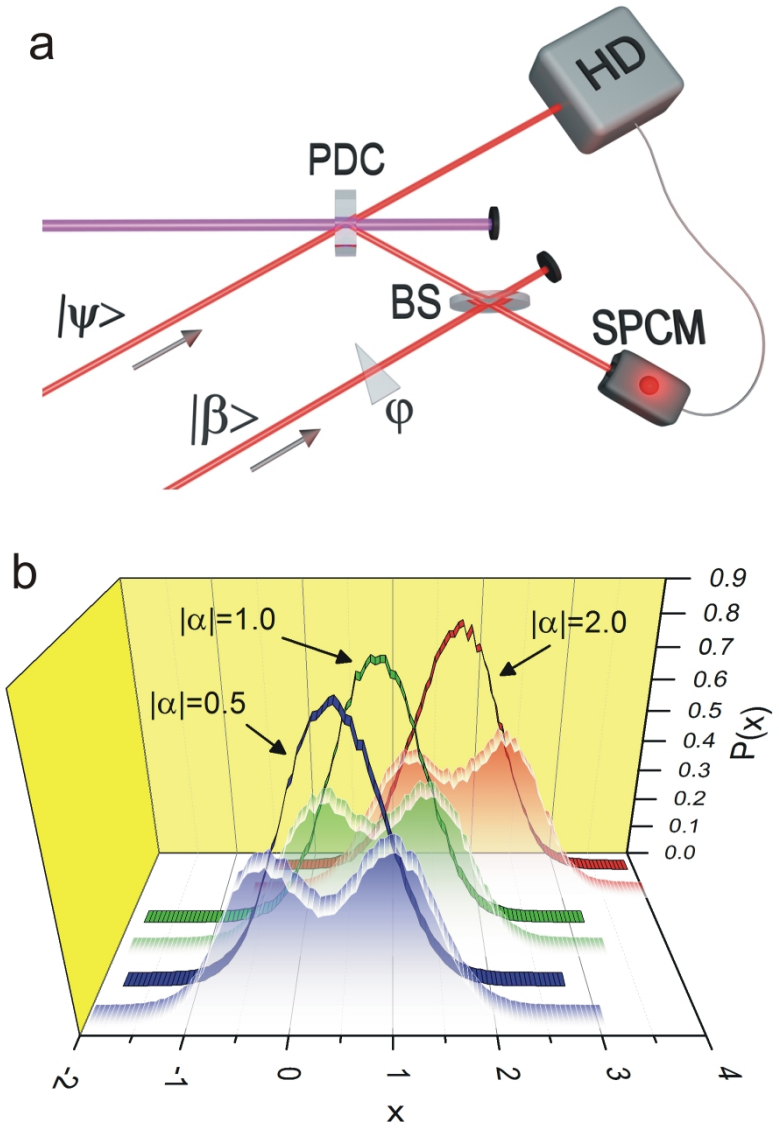

Figure 2.6: State orthogonaliser and cv qubit generator based on the photon creation operator $\hat{a}^\dagger$. a. Conceptual experimental scheme of the orthogonalizer and cv qubit generator based on photon addition by heralded stimulated PDC. A click in the single-photon-counting module (SPCM) normally heralds a single photon addition to the generic input $|\psi\rangle$ state. However, if the PDC idler mode is mixed with a coherent state $|\beta\rangle$ on a beamsplitter (BS) prior to detection, a superposition of the photon creation operator and the identity with adjustable weights and phases can be obtained. In the actual experiments coherent states $|\alpha\rangle$ were used as the input states and the operator superposition was implemented by using polarization modes. HD is a time-domain homodyne detector triggered by SPCM clicks. b. Raw measured x quadrature distributions (marginals of the Wigner function) for the input coherent states and for the corresponding results of the orthogonalisation procedure with $|\alpha| = 0.5, 1.0, 2.0$. This experiment was performed by collaborators on [62]

.

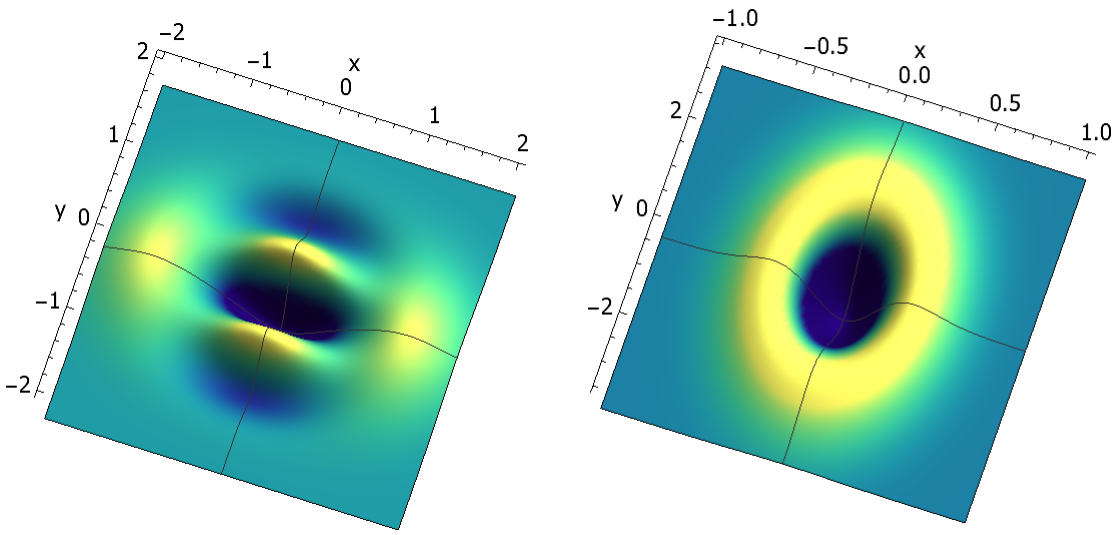

(a) (b)

Figure 2.7: Wigner functions for (a) the Schrödinger cat state $|\alpha\rangle + |-\alpha\rangle$ for $|\alpha| = 0.9$ and (b) the squeezed vacuum state $\hat{S}(\xi)|0\rangle$ for $\xi = 0.8$ following action of the orthogonaliser $\hat{O}_{a^\dagger}$. Darker (blue) colours represent regions of negative probability while lighter (yellow) colours represent regions of higher probability. Here, x and y denote the position and momentum quadratures.

up to an overall phase which is omitted to better see the similarity of the result to operator $\hat{O}_{a^\dagger}$.

Note that this scheme is equivalent to using displaced Fock states as orthogonal to coherent states. That is, $D(\alpha)|1\rangle$ is orthogonal to $|\alpha\rangle = D(\alpha)|0\rangle$. This is quickly demonstrated by noting the convolution of the displacement operator $D(\alpha)$ with the creation operator $\hat{a}^\dagger$:

$$D(\alpha)\hat{a}^\dagger D^\dagger(\alpha) = \hat{a}^\dagger - \alpha^* \mathbb{1}. \tag{2.37}$$

This is precisely the operator $\hat{O}_{a^\dagger}$.

2.3.3 Case 2: $\hat{n}$ as orthogonaliser

To further illustrate the generality of this orthogonalisation approach, we now consider a second scheme. The mean number of photons in a state is a fairly straightforward parameter to determine experimentally. We write the orthogonaliser in terms of mean photon number $\bar{n} = \langle \hat{n} \rangle$ and the number operator $\hat{n} \equiv \hat{a}^\dagger \hat{a}$ as

$$\hat{O}_n \equiv \hat{n} - \bar{n}\hat{\mathbb{1}}. \tag{2.38}$$

For this particular operator, the experimental setup conditionally produces the arbitrary superposition of operators

$$A\hat{a}^\dagger\hat{a} + B\hat{a}\hat{a}^\dagger, \tag{2.39}$$

which is proportional to $\hat{n} + \frac{B}{A+B}\hat{\mathbb{1}}$, as one can see using the bosonic commutation relation. As a result the generic orthogonal state can be straightforwardly produced by adjusting the setup of Fig.2.8a so that $\frac{B}{A+B} = -\bar{n}$. It should be noted that the orthogonaliser constructed from $\hat{n}$ does not necessarily produce a different orthogonal state than the operator $\hat{a}^\dagger$, and in fact two distinct operators produce orthogonal states that are not necessarily the same just as they are not necessarily different. That is, the orthogonaliser specifically produces a state orthogonal to the input it is directly acting on, unrelated to the use of a different orthogonaliser. This can be highlighted through applying the photon number orthogonaliser $\hat{O}_n$ to a coherent state $|\alpha\rangle$: in this case, $\hat{O}_n|\alpha\rangle$ produces the same orthogonal state in the previous example. In any case, we do not assume any knowledge about the initial state except its mean photon number. In Figs. 2.7(a), 2.7(b), 2.9(a), and 2.9(b) we illustrate how this operation is also able to orthogonalise the cat state and the squeezed vacuum. We emphasise again that while the use of this operation takes a state to one of its orthogonal states, these orthogonal states are not necessarily orthogonal to the states produced via a different operation. This is easily visible by comparing Figs.2.7(a) and 2.7(b) with Figs.2.9(a) and 2.9(b).

Just as we showed that the scheme of Fig.2.6a generates the operation $\hat{O}_{a^\dagger}$, we can show it works for $\hat{O}_n$. This approach begins with the expression $\hat{B}_{bc}(\mathrm{e}^{i\phi}\hat{a}^\dagger\hat{a}|1\rangle_b|0\rangle_c + \hat{a}\hat{a}^\dagger|0\rangle_b|1\rangle_c)$, where this time it is noted that $\hat{B}_{bc}|1\rangle_b|0\rangle_c = t|1\rangle_b|0\rangle_c + r|0\rangle_b|1\rangle_c$. Following the measurement again of $|1\rangle_b|0\rangle_c$, the resulting expression, up to a phase, is

$${}_b\langle 1|_c\langle 0|\hat{B}_{bc}(\mathrm{e}^{i\phi}\hat{a}^\dagger\hat{a}|1\rangle_b|0\rangle_c + \hat{a}\hat{a}^\dagger|0\rangle_b|1\rangle_c) \approx \hat{n} - \frac{r}{t-r}\mathbb{1}, \tag{2.40}$$

where $\frac{r}{t-r}$ can be set to equal $\bar{n}$ with the appropriate adjustment of the beamsplitter BS.

2.3.4 Preliminary conclusions

The work presented in the latter half of this chapter demonstrates the first experimental application of a universal orthogonalisation procedure for arbitrary cv optical states that relies on very limited preliminary information on the input states. The effectiveness of this technique both in orthogonalising the input state and in creating

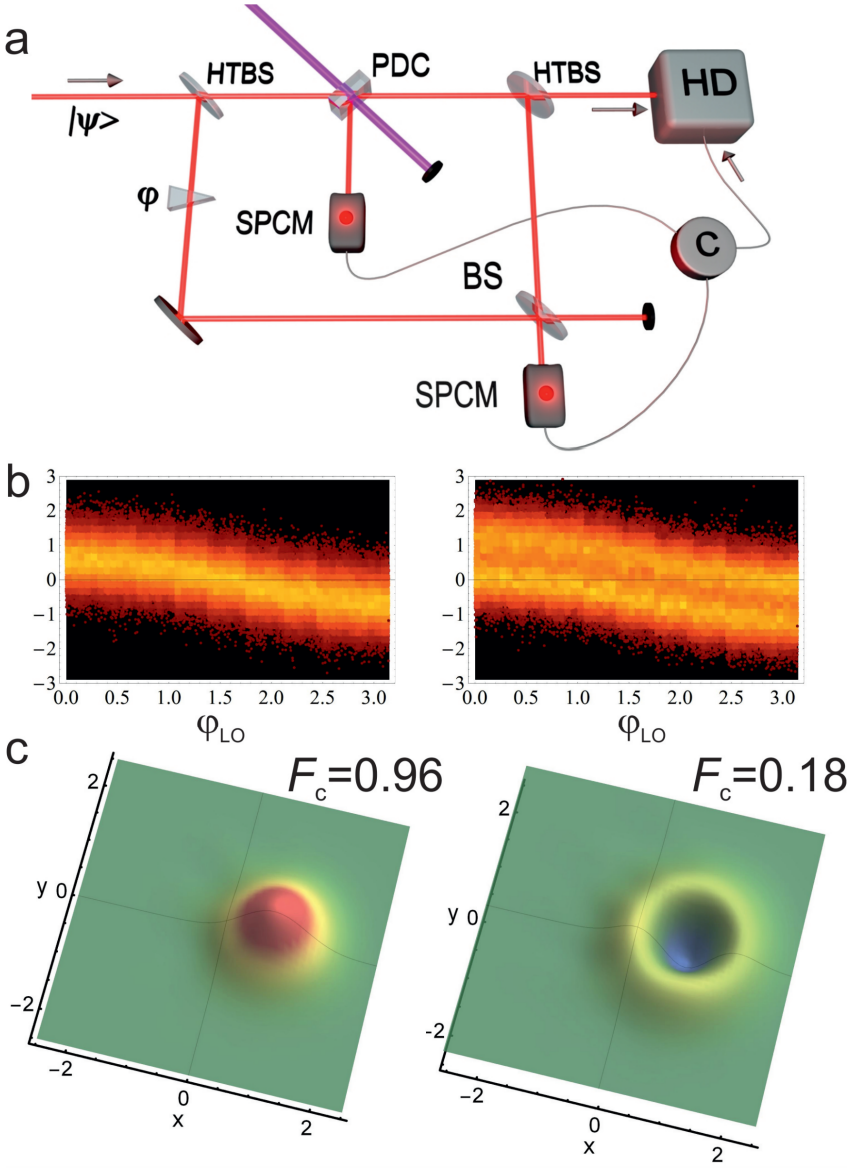

Figure 2.8: State orthogonaliser based on the photon number operator $\hat{n}$. (a) Conceptual experimental scheme for the orthogonaliser. HTBS are high-transmissivity beamsplitters and C is a coincidence logic circuit. (b) Experimental homodyne detection traces for the original input coherent state $|\alpha\rangle$ (left) and for the output state following orthogonalisation (right). The input coherent state amplitude was $|\alpha| = 0.78$, and 10 different values for the local oscillator phases were used. (c) Wigner functions of the input coherent state and the output orthogonal state (a displaced single-photon Fock state) as reconstructed from the homodyne data after corrected for the limited (70%) detection efficiency. This experiment was performed by collaborators on [62].

superpositions of orthogonal states was demonstrated through two experimental examples based on the photon creation and number operators. While the experimental demonstration was limited to input coherent states, we emphasise once again here

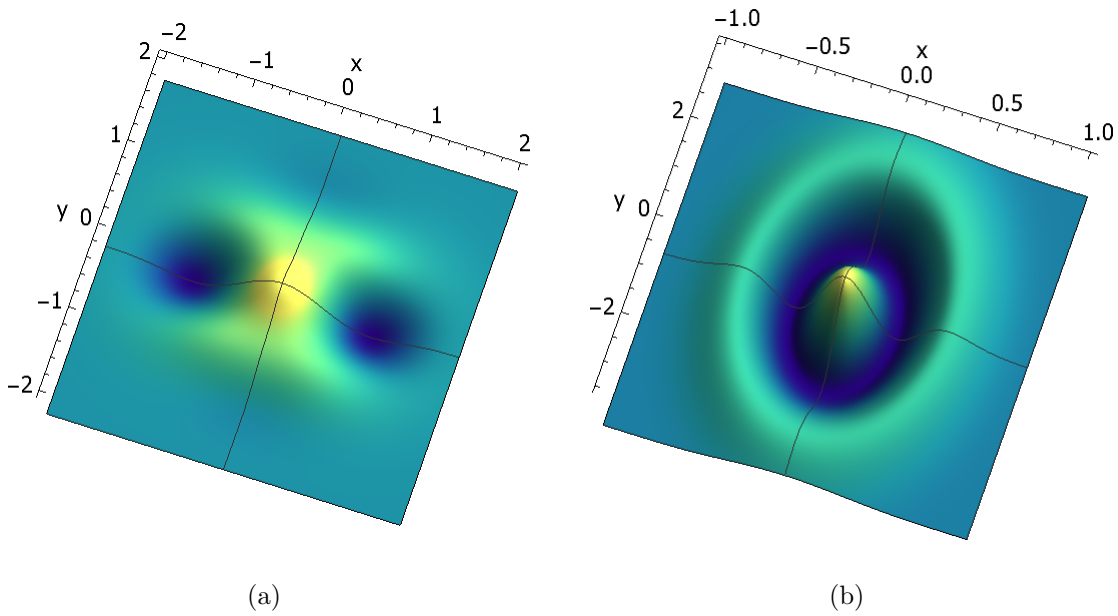

(a) (b)

Figure 2.9: Wigner functions for (a) the Schrödinger cat state $|\alpha\rangle + |-\alpha\rangle$ for $|\alpha| = 0.9$ and (b) the squeezed vacuum state $\hat{S}(\xi)|0\rangle$ for $\xi = 0.8$ following action of the orthogonaliser $\hat{O}_n$. Darker (blue) colours represent regions of negative probability while lighter (yellow) colours represent regions of higher probability. Here, x and y denote the position and momentum quadratures.

that the strategy is universal and a single adjustable parameter in the experimental setup is sufficient for achieving similar goals for any input pure state. To reaffirm this, we include theoretical examples of using the same operations to orthogonalise the Schrödinger cat state and the squeezed vacuum state. This means that, in principle we can use precisely the experimental scheme analysed in our work, but with different inputs.

Future work in this area naturally includes testing the system with different input states as well as extending it to larger intensity input fields. It would also be possible, outside of pure optics, to look at extensions of this general scheme to alternative physical systems including phononic states of trapped ions and nanomechanical oscillators [161]. Beyond these direct extensions, use of this method as a tool for quantum state engineering and using it to produce custom states is also feasible in the future. While we have demonstrated its applicability to small amplitude coherent states, by no means is this method limited to states of similar scale. Indeed, such a method could be applied to larger systems for use in the study of such foundational issues as tests of quantum-to-classical transition models [170].

2.4 Final remarks

This chapter has outlined two original models for producing a superposition of orthogonal states. The ability to generate such superpositions within continuous variable systems, which may then be used to form an orthogonal qubit basis, provides one approach for constructing a NOT gate – which is a fundamental component of information processing and is prohibited by quantum mechanics [159]. While the universal and arbitrary NOT gate is not possible in quantum mechanics, schemes such as the two presented here illustrate that it is possible to have a resource-efficient method for orthogonalising cv quantum states.

In the first analysis, we consider the generation of a superposition of a coherent state and an orthogonal state through conditional photon subtraction of a two-mode squeezed state. Choosing between either homodyne or heterodyne detection on one of the modes allows us to engineer either a superposition of a squeezed displaced state with an orthogonal state, or a displaced state with one of its orthogonal states, respectively. This work is limited by the difficulties of single-photon detection, as conditional photon subtraction with on-off APD detectors does not differentiate between single-photon subtraction and multi-photon subtraction. In the work as it is presented here, the non-Gaussian features of the output states are observed through the Wigner functions. However, future work could employ actual measures of non-Gaussianity to better qualify the output state. Such a measure is presented in Chapter 4.

The second analysis presents an experimentally-verified approach for producing an orthogonal state from a generic input. The two cases studied are the use of the creation operator $\hat{a}^\dagger$, and the photon number operator $\hat{n}$ acting on coherent states, Schrödinger cat states, and squeezed vacuum states. Experimental results are presented for the particular case of orthogonalising the input coherent states using both operators.

Chapter 3

Generating non-Gaussian states 2: multimode nonlinearity

3.1 The cubic resource state

The previous chapter on the generation of non-Gaussian states focused on superpositions of states with their orthogonal states, providing an additional entry in the catalogue of quantum states of light we can produce experimentally. This chapter presents another type of state to add to the catalogue, along with a method for extending the type of state presented to multiple modes. In particular, in the following work we illustrate the offline preparation of a non-Gaussian resource state, which can then be employed as a nonlinear gate on a generic quantum system. Specifically, the state is used as resource ancilla and mixed with an input of one's choice. Following detection of the ancilla with suitable feed-forward or post-selection, the characteristics of the ancilla state may be transferred to the input state. We therefore say that the state is used to enact a specific gate operation. This forms the backbone of the original results presented in this chapter, and is described in more detail later.

This approach to engineering quantum non-Gaussian states differs from the previous examples because, rather than a direct effort to generate the state, it focuses instead on nonlinear interactions. Understanding such interactions and their effect on the quantum state of the harmonic oscillator is imperative both for further development in the field of quantum optics as well as the long-standing goal of quantum information: universal quantum computation [14, 171]. Within quantum optics, nonlinear operations can be achieved probabilistically through interactions between the system and solid-state physical systems [172] and individual atoms or ions [173, 174], followed by discrete measurements. Combining this probabilistic approach with the method of introducing nonlinearity into a given system through a resource state an-

cilla, it is possible to use this approach for state processing procedures [94, 175, 176]. The non-Gaussian ancilla may then be mixed with the system through deterministic Gaussian operations and measurements. This limits the types of accessible systems, as while experiments that have demonstrated the fine control of cavity fields [177], trapped ions and circuit cavity electrodynamics do not currently allow the deterministic Gaussian operations and measurements necessary for deterministic implementation of high-order nonlinearities [94, 175, 176].

The work contained in the next few sections is motivated by the current research focus on the quantum cubic nonlinearity [175, 176, 178–181]. The cubic nonlinearity is of particular interest because it is possible to realise highly nonlinear quantum gates in a deterministic fashion through the concatenation of quadratic and cubic gates [182]. Furthermore, simple linear operations together with a single nonlinear operation are sufficient to construct arbitrary polynomial Hamiltonian transformations [14]. The cubic nonlinearity is described by the Hamiltonian

$$\hat{H} \propto \hat{x}^3. \tag{3.1}$$

This Hamiltonian is used to describe the so-called cubic phase state [175], which is written in its unnormalised form in terms of the position eigenstate

$$|\gamma\rangle = \int dx\ e^{i\gamma x^3}|x\rangle. \tag{3.2}$$

This state can serve as a resource for a cubic phase gate, written as $e^{i\gamma\hat{x}^3}$. Current experimental observations of such a nonlinearity, or states produced by it, are limited to approaches that approximate the cubic state to first order [176], as well as repeat-until-success type gates [183]. We focus on the former approach, as it forms the background to the work presented later in this chapter. This method was first proposed in [176], and was followed by a full experimental realisation in [184]. It should be noted that even the weak cubic interaction generates highly nonclassical states [178].

3.2 Deterministic gate operation

The primary motivation for generating such a nonlinear state – both in the single-mode case and in the two-mode case which forms the focus of the original work in this chapter – is to use the state as a nonlinear gate acting on a general system. Higher-order nonlinearity in cv systems has been studied, but almost exclusively in the single-mode case. In the next few sections we examine a deterministic multimode

nonlinear gate operation capable of acting on a generic cv system. The two-mode cubic Hamiltonian

$$\hat{H} \propto \hat{x}_1^2 \hat{x}_2 \tag{3.3}$$

is emulated using an approximation that truncates its expansion at first order. At this point, let us recall the result of [14]: an operation with Hamiltonian $i[\hat{A}, \hat{B}]$ may be approximatively implemented if one has access to Hamiltonians $\hat{A}$ and $\hat{B}$. This operation is engineered as quadratic in the interaction time t:

$$e^{i\hat{A}t} e^{i\hat{B}t} e^{-i\hat{A}t} e^{-i\hat{B}t} \approx e^{-[\hat{A},\hat{B}]t^2} + O(t^3). \tag{3.4}$$

The consequence of this is that we need not implement the unitary operation of the Hamiltonian we are interested in as it is sufficient to take only the quadratic approximation; for example, in the cubic case, it is sufficient to perform the operation

$$1 + i\chi\hat{x}^3 - \frac{\chi^2}{2}\hat{x}^6, \tag{3.5}$$

which is the lowest order expansion for which we can use the commutator method of Eq.(3.4). Since Eq.(3.5) is taken to be a valid approximation of the cubic state, we consider it as a best case scenario for the approximation. Unfortunately, since our goal is to generate an approximate form of the cubic state that can be tested experimentally, even the quadratic approximation requires too much fine tuning to successfully engineer at the current state of the art. As a result, we take the approximation one step further and truncate Eq.(3.5) at first order in χ, which is taken to be very small ($\mathcal{O}(10^{-2})$), following the work of [176]:

$$e^{i\chi\hat{x}^3} \approx 1 + i\chi\hat{x}^3. \tag{3.6}$$

This process is henceforth referred to as the weak approximation of the cubic state. Ideally, the cubic state is obtained by applying the non-truncated version of the cubic interaction Hamiltonian to an infinitely squeezed state. In keeping with the approximation, the weak cubic nonlinearity is approximated by [176]

$$\hat{S}(-r)(1 + i\chi\hat{x}^3)|0\rangle, \tag{3.7}$$

where r is the complex squeezing parameter. Since the squeezing operation does not affect the cubic behaviour of the state, in the further analysis of the cubic state as a

phase gate, the squeezing is ignored and we consider only the state

$$1 + i\chi\hat{x}^3|0\rangle = |0\rangle + i\chi\frac{3}{2\sqrt{2}}|1\rangle + i\chi\frac{\sqrt{3}}{2}|3\rangle. \tag{3.8}$$

This approximative state then acts as an ancilla for a nonlinear gate operation. It is coupled with the system states, and the nonlinearity is then imprinted on the target state through either a quantum non-demolition (QND) measurement [185] or feed-forward [92, 176]. The QND coupling

$$\hat{U}_{\text{QND}}(\lambda) = e^{i\lambda\hat{x}_1\hat{p}_2}, \tag{3.9}$$

where λ is a real-valued parameter, mixes the modes of the ancilla and system, while a probabilistic homodyne detection measurement (refer to Sec.2.2.3) ensures the nonlinear features of the ancilla are imprinted on the system. To illustrate, applying the operation of Eq.(3.9) to a position eigenstate $|x\rangle_1$ and the cubic state ancilla of Eq.(3.2), then performing homodyne detection represented by position basis state $|q\rangle_2$ on the ancilla, the resultant output is:

$$|\psi_{\text{out}}\rangle = {}_2\langle q|\hat{U}_{\text{QND}}|x\rangle_1|\gamma\rangle_2 \tag{3.10}$$

$$= e^{i\gamma(x+q)^3}|x\rangle_1. \tag{3.11}$$

It is then straightforward to write a quadratic (and therefore Gaussian) Hamiltonian [178]

$$\hat{H} = 3q\gamma(\hat{x}_1^2 + q\hat{x}_1 + \frac{q^2}{3}) \tag{3.12}$$

$$= e^{i(\gamma\hat{x}_1^3 - \gamma(\hat{x}_1+q)^3)}.$$

This transformation acts on Eq.(3.10) to yield precisely the cubic operation

$$e^{i\gamma\hat{x}_1^3}|x\rangle_1. \tag{3.13}$$

While the QND operation gives the desired result, much of this work is motivated to get results that may be achieved in a relatively straightforward manner experimentally. Since this is not the case with QND measurements despite experimental successes in cv quantum optics [186, 187], we seek a different approach. An alternative to using a QND coupling is to mix the system and ancilla with balanced beamsplitters, again accompanying this interaction with probabilistic homodyne detection, as illustrated in Fig.3.1. This is the gate operation considered in this work. Just like the QND

operation, this second method results in the nonlinearity being directly mapped to the system state. However, unlike the QND coupling, beamsplitting with homodyne detection introduces a level of squeezing into the system, which must be accounted for, or at least acknowledged, in the final result. The success of the gate operation is tested by choosing an appropriate target state that will serve to highlight whether the nonlinear features have been mapped as anticipated.

The nonlinearity is derived from the ancilla, which is prepared offline. The scheme for the preparation of this ancilla state as well as the method of extending the nonlinear features of the state to an additional mode are the subject of the next section. The discussion so far has focused on the single-mode cubic state, but it should be noted that the outcomes in terms of how the approximations are performed and how the measurements work are much the same for the two-mode case, which will become more central to the next discussion.

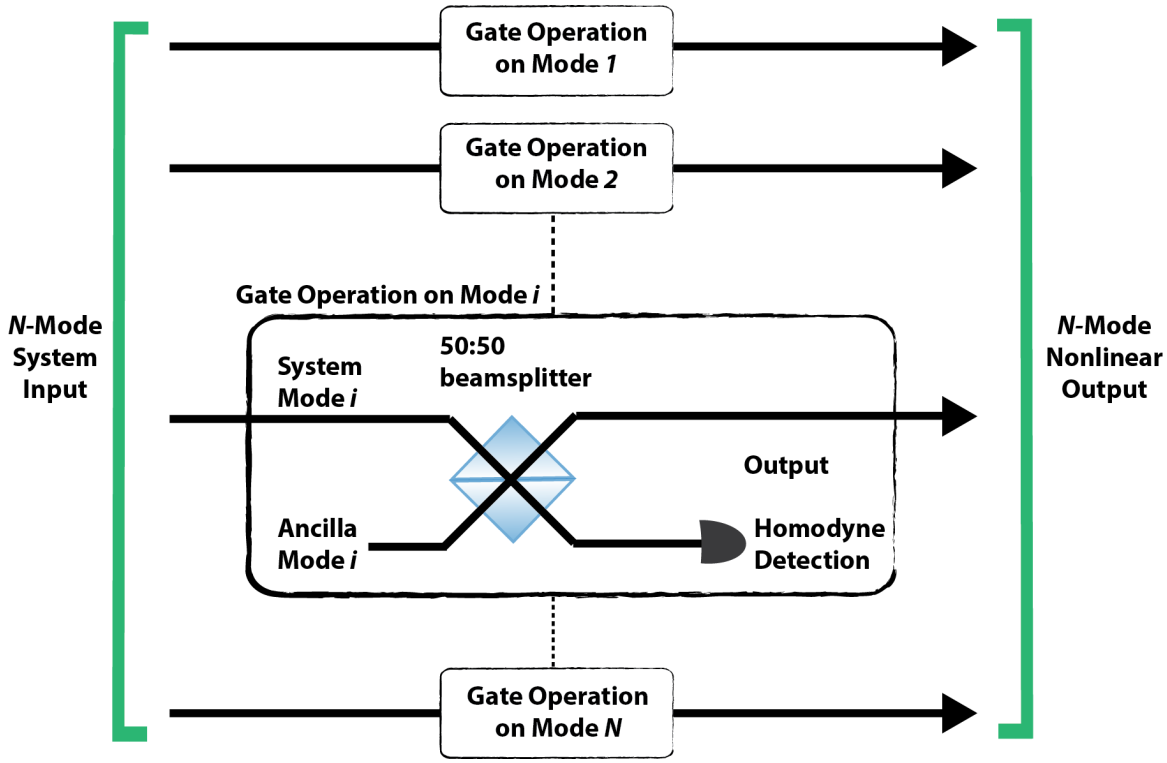

Figure 3.1: Scheme for the action of the gate operation for an N-mode system input. Each mode of the system is mixed on a balanced beamsplitter with the corresponding ancilla mode, which then undergoes homodyne detection. The outcome is either post-selected or fed-forward to the output state. The entire scheme effectively imprints the ancilla state features onto the system.

3.2.1 Realistic implementation

The key element of the gate described in the previous section is the ancilla, as it is this state that introduces the nonlinear features to the generic system. In this section we show how such an ancilla state is generated, notably for a two-mode state. The goal is to produce a state that simulates the ideal Hamiltonian $\hat{H} \propto \hat{x}_1^2\hat{x}_2$ in its first order approximation:

$$(1 + i\chi'\hat{x}_1^2\hat{x}_2)|00\rangle = |0\rangle_1|0\rangle_2 + \frac{i\chi'}{2\sqrt{2}}(|0\rangle_1 + \sqrt{2}|2\rangle_1)|1\rangle_2. \tag{3.14}$$

To create such a state experimentally, we propose beginning with an approximate form of the single mode cubic state, as described by Eq.(3.8). This resource state along with the single-photon Fock state acts as the input for the configuration that generates the two-mode cubic state. This initial two-mode state has the form:

$$|\psi\rangle_{1,2} = (1 + i\chi\hat{x}_1^3)|0\rangle_1|1\rangle_2. \tag{3.15}$$

This state acts as a highly nonlinear resource, upon which we perform conditional photon subtraction

$$\hat{O}_{1,2} = \hat{a}_1 + \gamma\hat{a}_2. \tag{3.16}$$

Here, as in its previous uses, $\hat{a}$ is the annihilation operator acting on either mode 1 or 2, and γ is a free, real-valued parameter. This operation yields a two-mode state where the order of the first mode is one less than the order of the original resource, with the second mode being of order 1. For example, in the case of the cubic state being used as a resource, the distribution works as:

$$\hat{x}_1^3 \to \hat{x}_1^2\hat{x}_2. \tag{3.17}$$

Implementation of the operation in Eq.(3.16) provides an accessible experimental approach to creating nonlinear multimode resource states. Furthermore, this resource state retains the features of the nonlinear state from which it was generated, allowing for a direct characterisation process. Application of the conditional photon subtraction operator $\hat{O}_{1,2}$ to $|\psi\rangle_{1,2}$ shows how the nonlinearity distribution scheme works, with the resulting state:

$$\hat{O}_{1,2}|\psi\rangle_{1,2} = \gamma|0\rangle_1|0\rangle_b + \frac{i3\chi}{2\sqrt{2}}(|0\rangle_1 + \sqrt{2}|2\rangle_1)|1\rangle_2 + \frac{i\chi\gamma}{2\sqrt{2}}(3|1\rangle_1 + \sqrt{6}|3\rangle_1)|0\rangle_2. \tag{3.18}$$

We then compare this superposition to the desired output state

$$(1 + i\chi' \hat{x}_1^2 \hat{x}_2)|00\rangle = |0\rangle_1|0\rangle_2 + \frac{i\chi'}{2\sqrt{2}}(|0\rangle_1 + \sqrt{2}|2\rangle_1)|1\rangle_2, \tag{3.19}$$

noting that the parameter χ' in Eq.(3.19) is equal to $3\frac{\chi}{\gamma}$ in Eq.(3.18) in order to have the superpositions equivalent up to some additional higher order terms. From these results, we can conclude that the conditional subtraction operation $\hat{O}_{1,2}$ effectively spreads the nonlinear features of the single-mode cubic state to a second mode. This operation is implemented experimentally in a setup described in Fig. 3.2.

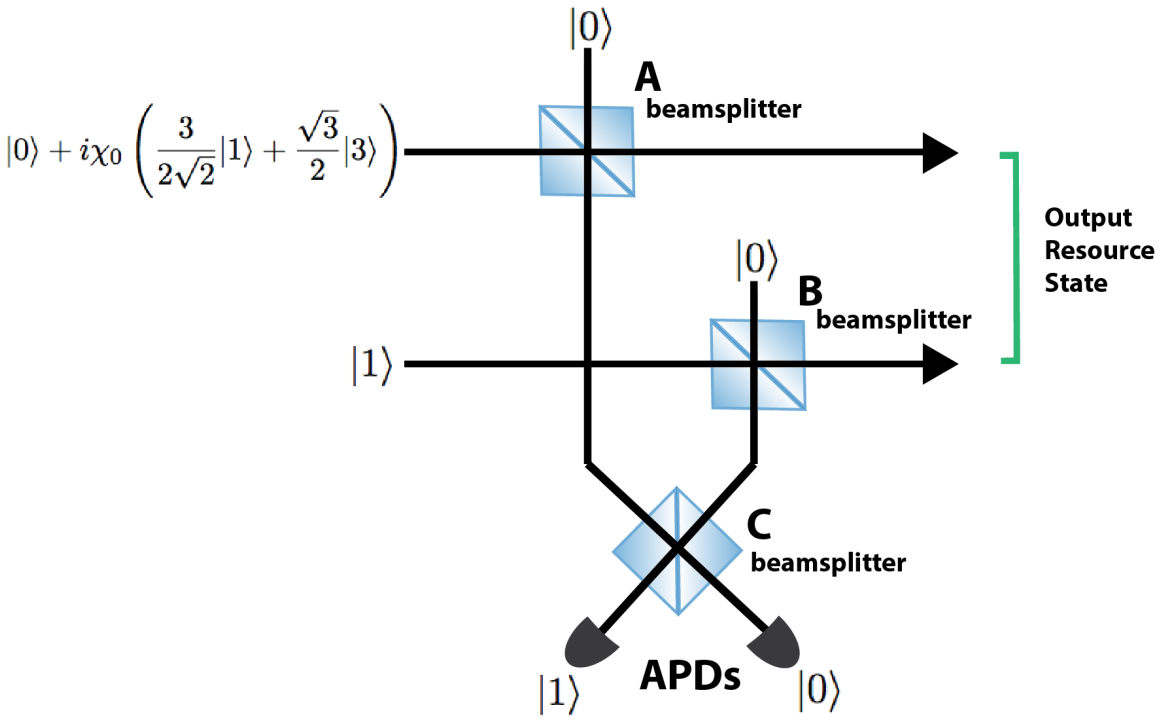

Figure 3.2: Optical setup for generating the two-mode resource state. The input states are the approximate cubic state and the single-photon state. These are put through high-transmissivity beamsplitters A and B, whose outputs are mixed across beamsplitter C before detection occurs. This action results in a conditional photon subtraction from the input modes. In the ideal case, single-photon detection happens following mixing at C, however calculations involving this scheme take into account the more common Avalanche Photo Diode (APD) detectors in order to show that the nonlinear features remain visible.

The conditional subtraction, as discussed previously in Sec. 2.2.1, is achieved via beamsplitting coupled with single-photon detection. In the case of Fig.3.2, this is accomplished through beamsplitters A and B, which are tuned to have transmissivity $t_A = t_B \approx 1$. At this extreme, the beamsplitter operator is effectively reduced to the photon annihilation operator $\hat{a}$ [70]. As a result the two beamsplitters A and

B produce the $\hat{a}_1$ and $\hat{a}_2$ components, respectively. The conditional action of these operators is the result of the beamsplitter C and the subsequent detection. By post-selecting on detection of a single photon at only one output from beamsplitter C, while the other output detects nothing, we are forcing the photon subtraction to occur at *either* beamsplitter A or B, but not both. In effect, we are erasing the photon pathway. The parameter γ in the operator $\hat{O}_{1,2}$ is a function of the transmissivity of beamsplitter C, and can be tuned to improve the quality of the output state.

To coincide with current experimental techniques, we consider the case where we use two APD detectors. The measurement operation on the two modes is therefore $(\mathbb{1} - |0\rangle\langle 0|) \otimes |0\rangle\langle 0|$ instead of $|1\rangle\langle 1| \otimes |0\rangle\langle 0|$, where $|0\rangle$ is the vacuum state and $|1\rangle$ the state with a single photon. With the weak cubic state of Eq.(3.15) as a resource, this scheme outputs the state in Eq.(3.18). The state produced by the setup of Fig. 3.2 contains extra terms due to the imperfections related to photon subtraction. Since the annihilation operator is not Hermitian, we instead use beamsplitters and detectors to emulate the operation. The transmissivity of beamsplitters A and B cannot be exactly 1 and therefore we do not implement the exact photon annihilation operation. The imperfect detection that is used to give a better understanding of whether this operation can be achieved experimentally means that more terms are kept in the expansion. Further, APD detection results in a mixed state output, which compounds the differences between the idealised and realistic cases. For ideal photon detectors, where a single photon is detected at one output and nothing at the other, the majority of the additional terms are eliminated, although the superposition is not reduced completely to the desired output due to the lack of perfect photon subtraction. In this scheme, we take the transmissivity of beamsplitters A and B to be 0.95, while beamsplitter C has a transmissivity of 0.99. The parameter χ of the input state is set at 0.09. We compare the ideal ancilla state from Eq.(3.19) (Fig. 3.3(a)) with the approximative ancilla generated using our setup of Fig.3.2 (Fig. 3.3(b)). In Fig. 3.3(a) we see that the vacuum term $|00\rangle\langle 00|$ dominates due to the approximation used. In the approximative version of the state, as shown in Fig.3.3(b), the nonlinear terms are still highly suppressed but may be amplified by a suitable choice of tunable parameters, notably the transmissivity of beamsplitter C.

3.3 Characterising the state

While we have proposed a novel method for generating a two-mode nonlinear state, it is not sufficient to abandon the analysis here. As the state is approximative, there exists some uncertainty as to whether the presence of the nonlinearity is verifiable, and we

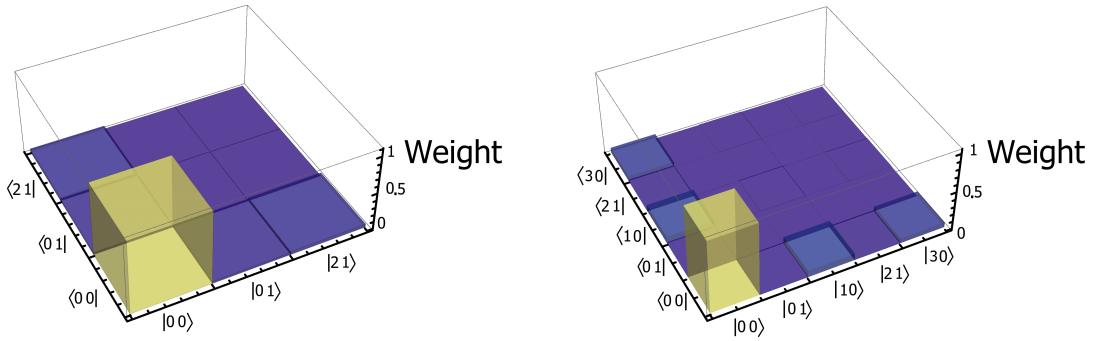

(a) (b)

Figure 3.3: (a) Histogram of elements of the density matrix for the ideal state $(\mathbb{1} + i\chi\hat{x}_1^2\hat{x}_2)|00\rangle$. (b) Histogram of density matrix elements of the two-mode state produced by Fig. 3.2. In both cases, only the nonzero density matrix elements are shown, with the magnitude of their coefficients corresponding to the height of the bars.

therefore consider three distinct methods of characterising the state. The first method directly analyses the output state of the setup in Fig. 3.2. The second and third methods are based on the proposed use of the state as a nonlinear gate, and tests the effectiveness of the operation by examining the nonlinear features of an output state following action of the gate on input coherent states. We will see that the desired nonlinear features of the state of Eq.(3.14) resulting from the weak approximation can actually be enhanced through the proposed state engineering scheme of Fig.3.2.

3.3.1 Direct characterisation

The first approach we employ to characterise the nonlinear state is to directly investigate the nonlinear features of the density matrix. In particular, we consider the density matrix in the coordinate representation,

$$\rho(x, x', x'', x''') = \langle x, x'|\rho|x'', x'''\rangle. \tag{3.20}$$

Inspecting the original form of the state, $(1+i\chi\hat{x}_1^2\hat{x}_2)|00\rangle$, it is clear that the imaginary components of the density matrix will be the ones to exhibit the nonlinearity we wish to observe. In fact, we expect the imaginary part to take the form of an exponentially suppressed cubic function in either mode, of form $x^3\mathrm{e}^{-x^2}$, illustrated in Fig. 3.4. In order to improve the visibility of the cubic features we set $x = x'$ and $x'' = -x'''$ in the calculation of Eq.(3.20). We then plot the imaginary part as a function of x, and in both the ideal (Fig.3.5(a)) and approximative (Fig.3.5(b)) cases, we see the expected cubic feature, although it should be noted that Fig. 3.5(a) is displaced and corresponds more precisely to a function of form $(\frac{1}{2}x - x^3)e^{-x^2}$. This is the first example where

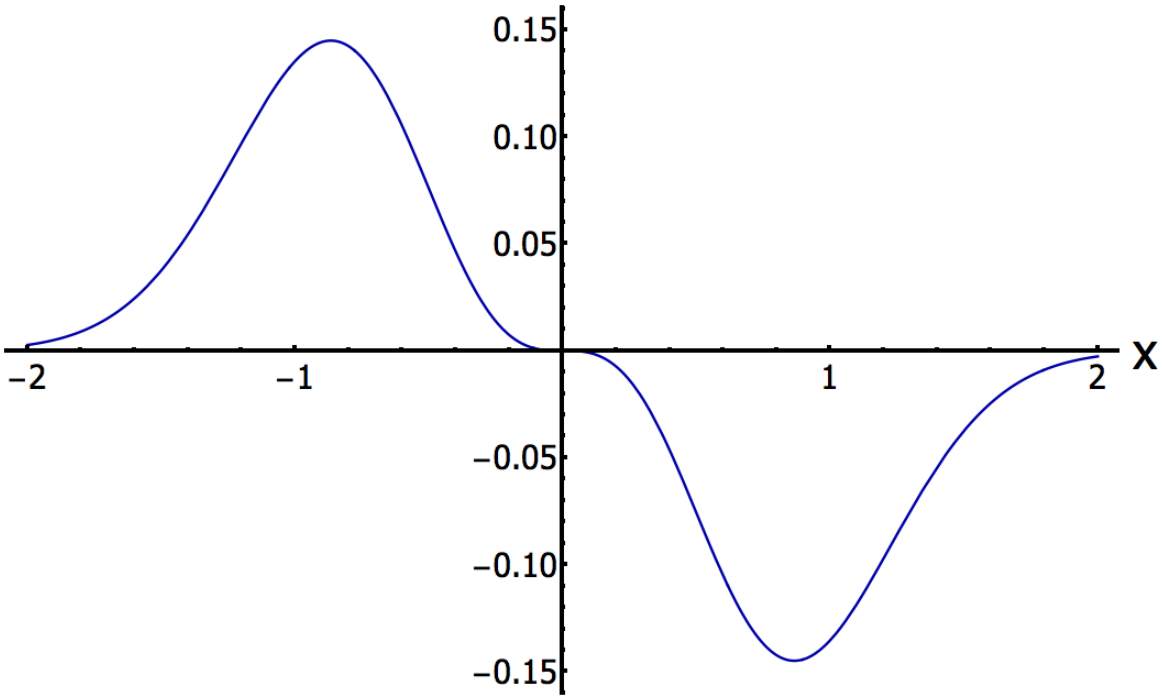

Figure 3.4: Plot of $f(x) = -x^3 e^{-x^2}$. This is what we expect to see when we plot the imaginary elements of the position representation of the density matrix for the state being considered in this chapter. This plot should be used as point of comparison for Figs. 3.5(a) and 3.5(b).

we can immediately note that the tunability of the engineered multimode state has actually allowed us to retrieve a state closer to the desired cubic state, while the ideal state in fact exhibits some displacement due to the weak approximation of Eq.(3.6).

3.3.2 Testing the phase gate

3.3.2.1 Moments

The second method of examining the resource state is to test its designated purpose as a phase gate by applying it to a two-mode coherent state $|\alpha\rangle|\beta\rangle$, where $0 \leq \alpha, \beta \leq 1$, as illustrated in Fig. 3.1. The gate is implemented by mixing the resource state ancilla and the input on balanced beamsplitters, then performing homodyne detection on the ancilla modes accompanied by either post-selection or feed-forward. For this analysis we use post-selection. This procedure results in an imprinting of the resource state on the input modes. A homodyne measurement of the quadratures of the output for the system modes can be used to determine the moments for position and momentum [188]. For the coherent state, these moments provide a straightforward way to determine whether the nonlinear ancilla has the expected form. In particular, the first moment of momentum for either mode of the input state is 0. The form of the first moment of

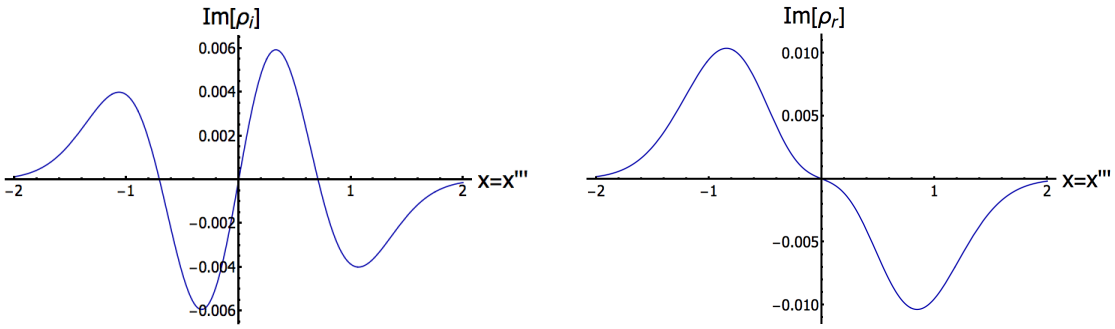

(a) (b)

Figure 3.5: (a) Plot of imaginary elements of the position representation of the density matrix ρ_i for the ideal state $(\mathbb{1} + i\chi\hat{x}_1^2\hat{x}_2)|00\rangle$. This plot exhibits a displacement which may be compensated in the case of the approximative resource state ρ_r. (b) Imaginary elements of the position representation of the density matrix for the approximative resource state ρ_r. The label x corresponds to those used to compute the density matrix, introduced in Eq.(3.20). These plots should be compared to that of Fig. 3.4, which is the ideal form assumed by the exact cubic state.

momentum for one mode can then be shown to be proportional to the second moment of the position of the other mode, up to some constant factor.

As we considered with the previous case, here we compare the operation with the ideal resource state with the approximative version. For the gate $e^{i\chi\hat{x}_1^2\hat{x}_2}$, we expect the relation

$$\langle p_2\rangle_{out} = \langle p_2\rangle_{in} + c\langle x_1^2\rangle_{in}, \tag{3.21}$$

where c is a real constant. This relationship is quickly seen by noting that, using the Baker-Campbell-Hausdorff formula [160],

$$e^{-i\chi\hat{x}_1^2\hat{x}_2}\hat{p}_2 e^{i\chi\hat{x}_1^2\hat{x}_2} = \hat{p}_2 + \chi\hat{x}_1^2. \tag{3.22}$$

As a result, for the coherent state input, we expect to see a quadratic relationship between the coherent state parameters and the moments. This calculation is then performed using the ideal and imperfect resource states as ancillas, mixing them with the coherent states using balanced beamsplitters and then performing homodyne detection on the ancilla modes. In Figs. 3.6(a) and 3.6(b) we compare the result of computing the moment $\langle p_2\rangle_{out}$ with $\langle p_2\rangle_{in} + c\langle x_1^2\rangle_{in}$. We see that in both the ideal and realistic cases both sides of Eq.(3.21) have the same form up to some displacement.

The displacement present in Fig. 3.6(a) is the result of the weak approximation performed in Eq.(3.6). Such a displacement exists in the realistic case as well, but due to the tunability of the photon subtraction operation it is possible to reduce the displacement of the final result. In both the ideal and realistic cases, the parameters

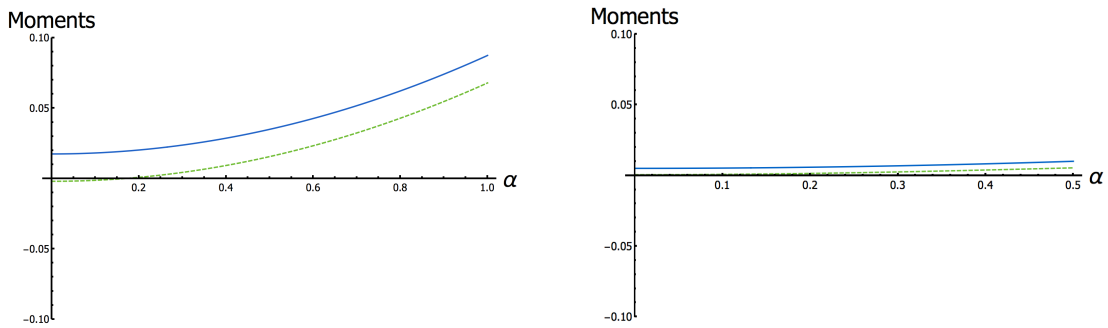

(a) (b)

Figure 3.6: A plot of the right and left-hand sides of Eq.(3.21), illustrating their proportionality, for (a) the ideal ancilla $(\mathbb{1} + i\chi\hat{x}_1^2\hat{x}_2)|00\rangle$, with $c = -0.035$ (b) the realistic case of imperfect photon subtraction with $c = -0.15$. In both cases the coherent state parameter β for the second mode is set to 0.The value of the first moment of the output momentum, $\langle p_2\rangle_{out}$ (green, dashed) and that of the input moments $\langle p_1\rangle_{in}+c\langle x_1^2\rangle_{in}$ (blue), is shown to be the same except for a displacement of ≈ 0.2, which is the result of the imperfect photon subtraction and detection operations performed in the scheme of Fig. 3.2
.

must be optimised in order to match both sides of Eq.(3.21), as a result, the two plots are not identical to each other.

3.3.2.2 Squeezing

As this is a two-mode state, we can take a similar approach and rather than analysing displacement, we look at squeezing of the quadratures of the output state following the nonlinear operation. If the variance of a given quadrature for one of the modes is less than $\frac{1}{2}$ then we say that mode is squeezed in that quadrature [160]. Further, the variances in the quadratures give insight into the nonlinear features of the output state, as we expect to witness nonlinear squeezing in a quadrature as a function of the amplitude of the input state in that mode, while the same squeezing would be linearly dependent on the amplitude of the other mode. We aim to quantify the squeezing of the output state following the application of the nonlinear gate to input coherent states $|\alpha\rangle_1|\beta\rangle_2$ for a range of values on the set $[0, 1]$ of α and β. The amount of squeezing is quantified by the smallest eigenvalue of the covariance matrix of the output state. We designate the smallest eigenvalue by the parameter $\lambda_i(\alpha, \beta)$, where i represents the mode for which the covariance matrix has been computed. Each of $\lambda_1(\alpha, 0)$, $\lambda_1(0, \beta)$, $\lambda_2(\alpha, 0)$, and $\lambda_2(0, \beta)$ are computed and plotted as the remaining coherent state parameter is varied from 0 to 1. This is illustrated in Figs. 3.7(a) and 3.7(b).

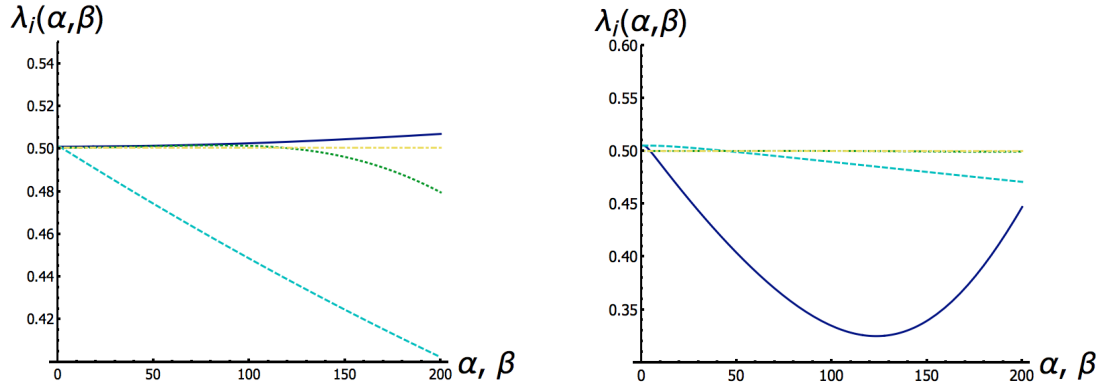

(a) (b)

Figure 3.7: A plot of the squeezing of the output state following the nonlinear gate operation for (a) the ideal case of $(\mathbb{1} + i\chi\hat{x}_1^2\hat{x}_2)|00\rangle$ and (b) the realistic case with imperfect photon subtraction. The squeezing is described by the smallest eigenvalue of the covariance matrix of the state, and labelled $\lambda_i(\alpha, \beta)$. Here we plot $\lambda_1(\alpha, 0)$ (dark blue, solid), $\lambda_1(0, \beta)$ (cyan, dashed), $\lambda_2(\alpha, 0)$ (green, dotted), and $\lambda_2(0, \beta)$ (yellow, dot-dashed). These eigenvalues are plotted against the free parameter α or β on the interval $[0, 1]$. The difference in these plots reinforces the observation that the approximate form of the state actually better emulates the desired outcome. We expect in the ideal case for squeezing to be exhibited in mode 1 as a function of α, illustrated by $\lambda_1(\alpha, 0) < 0.5$. The other eigenvalues are expected to not show significant deviation from the value 0.5. This is exactly what is observed in (b). In (a), we instead observe squeezing in mode 1 as a function of β. This occurs because the two modes are entangled and therefore while the squeezing in mode 1 as a function of α is too suppressed by the vacuum term to be witnessed, the corresponding entanglement to the mode 2 parameter β is still visible. Further explanation of this is contained in the accompanying text.

Just as we observed in the previous cases, the state generated through the scheme of Fig.3.2 actually better exhibits the desired nonlinear features than the so-called 'ideal' case. It is in this example that the difference is most visible – in fact, we notice that the expected squeezing in $\lambda_1(\alpha, 0)$ for the ideal case is not present at all, and instead we only witness squeezing in $\lambda_1(0, \beta)$. In the case of not witnessing squeezing in the desired mode, the argument falls back to the issue of the large vacuum contribution. In fact, the vacuum is approximately two orders of magnitude larger than either of the other terms in the superposition. As a result, in using a measure that relies fully on the two non-vacuum terms, we end up with a very poor characterisation of the state. The squeezing present in $\lambda_1(0, \beta)$ works as a better indicator of some nonlinearity being present, as it exists because of the entanglement between the two modes of the final state. As a result, while in Fig.3.7(a) we do not witness the desired squeezing, we can see that the two modes of the output state have been entangled. Turning to

Fig.3.7(b), however, we see exactly the desired outcome. We expect to see squeezing in $\lambda_1(\alpha, 0)$ as it is the mode containing the nonlinear superposition of $|0\rangle + |2\rangle$, and we do. This is directly the result of the ability to better tune the output state in order to enhance the nonlinear features.

3.4 Distributing nonlinearity across multiple modes

We have now presented a method for distributing the nonlinearity of the single-mode cubic state to a two-mode state. In fact, this scheme may be generalised further. In this section we illustrate the basic idea of spreading nonlinearity to additional modes. In particular, we show that conditional photon subtraction may be used to couple an additional mode to the original state by sharing the nonlinear features of the state with the new mode. In general the resource state for this operation may have an arbitrary number of modes, and is the result of applying the general operator

$$\hat{U}(\chi') = e^{i\chi' \prod_{i=1}^{M} \hat{x}_i^{j_i}} \tag{3.23}$$

to an infinitely squeezed state, where the exponents j_i are arbitrary positive integers, as is M. As in the cubic case illustrated earlier in this paper, this generalisation is achieved by approximating the higher order state as its first order expansion, taking the parameter χ' to be small:

$$\hat{U}(\chi') \approx \mathbb{1} + i\chi' \prod_{i=1}^{M} \hat{x}_i^{j_i}. \tag{3.24}$$

The operation used to distribute order-N nonlinearity to an additional mode is

$$\hat{a}_1^N + \gamma \hat{a}_2^N \tag{3.25}$$

where $\hat{a}_1$ and $\hat{a}_2$ are annihilation operators on modes 1 and 2, respectively. N is an arbitrary positive integer. The application of Eq.(3.25) to the two-mode state $(\mathbb{1} + i\chi'\hat{x}_1^M)\hat{x}_2^N|00\rangle$ will mix the initial states to produce the desired two-mode approximative state:

$$(\hat{a}_1^N + \gamma \hat{a}_2^N)(\mathbb{1} + i\chi'\hat{x}_1^M)\hat{x}_2^N|00\rangle_{1,2} = (\mathbb{1} + i\chi\hat{x}_1^{M-N}\hat{x}_2^N)|00\rangle_{1,2}. \tag{3.26}$$

This is best understood by noting that the annihilation operator product $\hat{a}^N$ commutes with the position operator with a constant remainder. Therefore, since this operation is applied to the vacuum, the net effect is for $\hat{a}^N$ to annihilate N position operators.

The result is a distribution of nonlinear features from the Hamiltonian $\hat{H}' \propto i\chi'\hat{x}^M$ to a two-mode Hamiltonian $\hat{H} \propto i\chi\hat{x}_1^{M-N}\hat{x}_2^N$.

The key component of this scheme is the operation Eq.(3.25). To demonstrate that this operator may be exactly produced by systematic application of conditional photon subtraction, we begin by defining conditional photon subtraction with a carefully chosen phase: $\hat{a}_1 + \gamma^{1/N}e^{i\phi_j}\hat{a}_2$. The tunable parameter γ has the same purpose as before. We focus on constraining the phase parameter ϕ_j. We claim it is possible to choose the phase ϕ_j such that

$$(\hat{a}_1 + \gamma^{1/N}e^{i\phi_j}\hat{a}_2)^N = \hat{a}_1^N + \gamma\hat{a}_2^N. \tag{3.27}$$

Suppose we choose ϕ_j to be evenly distributed between 0 and 2π, allowing us to write $\phi_j = j\frac{2\pi}{N}$. We now look at the expansion of the left hand side of Eq.(3.27):

$$(\hat{a}_1 + \gamma^{1/N}e^{i\phi_j}\hat{a}_2)^N = \sum_{k=0}^{N}\binom{N}{k}\hat{a}_1^{N-k}\hat{a}_2^k\gamma^{k/N}\left(\sum_{S_k}\prod_{j\in S_k}\mathrm{e}^{ij\frac{2\pi}{N}}\right). \tag{3.28}$$

In particular, we focus on the final summation in brackets, which we label z,

$$z = \sum_{S_k}\prod_{j\in S_k}\mathrm{e}^{ij\frac{2\pi}{N}}. \tag{3.29}$$

This term is equal to 1 when the binomial parameter $k = 0$, but for all other values of k we leave it in this general form. The notation S_k denotes all possible subsets of k elements from the set of integers $[1, N]$. In order for our claim in Eq.(3.27) to be true, we require that $z = 0$ for all values of k except 0 and N. At $k = 0$ we define $z = 1$ in order to satisfy the expansion, while at $k = N$ it can be shown with the use of trigonometric identities that $z = 1$. For $k \in [1, N-1]$, we observe that for each k, z is the sum of all possible products of $e^{ij\frac{2\pi}{N}}$. Furthermore, we note that for each k, the ϕ_j are evenly distributed and therefore the angle between consecutive ϕ_j is $\theta = k\frac{2\pi}{N}$. Since each z contains all possible subsets, rotating z by the phase $e^{i\theta}$ does not change z. Therefore, we conclude $z = 0$ must be true as it is the only solution to the equation $e^{i\theta}z = z$ for the given θ. We note that this is not the case for $k = 0, N$ since in these cases $e^{i\theta} = 1$ and we cannot draw a conclusion about the z. Thus Eq.(3.27) holds.

We have therefore shown that repeated, phase-controlled conditional photon subtraction is capable of generating highly nonlinear entangled two-mode states out of two nonlinear single-mode states. Nonlinear states of higher-than-cubic-order may be generated from the cubic state and lower order states, as discussed in Sec.3.2. Furthermore, additional modes may be incorporated into this state provided that the

conditional subtraction operation occurs between the weak approximation mode – that is, mode 1 in Eq.(3.26).

It is this generalisation of the scheme for distributing nonlinearity that provides the greatest incentive for further analysis. We studied the specific case of the two-mode Hamiltonian $\hat{H} \propto \hat{x}_1^2\hat{x}_2$, but the use of such an interaction for quantum information protocols remains an area requiring further analysis. However, with a scheme for distributing this nonlinearity beyond the two-mode case we can also consider the case where we use conditional photon subtraction to generate the three-mode state, which may be used to produce the Hamiltonian

$$\hat{H} \propto \hat{x}_1\hat{x}_2\hat{x}_3. \tag{3.30}$$

Such a balanced superposition of operators is already familiar in the two-mode case, where it can be used to generate a controlled-NOT (CNOT) gate operation in continuous variables [189]. In the three-mode case, this operation could be examined as a controlled-controlled-NOT gate. While the controlled-controlled-NOT gate can be generated from a combination of CNOT gates, the direct generation of such gate could provide a more resource-efficient approach.

3.5 Final remarks

In this chapter we have described in detail a model for generating multimode non-Gaussian states. Using conditional photon subtraction, we have found that the weak approximation of the cubic nonlinear state presented in [176] can be expanded to a two-mode state that exhibits the same cubic features. The basis of using a weak approximate version of the state was discussed, and it was shown that the weak cubic single-mode state acts as a good resource to generate the two-mode state. The generation of this two-mode state is presented both in the ideal case and through a more realistic experimental setup. It should be noted that even in the ideal case, there are additional higher-order terms present in the two-mode state, and as a result a consistent displacement is observed in the final state. As displacements can be compensated experimentally, and since it does not suppress the defining nonlinear features of the state, this is not a cause for concern.

The original component of this chapter, comprising the full presentation and analysis of the two-mode cubic state, represents a first step toward taking the cubic state and making use of its features to extend them across multiple modes. States of two or more modes are the basic requirement for testing entanglement in systems, and the

ability to generate non-Gaussian entangled states provides a fertile ground for further study in this area. Entanglement of non-Gaussian states remains a major research topic [190–194], and the ability of non-Gaussian operations to enhance entanglement has been experimentally demonstrated in the case of photon subtraction [25, 26, 195]. Such investigations provide strong motivation for future work with the particular state discussed above.

Finally, several limitations to this proposal should be acknowledged. The weak approximation itself introduces a dominant vacuum term in the cubic state expression, suppressing the key nonlinear features. While the analysis has shown that it is still possible to characterise the non-Gaussian state with this term present – meaning that the state is still useful for enacting the desired nonlinear gate – not all characterisation methods are practical. For example, any effort to test the fidelity of the output state from Fig.3.2 against the idealised weak approximation of the two-mode state would find that the output shares almost equally high fidelity with the vacuum state itself. It is for this reason that alternative approaches were used to characterise the output state and the effect of the phase gate operation. In addition, while it was shown that, in theory, multiple conditional photon subtraction operations can be used to engineer a multimode non-Gaussian state to arbitrary order in $\hat{x}$, there are restrictions in the practical application of such an operation. Specifically, even in the case of moving from one mode to two it was shown that additional terms in the superposition are generated. This problem is exacerbated with further applications of the subtraction operation and as a result the desired features of the state become increasingly suppressed.

Chapter 4

Characterising non-Gaussian states

4.1 Introduction to tests of non-Gaussianity

Up until this point, the discussion has centred on different methods of generating non-Gaussian states. It is insufficient, however, to claim that a particular type of state has been created without providing suitable witnesses to the defining feature of such a state. This recalls an original point of discussion within quantum mechanics – where is the boundary between the classical and the quantum? Indeed, the classification of quantum states according to classical/non-classical and Gaussian/non-Gaussian paradigms remains a major research focus within the field of quantum information. The bulk of the literature has focused on distinguishing non-classical states, either based on phase-space distributions [4, 5, 67, 196–204], ordered moments [42, 58, 205], or information-theoretic arguments [49, 206–213]. More extensive effort has gone toward characterising states with positive Wigner function [73, 214–217] as well as distinguishing Gaussian and non-Gaussian states [55, 61, 218]. These results include examining classes of states for which the Wigner function is negative [73, 214, 215], as well as utilising the negativity of the Wigner function as an operational resource for quantum computation [216, 217]. These measures have been used to characterise, for example, experimentally generated non-Gaussian states [38, 39, 219], although they fail to discriminate between states written as mixtures of Gaussian states and so-called quantum non-Gaussian (QNG) states.

In this chapter we will describe a proposal for identifying these QNG states based on bounding linear functionals. We begin with a more complete presentation of what it means for a state to be QNG as well as how to test for this feature, and then discuss how we can define certain functions of these states. We then proceed to define a set of functionals based on phase-space quasiprobability distributions and stipulate a set of criteria with which one may use the bounds of the functionals to identify QNG

states. To illustrate the use of these criteria, we consider three cases of known QNG states evolving in a lossy channel and show that not only could the criteria be used to identify QNG states, but also serves to quantify the amount of loss that can be tolerated in a channel before the QNG features of the input state may no longer be identified. Finally we estimate the error on the bounding functions to complete the examination of these QNG witnesses. This work has been published in [63].

4.2 Quantum non-Gaussianity

Distinguishing between non-Gaussian states and QNG states is an important pursuit, since QNG states may only be produced by means of highly nonlinear processes, while a number of non-Gaussian states can be generated from mixtures of Gaussian states. As a result, witnessing QNG can certify that processes such as Fock state generation, Kerr interaction, photon addition/subtraction operations, or conditional number detections have occurred [220]. Initial efforts to detect QNG were carried out in [60, 220] by deriving witnesses based on photon-number probabilities and the Wigner function, respectively. Already, the criterion [60] was used to detect QNG states produced in a variety of experimental settings [221–223].

In order to better define what it means for a state to be quantum non-Gaussian, we begin by defining the Gaussian convex hull

$$\mathcal{G} = \left\{ \rho \in \mathcal{B}(\mathcal{H}) \mid \rho = \int d\boldsymbol{\lambda}\, p(\boldsymbol{\lambda}) |\psi_G(\boldsymbol{\lambda})\rangle\langle\psi_G(\boldsymbol{\lambda})| \right\}, \tag{4.1}$$

where $p(\boldsymbol{\lambda})$ can be an arbitrary probability distribution, $|\psi_G(\boldsymbol{\lambda})\rangle$ are pure Gaussian states and $\mathcal{B}(\mathcal{H})$ is the set of bounded operators[1]. It is possible to parametrise all pure single-mode Gaussian states in terms of the displacement and squeezing operators as $|\psi_G(\boldsymbol{\lambda})\rangle = D(\alpha)S(\xi)|0\rangle$, where $|0\rangle$ is the vacuum state, α, ξ are arbitrary complex numbers and $\boldsymbol{\lambda} = \{\alpha, \xi\}$. While it might be clear that the set $\mathcal{G}$ contains pure as well as mixed Gaussian states, it is important to note that non-Gaussian states that are mixtures of Gaussian states, for example those states which are mixtures of squeezed and coherent states, are also contained with $\mathcal{G}$. Based on this, we can therefore define what it means for a state to be QNG: *a quantum state ρ is quantum non-Gaussian iff $\rho \notin \mathcal{G}$.*

The importance of QNG in the field of quantum optics can be illustrated with a simple example: consider preparing a single-mode field in the vacuum state. It may

[1] A bounded operator is any operator for which the spectrum of its eigenvalues is a closed, bounded and non-empty subset of the complex plane. [224]

easily be verified that states belonging to $\mathcal{G}$ can be prepared by applying a combination of Gaussian operations and classical randomisation, while, in order to prepare a QNG state $\rho \notin \mathcal{G}$ starting from a vacuum field, a non-Gaussian operation is imperative. Such operations include the application of Hamiltonian more than quadratic in the mode operators, or probabilistic non-Gaussian operations like photon addition and subtraction [70].

4.3 Quantum non-Gaussian witnesses in the phase space

Now that we have a definition for quantum non-Gaussianity and motivation for why we may be interested in classifying this particular set of states, we can look at a general approach to witnessing such states. Let us consider an experiment whose output is a single-oscillator quantum state ϱ. Suppose that the data collected from this experiment allows us to estimate two things: a quantity $\Phi[\varrho]$, where Φ is a *linear* functional on the space of quantum states, and a bound n on the average photon number, that is $\mathrm{Tr}\left[\varrho\hat{a}^\dagger\hat{a}\right] \leq n$. With this small amount of information about the state, it is possible to learn about the QNG character of ϱ. Consider the convex subsets of $\mathcal{G}$ for any $n \geq 0$:

$$\mathcal{G}_n \equiv \{\varrho_G \in \mathcal{G} | \mathsf{Tr}[\varrho_G\, \hat{a}^\dagger\hat{a}] \leq n\}. \tag{4.2}$$

On this set, we define the bound function

$$B(n) \equiv \min_{\varrho_G \in \mathcal{G}_n} \Phi[\varrho_G]. \tag{4.3}$$

To interpret this: $B(n)$ is the lowest possible value that $\Phi[\varrho]$ could take such that the assumptions

1. $\varrho \in \mathcal{G}$
2. $\mathrm{Tr}\left[\varrho\hat{a}^\dagger\hat{a}\right] \leq n$

are satisfied. It should be stated that, if we find the quantity $\Phi[\varrho]$ to be less than $B(n)$, the conclusion we must draw is that $\varrho \notin \mathcal{G}$. In contrast, finding $\Phi[\varrho] \geq B(n)$ must be interpreted as inconclusive. We define the bounding function as a minimum as a choice – it is equally possible to consider $B(n)$ to be the maximum of the set of linear functionals, which would then change the definition of the criteria presented later.

Establishing $B(n)$ as the bounding function indicates that the crucial step in determining the bound on the state will be calculating $B(n)$ for a given Φ. In general

this becomes an issue of linear optimisation over an infinite-dimensional parameter space, although this potential issue can be simplified by exploiting the properties of $B(n)$. It is sufficient to determine the constrained minimum of Φ among the set of pure Gaussian states as well as Rank-2 mixtures of Gaussian states. We therefore conclude that for a fixed Φ and n, it is enough to optimise over only a finite number of parameters in order to find $B(n)$. These results are derived in Appendix A.1.

We now move forward to show that the structure of the states in Eq.(4.1) implies nontrivial constraints on their associated quasiprobability distributions. Consequently we can use these constraints – and more specifically, their violation – to determine QNG. In the remainder of this chapter we focus on the use of generalised quasiprobability distributions as witnesses of QNG. We begin with the results of [220], which compute a bound for the Wigner function of a general quantum state ϱ belonging to the Gaussian convex hull:

$$W[\varrho](0) \geq \frac{2}{\pi} \exp\{-2n(1+n)\} , \qquad n = \mathrm{Tr}[\varrho a^\dagger a] . \tag{4.4}$$

We take this initial result and illustrate that bounds can be found for general s-parametrised quasiprobability distributions instead, and that this more general result can yield further information about a state. We write the generalised quasiprobability distribution as convolution of the Wigner function [225]. That is, for quantum state ϱ,

$$Q_s[\varrho](\alpha) = \frac{1}{\pi^2} \int d^2\xi \; \chi[\varrho](\xi, s) \mathrm{e}^{\alpha\xi^* - \alpha^*\xi}, \tag{4.5}$$

where $\chi[\varrho](\xi, s)$ is the s-ordered characteristic function

$$\chi[\varrho](\xi, s) = \mathrm{Tr}\, \varrho \hat{D}(\xi) \mathrm{e}^{s|\xi|^2/2}. \tag{4.6}$$

As discussed in Chap.1, the quasiprobability parameter s takes three standard values: $s = 1$ is the Glauber-Sudarshan P-function [4, 5], $s = 0$ is the Wigner function [67], and $s = -1$ is the Husimi Q-function [71]. In order to avoid problems associated with singularities in the quasiprobability distributions, we will require $s < 0$. Furthermore, while the bound may no longer contain some of the appealing properties of a quasiprobability distribution when $s < -1$, we do not exclude such a value in order to obtain some useful and experimentally-friendly QNG criteria. These criteria are the topic of the next section.

4.3.1 General QNG criteria

Following an introduction of the general process behind bounding linear functionals on the Gaussian convex hull, along with the fact that this concept has been applied to the Wigner function, we now establish a set of criteria for using generalised quasiprobability distributions to witness QNG. In order to formulate this problem in the language of Sec. 4.3, we first note that the general quasiprobability distribution $Q_s[\varrho](\alpha)$ is a linear functional of the state ϱ at fixed s and α. As a result, fixing a value of $s < 0$ and assuming $\mathrm{Tr}[\varrho \hat{a}^\dagger \hat{a}] \leq n$, we investigate whether the structure presented in Eq.(4.1) implies a non-trivial bound on possible values assumed by Q_s. To better relate the notions of Sec. 4.3 to the formalism of quasiprobability distributions, we define:

$$B_s(n) \equiv \min_{\varrho \in \mathcal{G}_n} Q_s[\varrho](0). \tag{4.7}$$

To clarify, we designate the function $B_s(n)$ to represent the minimum value that the general quasiprobability distribution Q_s takes over the set of states $\varrho \in \mathcal{G}_n$. In order to determine this bound, the parameter α must be fixed, and without loss of generality we choose $\alpha = 0$ throughout this analysis. Writing this bound is possible because for every $s < 0$, $B_s(n)$ is positive and convex. Furthermore, $B_s(n)$ is shown to be strictly decreasing in n, $B_s(n) \to 0$ as $n \to \infty$, and the minimising state in $\mathcal{G}_n$ has an average photon number exactly equal to n, which is shown in full detail in Appendix A.2. Since the functions B_s are therefore non-trivial, we exploit them to formulate a set of criteria we can use to witness QNG.

Criterion 1: For a quantum state ϱ, define the QNG witness

$$\Delta_s^{(a)}[\varrho] = Q_s[\varrho](0) - B_s(\bar{n}) \tag{4.8}$$

where $\mathrm{Tr}[\varrho a^\dagger a] \leq \bar{n}$. Then,

$$\Delta_s^{(a)}[\varrho] < 0 \implies \varrho \notin \mathcal{G}, \tag{4.9}$$

that is, ϱ is quantum non-Gaussian.

Criterion 2: Consider now a quantum state ϱ and a Gaussian map $\mathcal{E}_G$, or a convex mixture of such maps. Define:

$$\Delta_s^{(b)}[\varrho, \mathcal{E}_G] = Q_s[\mathcal{E}_G(\varrho)](0) - B_s(\bar{n}_{\mathcal{E}}) \tag{4.10}$$

where $\mathrm{Tr}[\mathcal{E}_G(\varrho) a^\dagger a] \leq \bar{n}_{\mathcal{E}}$. Then,

$$\exists\ \mathcal{E}_G \text{ s.t. } \Delta_s^{(b)}[\varrho, \mathcal{E}_G] < 0 \implies \varrho \notin \mathcal{G}. \tag{4.11}$$

We now review the proof for these criteria in the case of the Wigner function Q_0. A proof for the general quasiprobability distribution Q_s was not possible analytically by us, however the methodology holds for other values of s provided the functions do not exhibit any discontinuous behaviour. The full details of these proofs is provided in [220].

Lemma 1: For a pure single-mode Gaussian state $|\psi_G\rangle$, the value of the Wigner function at the origin of phase space is bounded from below according to

$$Q_0[|\psi_G\rangle\langle\psi_G|](0) \geq \frac{2}{\pi} e^{-2n(1+n)}, \tag{4.12}$$

where $n = \langle\psi_G|\hat{n}|\psi_G\rangle$.

Outline of Proof. We write the generic pure single-mode Gaussian state as $|\psi_G\rangle = \hat{D}(\alpha)\hat{S}(\xi)|0\rangle$, for $\alpha = |\alpha|e^{i\theta}$, $\xi = re^{i\phi} \in \mathbb{C}$ and $r > 0$. The Wigner function at the origin can therefore be written as

$$Q_0[|\psi_G\rangle\langle\psi_G|](0) = \frac{2}{\pi} e^{-2|\alpha|^2[\cosh 2r - \cos(2\theta+\phi)\sinh 2r]}. \tag{4.13}$$

Minimising the value of the Wigner function therefore corresponds to maximising the function

$$g(\alpha, \xi) = 2|\alpha|^2[\cosh 2r - \cos(2\theta + \phi)\sinh 2r]. \tag{4.14}$$

Maximising first by choosing phases such that $2\theta + \phi = \pi + 2k\pi$ ($k \in \mathbb{N}$), we then introduce the displacement and squeezing photon numbers $n_d = |\alpha|^2$ and $n_s = \sinh^2 r$, which obey $n = n_d + n_s$. This allows us to write the function $g(\alpha, \xi)$ as

$$g(\alpha, \xi) \leq 2(n - n_s)[2n_s + 1 + 2\sqrt{n_s(1 + n_s)}]. \tag{4.15}$$

For a given mean photon number n, then, this expression can be maximised with respect to the squeezed photon number n_s:

$$n_s = \frac{n^2}{1 + 2n}, \tag{4.16}$$

giving

$$g(\alpha, \xi) \leq 2n(1 + n), \tag{4.17}$$

which yields the Wigner function bound

$$Q_0[|\psi_G\rangle\langle\psi_G|] \geq \frac{2}{\pi} e^{-2n(1+n)}. \tag{4.18}$$

■

This bound is then generalised for generic mixture of Gaussian states.

Proposition 1: For any single-mode quantum state ϱ belonging to the Gaussian convex hull $\mathcal{G}$ of Eq.(4.1), the lower bound of the Wigner function at the origin is

$$Q_0[\varrho](0) \geq \frac{2}{\pi} e^{-2\bar{n}(1+\bar{n})}, \tag{4.19}$$

where $\bar{n} = \mathrm{Tr}[\varrho \hat{n}]$.

Outline of Proof. Define an index λ, containing information on displacement α and squeezing ξ, to label every Gaussian state in the convex mixture $|\psi_G(\lambda)\rangle = \hat{D}(\alpha)\hat{S}(\xi)|0\rangle$. It is then equivalent to consider the index in terms of variables $\lambda = \{n, n_s, \theta, \phi\}$. We can then exploit the linearity of the Wigner function and the result of Eq.(4.18) to write

$$\begin{aligned} Q_0[\varrho](0) &= \int d\lambda p(\lambda) Q_0[|\psi_G(\lambda)\rangle\langle\psi_G(\lambda)|](0) \\ &\geq \frac{2}{\pi} \int d\lambda p(\lambda) e^{-2n(1+n)}. \end{aligned} \tag{4.20}$$

We then define a probability distribution with respect to variable n:

$$p'(n) = \int_0^n dn_s \int_0^{2\pi} d\phi \int_0^{2\pi} d\theta \; p(\lambda), \tag{4.21}$$

which allows us to rewrite the Wigner function as

$$Q_0[\varrho](0) \geq \frac{2}{\pi} \int_0^\infty dn \; p'(n) e^{-2n(1+n)}. \tag{4.22}$$

We then define the function

$$B_{\min}(n) = \frac{2}{\pi} e^{-2n(1+n)}, \tag{4.23}$$

which we, through studying the second derivative, determine to be convex for $n \geq 0$. Consequently,

$$\int_0^\infty dn \; p'(n) B_{\min}(n) \geq B_{\min}\left[\int_0^\infty dn \; p'(n) n\right] = B_{\min}(\bar{n}), \tag{4.24}$$

since we can write $\bar{n} = \int_0^\infty dn \; p'(n) n = \mathrm{Tr}[\varrho \hat{n}]$. This last inequality gives us directly the desired result:

$$Q_0[\varrho](0) \geq \frac{2}{\pi} e^{-2\bar{n}(1+\bar{n})}. \tag{4.25}$$

■

This result provides the motivation for writing Criterion 1. We can extend this result in order to justify Criterion 2 as well by considering the state evolving under a Gaussian map $\mathcal{E}_G$.

Proposition 2: For a single-mode quantum state $\varrho \in \mathcal{G}$ and any given Gaussian map $\mathcal{E}_G$, or a convex mixture thereof, the following holds:

$$Q_0[\mathcal{E}_G(\varrho)] \geq \frac{2}{\pi} e^{-2\bar{n}_{\mathcal{E}}(1+\bar{n}_{\mathcal{E}})}, \tag{4.26}$$

where $\bar{n}_{\mathcal{E}} = \mathrm{Tr}[\mathcal{E}_G(\varrho)\hat{n}]$.

Outline of Proof. For a quantum state ϱ that can be written as a mixture of a Gaussian state and a Gaussian map $\mathcal{E}_G$ (or a convex mixture thereof), the output can also be written as a mixture of Gaussian states:

$$\varrho' = \mathcal{E}_G(\varrho). \tag{4.27}$$

As a result, we can exactly substitute ϱ' for the state in the result of Proposition 1. ■

To reiterate, we note that for both criteria the proof follows much the same structure, since the difference between the two is that a Gaussian map $\mathcal{E}_G$ has been applied to the state in Eq.(4.11). This changes the mean photon number, but has no impact on the actual procedure for determining the bound. It is noted, however, that the monotonicity of B_s implies that it becomes more difficult to satisfy the criteria as $\bar{n}$ and $\bar{n}_{\mathcal{E}}$ are increased, since both $\Delta_s^{(a)}$ and $\Delta_s^{(b)}$ would correspondingly increase. As a consequence of this, we apply these witnesses for $\mathrm{Tr}[\varrho a^\dagger a] = \bar{n}$ and $\mathrm{Tr}[\mathcal{E}_G(\varrho)a^\dagger a] = \bar{n}_{\mathcal{E}}$ for the remainder of this chapter in order to improve our chances of detecting QNG. Alternatively, within the experimental context it may be more practical to estimate an upper bound to the average photon number, as opposed to determining its precise value. It is therefore important to note that these criteria provide sufficient but not necessary bounds, although the determined bound is still valid.

4.3.2 Near-optimality of pure states

We will now take a moment to discuss some of the implications of this optimisation. As mentioned in Sec.4.3, we are able to restrict the optimisation of Eq.(4.7) to Rank-1 (meaning pure) and Rank-2 mixtures of Gaussian states. Despite this more open restriction, we have found strong numerical evidence that the minimum is reached by the pure Gaussian state. In fact, we have proven the so-called near-optimality of pure Gaussian states for the various s-values of interest using a semi-analytical

approach whose details are contained in Appendix A.3. A pure state lower bound to each quasiprobability distribution can be defined as

$$B_s^P(n) \equiv \min_{|\psi_G\rangle} \left\{ Q_s[|\psi_G\rangle\langle\psi_G|](0) \mid \langle\psi_G|a^\dagger a|\psi_G\rangle \leq n \right\}, \tag{4.28}$$

where the $|\psi_G\rangle$s are pure Gaussian states. It is obvious that the bound of Eq.(4.28) is easier to compute than that of Eq.(4.7), however $B_s^P(n) \geq B_s(n)$, since we can not exclude that the minimum may be reached by a Rank-2 state. Nevertheless, our numerical studies for the cases $s = \{-1/4, -1/2, -1, -2, -3\}$ provide the bound

$$\left| B_s^P(n) - B_s(n) \right| \lesssim n \cdot 10^{-15}, \tag{4.29}$$

meaning that, for a wide range of average photon numbers, the pure state lower bound $B_s^P(n)$ is an excellent approximation to the true bound $B_s(n)$. Direct calculations related to this bound are given in more detail in Appendix A.4. The level of approximation provided by Eq.(4.29) is sufficient to guarantee the validity of our findings in the following sections.

4.4 QNG of states in a lossy channel

Now that we have discussed in some detail how we are able to establish a bound on QNG states, we can move forward to testing the effectiveness of our QNG criteria introduced in Sec.4.3.1. Specifically, we will investigate the performance of these criteria in certifying that pure non-Gaussian states evolving in a lossy channel remain quantum non-Gaussian.

The master equation [226] described the evolution of pure non-Gaussian states evolving in a lossy bosonic channel is

$$\dot{\varrho} = \frac{\gamma}{2}(\hat{a}\varrho\hat{a}^\dagger - \hat{a}^\dagger\hat{a}\varrho) + h.c. \tag{4.30}$$

The quantum channel $\mathcal{E}_\epsilon$ corresponding to this is Gaussian, and may be characterised by a single parameter $\epsilon = 1 - e^{-\gamma t}$. It is this parameter that we need to maximise in order to test the violation of the QNG criteria. To better quantify this violation, we define

$$\epsilon_s^{(a)}[\varrho] = \max\{\epsilon \ : \Delta_s^{(a)}[\mathcal{E}_\epsilon(\varrho)] \leq 0\}, \tag{4.31}$$

$$\epsilon_s^{(b)}[\varrho] = \max\{\epsilon \ : \exists \mathcal{E}_\mathsf{G} \text{ s.t. } \Delta_s^{(b)}[\mathcal{E}_\epsilon(\varrho), \mathcal{E}_\mathsf{G}] \leq 0\}, \tag{4.32}$$

the maximum values of the parameter for which the QNG criteria of Eqs.(4.9) and (4.11) are violated.

We note here that for $\epsilon > \frac{1}{2}$, no negativity of the Wigner function may be observed. Therefore we investigate values of $\epsilon_s^{(a)}$ and $\epsilon_s^{(b)}$ larger than this in order to determine whether the criteria are able to detect QNG states with positive Wigner function.

In the next three sections we will examine three distinct cases of quantum non-Gaussian states evolving in a lossy channel: the Fock state [160], the photon-added coherent (PAC) state [35, 36], and the photon-subtracted squeezed (PSS) state [227]. In each case, we are seeking to optimise our ability to witness QNG. As a result, in the Fock state case it is sufficient to employ only the first criteria (Eq.(4.9)), comparing the witnesses $\Delta_s^{(a)}$ for different initial Fock states. For the PAC and PSS states, we look at both witnesses $\Delta_s^{(a)}$ and $\Delta_s^{(b)}$. We consider three values of the parameter s for $\Delta_s^{(a)}$: the special cases $s = 0$, $s = -1$ corresponding respectively to the Wigner and Husimi-Q functions, and adding a third case at $s = -2$. We evaluate the quasiprobability distributions at the origin of phase-space:

$$Q_s[\varrho](0) = \frac{2}{\pi(1-s)} \sum_m (-1)^m \left(\frac{1+s}{1-s}\right)^m \langle m|\varrho|m\rangle \, . \tag{4.33}$$

We take a moment now to discuss the feasibility of measuring such states. This expression depends only on the photon-number probabilities $p_m = \langle m|\varrho|m\rangle$. Consequently, it may be measured experimentally using photon-number resolving detectors. Even more interestingly, the Wigner function at the origin corresponds to the average value of the parity operator $\Pi = (-)^{a^\dagger a}$, while the Husimi Q-function at the origin is the projection over the vacuum state $Q_{-1}[\varrho](0) = \langle 0|\varrho|0\rangle$, which may be measured using an APD on-off detector, a photon-number resolving detector, or through heterodyne detection [228]. If we instead consider values of $s < -1$, we see that that $Q_s[\varrho](\alpha)$ corresponds to the rescaled heterodyne probability distribution, obtained by means of detectors with efficiency $\eta = 2/(1-s)$, such that for $s = -2$ we have $\eta = 2/3$ [229].

Examining the parameter characterising the lossy channel, ϵ, more carefully, we see it also has a physical interpretation. While it is supposed to be unknown, and our stated goal in this work is to identify only the maximum value of noise such that our criteria are still able to detect QNG states, the inefficiency of the detector is in fact known to the experimentalist since it may be determined by probing the detector with known states. As a result, considering different values of s is equivalent to detecting QNG of unknown states evolving in a lossy channel, where each s corresponds to a different choice of detector. This is illustrated in Fig.4.1.

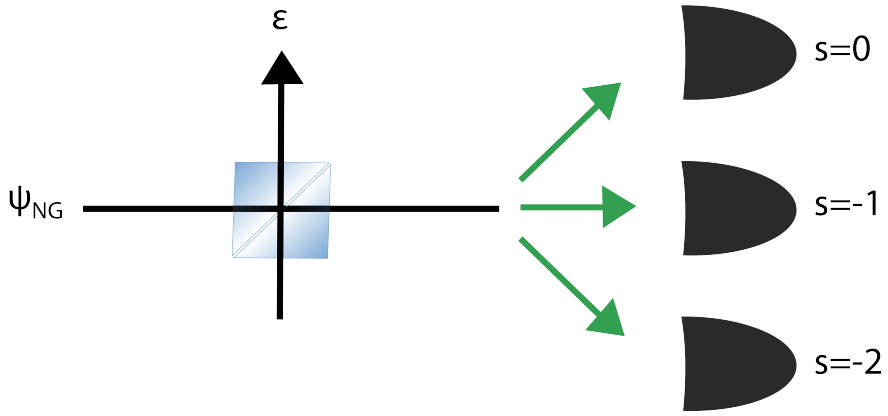

Figure 4.1: We send a non-Gaussian state through a channel with loss ϵ and choose the detector with which to measure it. The $s = 0$ detector correspond to parity measurement, $s = -1$ to the probability of vacuum detection, while $s = -2$ corresponds to an inefficient vacuum detection with efficiency $\eta = 2/3$.

With respect to the examination of $\Delta_s^{(b)}$, we focus on the special cases of $s = 0$ and $s = -1$. In both cases we discover that the witnesses derived for small values of s show a larger robustness against loss, and that this is particularly true in the low energy regime.

4.4.1 Fock States

The first state we consider is the Fock state $|m\rangle$ [160], which evolves in a lossy channel as

$$\mathcal{E}_\epsilon(|m\rangle\langle m|) = \sum_{l=0}^{m} \binom{m}{l} (1-\epsilon)^l \epsilon^{m-l} |l\rangle\langle l| \,. \tag{4.34}$$

We compute the corresponding s-parametrised quasiprobability distribution at the origin using the formula for a generic Fock state

$$Q_s[|m\rangle\langle m|](0) = \frac{2}{\pi(1-s)} (-1)^m \left(\frac{1+s}{1-s}\right)^m \,. \tag{4.35}$$

Using this result, we calculate the values of the witnesses $\Delta_s^{(a)}$ as well as maximum values of the noise parameter $\epsilon_s^{(a)}$ for which the bounds are violated. These values are plotted in Fig. 4.2 as a function of the Fock number m and for different values of the s parameter. It is somewhat surprising to observe that the witnesses seem to increase in sensitivity as s decreases (becomes more negative), meaning they provide a larger value of $\epsilon_s^{(a)}$ in the relevant range $m \leq 5$. With some thought, however, this can be explained by examining Figs. 4.3(a) and 4.3(b). The pertinent information in

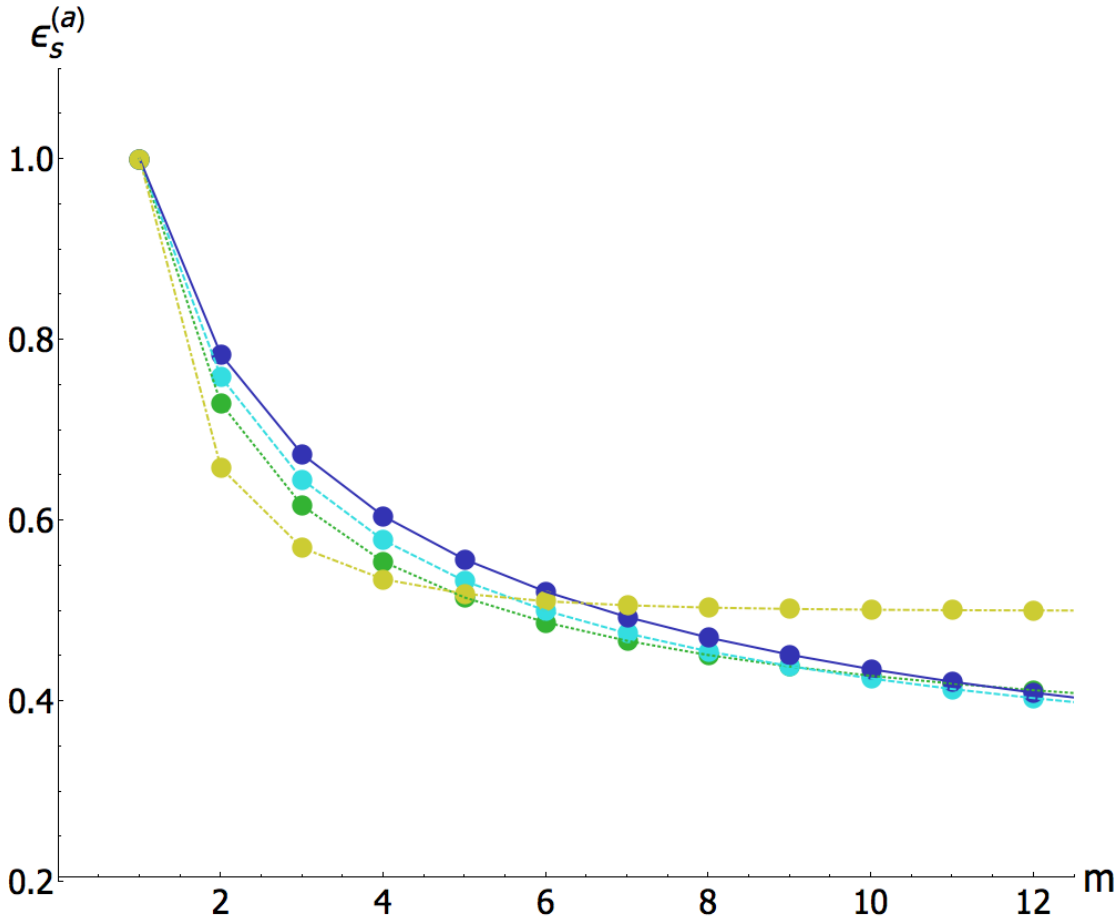

Figure 4.2: Maximum value of the loss parameter $\epsilon_s^{(a)}$ such that the bounds are violated, as a function of the initial Fock number m and for different values of s: yellow (dot-dashed), $s = 0$; green (dotted), $s = -1/2$; cyan (dashed), $s = -1$; blue (solid), $s = -2$.

these plots is where the curves cross the horizontal axis as this indicates the value of ϵ for which the bound is violated. Consequently, this value of ϵ corresponds to the maximum value of the noise parameter as plotted in Fig. 4.2. In order to understand the apparent increase in sensitivity of the witnesses for smaller values of s, we then examine the magnitude of $\Delta_s^{(a)}$ in Figs. 4.3(a) and 4.3(b). We immediately notice a tradeoff in the behaviour of the witnesses $\Delta_s^{(a)}$ for the Fock state $|1\rangle$ in Fig. 4.3(a). We can observe that the absolute value of $\Delta_s^{(a)}$ is decreasing with decreasing values of s. This monotonic behaviour is lost for the Fock state $|3\rangle$ (see Fig. 4.3(b)), for higher Fock states we can draw similar conclusions. What this means is that, while in principle one is able to detect QNG for larger values of the noise parameter by decreasing s, the amount of violation quantified by the witness $\Delta_s^{(a)}$ may be generally smaller. The impact of this tradeoff on an experimental effort to detect QNG cannot be assessed without a thorough analysis of the propagation of experimental errors for

the various witnesses. A preliminary effort at such error analysis is illustrated later, in Sec. 4.5.

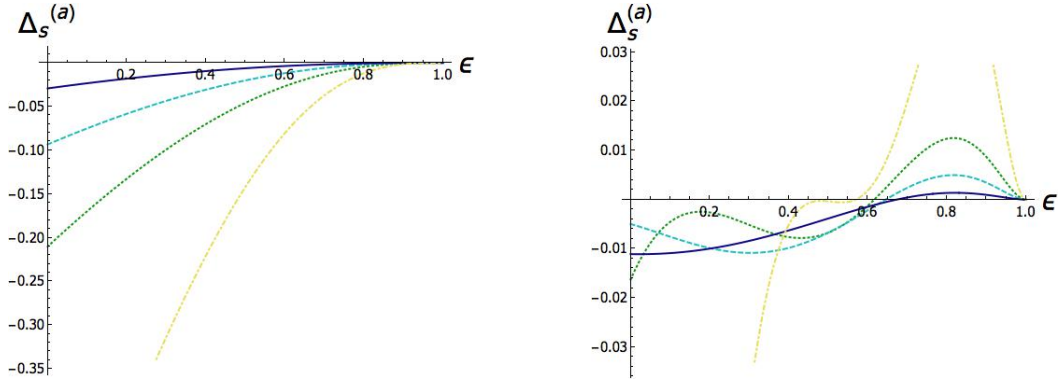

(a) (b)

Figure 4.3: QNG witnesses $\Delta_s^{(a)}$ for initial Fock states (a) $|1\rangle$ and (b) $|3\rangle$ as a function of the lossy parameter ϵ and for different values of s: yellow (dot-dashed), $s = 0$; green (dotted), $s = -1/2$; cyan (dashed), $s = -1$; blue (solid), $s = -2$. We are interested in where these curves first intersect with the horizontal axis, as it indicates the maximum value of the noise parameter ϵ for which we can detect QNG using the proposed witnesses. Furthermore, the magnitude of the parameter $\Delta_s^{(a)}$ indicates the amount of QNG we are witnessing. As a result, we are only interested in the behaviour of the plots near and below the horizontal axis.

4.4.2 Photon-added Coherent States

The next initial quantum non-Gaussian state we examine is the PAC state [35, 36], defined as

$$|\psi_{\text{PAC}}\rangle = \mathcal{N}\hat{a}^\dagger|\alpha\rangle, \tag{4.36}$$

where $\mathcal{N}$ is the normalisation factor. Its average photon number is

$$\bar{n}_0^{\text{PAC}} = \frac{\alpha^4 + 3\alpha^2 + 1}{1 + \alpha^2}, \tag{4.37}$$

for $\alpha \in \mathbb{R}$. The s-parametrised quasiprobability distributions are determined using the convolution expression presented in [225]:

$$Q_{s'}[\varrho](\alpha) = \frac{2}{\pi(s - s')} \int d^2\beta \; Q_s[\varrho](\beta) \; \mathrm{e}^{-\frac{2|\alpha-\beta|^2}{(s-s')}}, \tag{4.38}$$

where this expression is valid for $s' < s$. It is from this expression that we then compute the values of the witnesses $\Delta_s^{(a)}$.

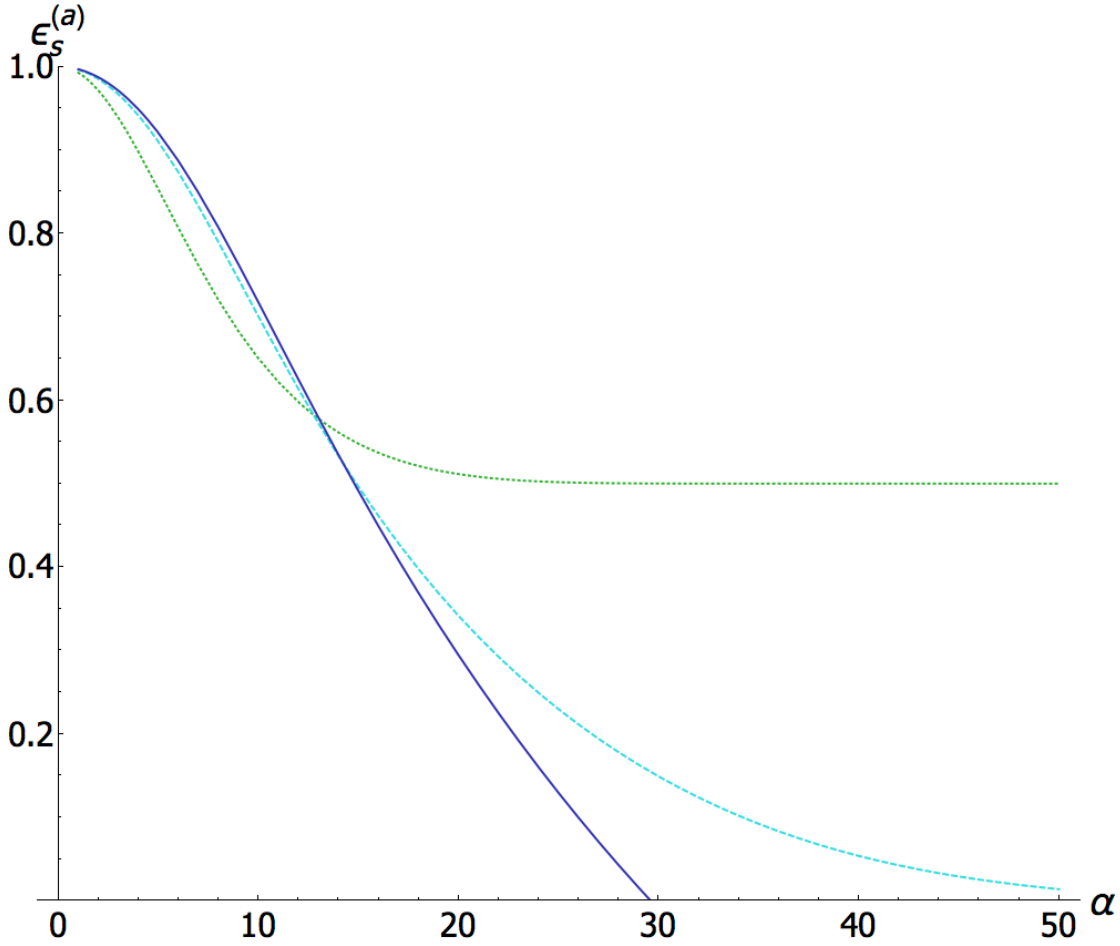

Figure 4.4: Maximum value of the loss parameter $\epsilon_s^{(a)}$ such that the bounds are violated, as a function of the coherent state parameter α and for different values of s: green (dotted), $s = 0$; cyan (dashed), $s = -1$; blue (solid), $s = -2$.

As may be observed from Fig. 4.4, the loss parameter for the PAC states exhibits similar features as it did for the Fock state. That is, smaller values of s produce a more effective bound for certifying QNG in a noisy PAC state, provided the parameter α is smaller or equal to about 10. As in the previous case, however, there is evidence that there exists a compromise between a tighter bound and the amount of violation quantified by the criterion $\Delta_s^{(a)}$ – in effect, the magnitude of the parameter decreases for lower values of s.

For the PAC state, we also consider the effect of the second optimised witness of Eq.(4.10), which requires a few additional steps in the analysis. First, we observe that the minima of the witness $\Delta_s^{(b)}[\varrho, \hat{D}(\beta)]$ for the quasiprobability distributions are displaced from the origin of the phase space, and we can in fact decrease the QNG indicator by displacing the minimum back to the origin. We therefore compute the

displaced photon number for the new quasiprobability distribution $Q_s[\varrho](-\beta)$:

$$\bar{n}^{\mathrm{PAC}}(\beta) = (1-\epsilon)|\beta|^2 \bar{n}_0^{\mathrm{PAC}} + \sqrt{1-\epsilon}(\beta^* \langle \hat{a} \rangle_0 + \beta \langle \hat{a}^\dagger \rangle_0), \tag{4.39}$$

where $\langle A \rangle_0 = \langle \psi_0 | A | \psi_0 \rangle$, and for $|\psi_0\rangle = |\psi_{\mathrm{PAC}}\rangle$,

$$\langle \hat{a} \rangle_0 = \langle \hat{a}^\dagger \rangle_0 = \frac{\alpha(2+\alpha^2)}{1+\alpha^2}. \tag{4.40}$$

Minimising $\Delta_s^{(b)}[\varrho, \hat{D}(\beta)]$ over possible displacement parameters β, we see that we can approximate the optimal values of β, for large values of ϵ and $\alpha \gtrsim 1.5$, as

$$\beta_{\mathrm{opt}} \simeq -\alpha\sqrt{1-\epsilon} = -\alpha e^{-\gamma t/2}, \tag{4.41}$$

which is roughly the same for the Wigner and Q functions. We then set $\beta = \beta_{\mathrm{opt}}$ in order to compare the values of the QNG witness based on the second criterion for $s = 0$ and $s = -1$. Numerical investigations performed as part of this original work indicate that $\epsilon_s^{(b)} \simeq 1$ for all possible values of α. No root can be found for general α as analytic optimisation was tried but not feasible.

4.4.3 Photon-subtracted Squeezed States

Our third and final case study for testing the QNG witness is the photon-subtracted squeezed state [227], defined as $|\psi_{\mathrm{PSS}}\rangle = \mathcal{N}\hat{a}\hat{S}(r)|0\rangle$, where squeezing parameter r is taken to be real. The average photon number for the PSS state is

$$\bar{n}_0^{\mathrm{PSS}} = 3\sinh^2 r + 1. \tag{4.42}$$

We compute the quasiprobability distribution for this state using the convolution of Eq.(4.38). Upon determining the bounds, we again notice that the characteristics demonstrated by the Fock and PAC states are exhibited by the PSS state. In this case, increasingly negative values of s allow for larger values of the loss parameter $\epsilon_s^{(a)}$, provided we have squeezing parameter $r \lesssim 8$. This is illustrated in Fig.4.5(a). Once again, this represents a loss in the quantity of violation described by $\Delta_s^{(a)}$.

In this final case we also examine the second QNG witness, $\Delta_s^{(b)}$. Just as the PAC states inherit a displacement following Gaussian evolution, PSS states inherit additional squeezing on the evolved state. We can use the optimised witness of Eq.(4.10) to take these squeezing operations into consideration. Adjusting the bound for the PSS state is not as straightforward, however, since the Wigner and the Q functions change differently under squeezing. The Wigner function at the origin is unchanged by

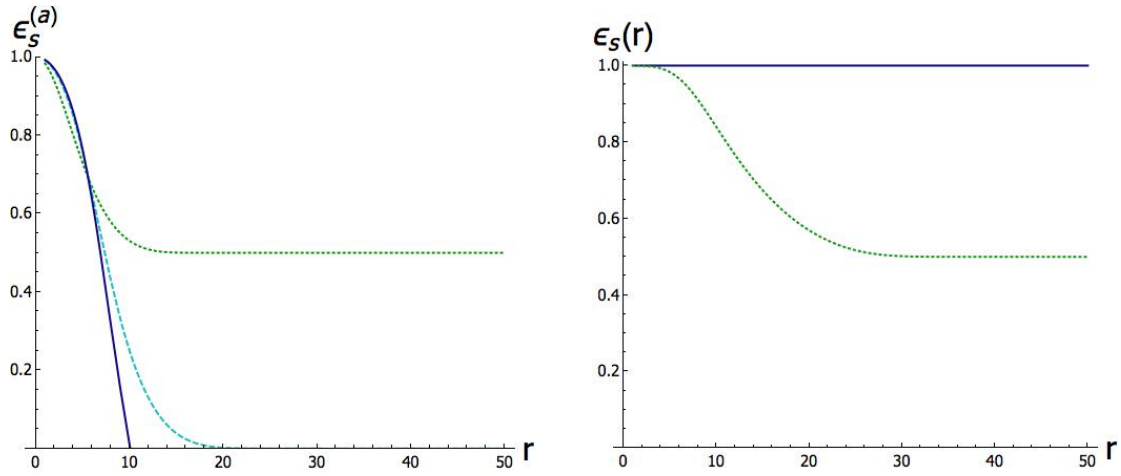

(a) (b)

Figure 4.5: Loss parameters for PSS states. (a) Maximum value of the loss parameter $\epsilon_s^{(a)}$ such that the bounds are violated, as a function of the squeezing parameter r and for different values of s: green (dotted), $s = 0$; cyan (dashed), $s = -1$; blue (solid), $s = -2$. (b) A comparison between the maximum values of the noise parameter $\epsilon_s^{(b)}$ for PSS states by using the Wigner function criterion (green dotted line) and the Q function criterion (blue solid line).

the squeezing operation, but the Q function is not similarly invariant and as a result the following argument for the optimisation of the squeezing parameter is valid only for the Wigner function. It will quickly become evident, however, that this doesn't prove to be a problem. To compute this new bound, we first find the value $q_{\rm opt}$ that minimises the average photon number of $\hat{S}(q)\rho\hat{S}^\dagger(q)$,

$$\bar{n}^{\rm PSS}(q) = (1-\epsilon)[\bar{n}_0^{\rm PSS}(\mu_q^2+\nu_q^2) + \mu_q\nu_q(\langle\hat{a}^2\rangle_0 + \langle\hat{a}^{\dagger 2}\rangle_0)] + \nu_q^2, \tag{4.43}$$

where $\mu_t = \cosh t$, $\nu_t = \sinh t$ and for an initial PSS state $|\psi_{\rm PSS}\rangle$, $\langle\hat{a}^2\rangle_0 = \langle\hat{a}^{\dagger 2}\rangle_0 = 3\mu_r\nu_r$. The optimal squeezing value is then evaluated analytically:

$$q_{\rm opt} = -\text{arccosh}(\mu_{\rm opt}) \tag{4.44}$$

$$\mu_{\rm opt} = \frac{1}{\sqrt{2}}\left(1 + \frac{6(1-\epsilon)\mu_r^2 + 4\epsilon - 3}{\sqrt{(4\epsilon-3)^2 + 12(1-\epsilon)\epsilon\mu_r^2}}\right)^{1/2}. \tag{4.45}$$

Similar to the PAC state analysis, we now assign the squeezing parameter its optimal value $q_{\rm opt}$ and plot the criterion as a function of ϵ. It is at this point that we can illustrate why optimising the squeezing for the Q function was unnecessary. We plot both the Wigner and Q functions in Fig. 4.5(b) and observe that, while $q_{\rm opt}$ is only optimised for the Wigner function, the maximum noise $\epsilon_s^{(b)}$ for the Q function

for this value of s is 1 for all values and therefore already gives the desired result. Therefore, while this is not the optimal squeezing for the Q function, it is sufficient to detect QNG by means of the Q function-based witness.

4.5 Error estimation on bounds

Now that we have looked at three case studies for testing whether our QNG witnesses do indeed certify quantum non-Gaussianity, we look more carefully at the notion that a tradeoff exists between the amount of information quantified by these witnesses and the tightness of the bound. While a full error propagation evaluating the various witnesses is left to future work, we instead evaluate the bounds $B_s(n)$ for the different s-values, based on uncertainty in the mean photon number n. In order to best approximate the realities of experiment in determining the error on the bound, we suppose that we have a photon number resolving detector with which we would like to measure different average values of n that we assign to a set n_{avg}. These are discretised values covering the desired range of n. Experimentally, the state would need to be measured k times, with k ideally large. Due to this, we define our n_{tot} as the total number of photons measured over k trials:

$$n_{tot} = k \times n_{avg}. \tag{4.46}$$

We have assumed a Poissonian distribution, as we expect the states to be independent of each other. Since we wish to evaluate the bound for an average $n = n_{avg}$, we divide by k before computing the means and variances of the bounds. Fig. 4.6 shows the result of these calculations, with all results normalised so the bounds evaluate to 1 at $n_{avg} = 0$. Specifically, from this figure we see that the error on the bounding functions $B_s(n)$ does not change with different values of s. As a result, any errors derived from the measurement of the quasiprobability distribution values $Q_s[\varrho](\alpha)$ are likely to have a large impact when the proposed witnesses are used in a real experiment.

4.6 Final Remarks

Over the course of this chapter we have presented a general method for deriving sufficient but not necessary bounds of linear functionals on the Gaussian convex hull. Having introduced the properties of the bounds, we used them to define QNG witnesses based on s-parametrised quasiprobability distributions, with $s < 0$. The witnesses work by bounding the average photon number of the quantum state from above and

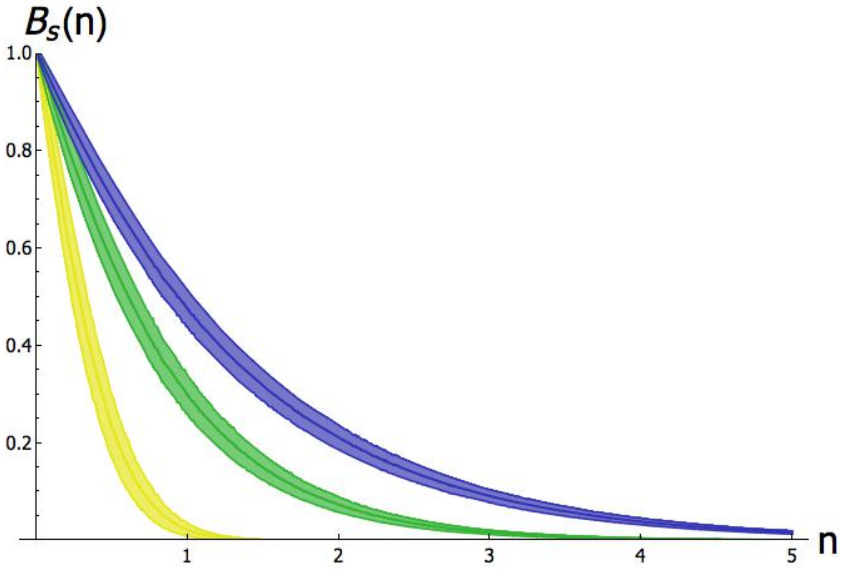

Figure 4.6: Error on the (renormalised) bounding functions $B_s(n)$ for (from top to bottom) s=0 (blue), s=-1 (green), and s=-2 (yellow).

then measuring the resulting quasiprobability distribution for a given point in phase space. In general, this point is taken to be the origin. We find that we can express a detection-independent bound for classifying quantum non-Gaussian states.

Three separate cases studies are examined to illustrate the use of these witnesses. We test criteria for a range of s-values for each of the Fock, PAC, and PSS states. The motivation for evaluating the bound for different values of s comes from the ability to associate the s value with different types of detection used in experiment. For example, while $s = 0, -1$ correspond to the Wigner and Q functions respectively, $s = -2$ can be compared to an inefficient measurement of the Q function. Since it is possible to know the inefficiency of the detector from trials using known states, having s assume values less than -1 allows us to generalise our description by removing the dependence on the type and quality of detection. Looking at the bound for these different states, it is observed that there exists a region for which a smaller s-value provides a witness for QNG and allows more channel loss than the Wigner function bound originally considered [220]. This is actually describing a tradeoff between the maximum allowable loss for which we can witness QNG, and the amount of violation quantified by our criterion. In general the magnitude of violation is smaller for smaller values of s.

The presence of this tradeoff provides a strong incentive for future work on this subject, including a better understanding of the value of this tradeoff. In effect, with this as with many other bounds used in quantum mechanics, it is important to understand the cost of tightening the bound.

Conclusions

Non-Gaussianity has proven to be an invaluable resource for quantum information processing tasks in the continuous variable regime. The ability to generate non-Gaussian states is a requirement in order to achieve universal quantum computation, and has demonstrated enhancements to current quantum information protocols, including quantum teleportation, quantum cloning, and dense coding, as well as uses in improving storage. Such states have also been shown to be necessary for long distance protocols based on entanglement distillation and swapping. The accessibility of such states has proven to be a challenge experimentally, however, as they require a nonlinear operation like photon addition or subtraction, or the application of a Hamiltonian that is more than quadratic in the bosonic mode operators.

This thesis has studied two distinct methods of generating such non-Gaussian states, as well as presenting a method for characterising a specific set of non-Gaussian states that can only be generated by means of such highly nonlinear processes as Fock state generation, Kerr interaction, photon addition and subtraction operations, or conditional photon number detections. We began with an overview of quantum information processing in continuous variables in order to both introduce the formalism required for the original work presented later, as well as to motivate the need for non-Gaussian states and operations in quantum information.

The first type of non-Gaussian quantum states considered are superpositions of orthogonal states. These states have applications in quantum cloning protocols as well as approximating a cv universal NOT operation. Two distinct proposals have been presented for generating such superpositions. In the first, we demonstrate a scheme for producing the superposition of the photon creation and annihilation operations through conditional photon subtraction on a two-mode squeezed state. Such a superposition has been shown to achieve orthogonalisation of any pure continuous input field [161]. While this scheme is limited, it is shown that by varying the type of detection performed on one of the modes of the original tms state, we can engineer either a squeezed displaced state or a coherent state.

A general method for producing a superposition of a state and one of its orthogonal

states is also presented, relying only on knowledge of the mean value of the operator chosen as the orthogonaliser, given the input state. This operation is not limited to producing only a superposition, but can directly orthogonalise a general input state. The experimental realisation of such an orthogonaliser was also achieved for a coherent state input, using both the creation operator and the photon number operator as orthogonalisers, while the theory of using these operators to orthogonalise the single-mode squeezed vacuum and the Schrödinger cat state is also explored.

The second method for generating non-Gaussian states actually considers the use of such states as resources for a non-Gaussian gate operation on an independent system. In particular, it examines the distribution of higher-order nonlinearities across multiple modes, focusing on the case of distributing the single-mode cubic state $\hat{x}^3$ across two modes $\hat{x}_1^2\hat{x}_2$. States of two or more modes are needed in order to test entanglement in a system, and the ability to produce non-Gaussian entangled states is an area that has not yet been well-explored. The extension to general multimode state generation starting from a single-mode higher-order state is also presented, where it is shown that repeated, phase-controlled conditional photon subtraction is capable of generating highly nonlinear entangled two-mode states.

Finally, we present a set of witnesses for quantum non-Gaussianity based on general s-parametrised quasiprobability distributions. This work was motivated by the need for qualifying not just non-Gaussian states, but states which can only be created by a non-Gaussian operation. We call these states quantum non-Gaussian, to differentiate them from non-Gaussian states which could be made by a combination of Gaussian operations and classical randomisation. We test the presented witnesses for a range of s-values for each of Fock, photon-added coherent, and photon-subtracted squeezed states, and note that by evaluating the bound at different values of the quasiprobability distribution parameter s, we can directly observe the effect of different detection inefficiencies on our ability to witness quantum non-Gaussianity. Furthermore, we illustrate that, while smaller s-values allow more channel loss while still witnessing QNG, this amounts to a tradeoff between the maximum allowable loss, and the amount of violation quantified by our criterion.

While we have explored a number of novel approaches for both generating and characterising non-Gaussian quantum states, this work also highlights several avenues for further investigations. In particular, the application of our QNG criteria on the non-Gaussian states we generate is a natural first extension to the work. With respect to the orthogonal states and separately from experimental improvements, testing the application of such states as tools in quantum information protocols is a feasible future step. In the case of the multimode non-Gaussian state generation, it would be

interesting to study such states from the perspective of their entanglement characteristics. Indeed, understanding the full practical application of such states remains mostly unexplored. At last, further examination of the tradeoff between the ability to characterise quantum non-Gaussian states and the amount of violation quantified by the criteria introduced here is another important next step.

While this thesis presents several approaches for generating and characterising non-Gaussian states, the full range of applicability of the results presented here remains to be discovered.

References

[1] A. Einstein, Physikalische Zeitschrift **18**, 121 (1917).

[2] T. H. Maiman, Nature **187**, 493 (1960).

[3] P. A. M. Dirac, Proceedings of the Royal Society of London A **114** (1927).

[4] R. J. Glauber, Physical Review **131** (1963).

[5] E. C. G. Sudarshan, Physical Review Letters **10** (1963).

[6] L. Mandel, Physica Scripta **T12**, 34 (1986).

[7] L. Davidovich, Reviews of Modern Physics **68** (1996).

[8] P. G. Kwiat, K. Mattle, H. Weinfurter, and A. Zeilinger, Physical Review Letters **75** (1995).

[9] H. Kosaka, A. Tomita, Y. Nambu, T. Kimura, and K. Nakamura, Electronics Letters **39** (2003).

[10] M. Aspelmeyer, T. Jennewein, M. Pfennigbauer, W. R. Leeb, and A. Zeilinger, IEEE Journal of Selected Topics in Quantum Electronics **9** (2003).

[11] C. Gobby, Z. L. Yuan, and A. J. Shields, Applied Physics Letters **84** (2004).

[12] D. P. DiVincenzo, Science **270**, 255 (1995).

[13] S. Lloyd, Scientific American **273** (1995).

[14] S. Lloyd and S. L. Braunstein, Physical Review Letters **82** (1999).

[15] S. L. Braunstein and P. van Loock, Reviews of Modern Physics **77**, 513 (2005).

[16] U. Leonhardt, *Measuring the Quantum State of Light* (Cambridge University Press, 1997).

[17] D. F. Walls and G. J. Milburn, *Quantum Optics* (Springer, 1994).

[18] L. Vaidman, Physical Review A **49** (1994).

[19] F. Grosshans, G. V. Assche, J. Wenger, R. Brouri, N. J. Cerf, and P. Grangier, Nature **421**, 238 (2003).

[20] V. Bužek and M. Hillery, Physical Review A **54** (1996).

[21] N. J. Cerf and S. Iblisdir, Physical Review A **62** (2000).

[22] N. J. Cerf, A. Ipe, and X. Rottenberg, Physical Review Letters **85** (2000).

[23] S. L. Braunstein, N. J. Cerf, S. Iblisdir, P. van Loock, and S. Massar, Physical Review Letters **86** (2001).

[24] J. Fiurášek, Physical Review Letters **86** (2001).

[25] A. Ourjoumtsev, A. Dantan, R. Tualle-Brouri, and P. Grangier, Physical Review Letters **98** (2007).

[26] H. Takahashi, J. S. Neergaard-Nielsen, M. Takeuchi, M. Takeoka, K. Hayasaka, A. Furusawa, and M. Sasaki, Nature Photonics **4**, 178 (2010).

[27] Y.-Q. Zhang and J.-B. Xu, Journal of Modern Optics **58** (2011).

[28] K. Jensen, W. Wasilewski, H. Krauter, T. Fernholz, B. M. Nielsen, M. Owari, M. B. Plenio, A. Serafini, M. M. Wolf, and E. S. Polzik, Nature Physics **7**, 13 (2011).

[29] T. Opatrný, G. Kurizki, and D.-G. Welsch, Physical Review A **61** (2000).

[30] A. I. Lvovsky, H. Hansen, T. Aichele, O. Benson, J. Mlynek, and S. Schiller, Physical Review Letters **87** (2001).

[31] P. A. Franken, A. E. Hill, C. W. Peters, and G. Weinreich, Physical Review Letters **7** (1961).

[32] W. Wasilewski, T. Fernholz, K. Jensen, L. S. Madsen, H. Krauter, C. Muschik, and E. S. Polzik, Optics Express **17** (2009).

[33] J. S. Neergaard-Nielsen, M. Takeuchi, K. Wakui, H. Takahashi, K. Hayasaka, M. Takeoka, and M. Sasaki, Physical Review Letters **105** (2010).

[34] A. I. Lvovsky and S. A. Babichev, Physical Review A **66** (2002).

[35] A. Zavatta, S. Viciani, and M. Bellini, Science **306**, 660 (2004).

[36] A. Zavatta, S. Viciani, and M. Bellini, Physical Review A **72** (2005).

[37] D. Leibfriend, E. Knill, S. Seidelin, J. Britton, R. B. Blakestad, J. Chiaverini, D. B. Hume, W. M. Itano, J. D. Jost, C. Langer, et al., Nature **438**, 639 (2005).

[38] A. Allevi, A. Andreoni, F. A. Beduni, M. Bondani, M. G. Genoni, S. Olivares, and M. G. A. Paris, Europhysics Letters **92** (2010).

[39] M. Barbieri, N. Spagnolo, M. G. Genoni, F. Ferreyrol, R. Blandino, M. G. A. Paris, P. Grangier, and R. Tualle-Brouri, Physical Review A **82** (2010).

[40] A. Zavatta, V. Parigi, and M. Bellini, Physical Review A **75** (2007).

[41] G. Vidal and R. F. Werner, Physical Review A **65** (2002).

[42] T. Kiesel, W. Vogel, V. Parigi, A. Zavatta, and M. Bellini, Physical Review A **78** (2008).

[43] U. M. Titulaer and R. J. Glauber, Physical Review **140** (1965).

[44] T. Kiesel, W. Vogel, B. Hage, J. DiGuglielmo, A. Samblowski, and R. Schnabel, Physical Review A **79** (2009).

[45] A. Mari, K. Kieling, B. M. Nielsen, E. S. Polzik, and J. Eisert, Physical Review Letters **106** (2011).

[46] V. V. Dodonov, O. V. Man'ko, V. I. Man'ko, and A. Wünsche, Journal of Modern Optics **47**, 633 (2000).

[47] V. V. Dodonov and V. B. Renó, Physics Letters A **308**, 249 (2003).

[48] P. Marian, T. A. Marian, and H. Scutaru, Physical Review A **69** (2004).

[49] P. Marian, T. A. Marian, and H. Scutaru, Physical Review Letters **88** (2002).

[50] D. Bures, Transactions of the American Mathematical Society **135**, 199 (1969).

[51] A. Wehrl, Reviews of Modern Physics **50** (1978).

[52] V. Vedral, M. B. Plenio, M. A. Rippin, and P. L. Knight, Physical Review Letters **78** (1997).

[53] V. Vedral and M. B. Plenio, Physical Review A **57** (1998).

[54] V. Vedral, Reviews of Modern Physics **74**, 197 (2002).

[55] M. G. Genoni, M. G. A. Paris, and K. Banaszek, Physical Review A **78** (2008).

[56] J. K. Asbóthe, J. Calsamiglia, and H. Ritsch, Physical Review Letters **94** (2005).

[57] D. N. Klyshko, Physics Letters A **213**, 7 (1996).

[58] E. V. Shchukin and W. Vogel, Physical Review A **72** (2005).

[59] E. Shchukin, T. Richter, and W. Vogel, Physical Review A **71** (2005).

[60] R. Filip and J. L. Mišta, Physical Review Letters **106** (2011).

[61] M. G. Genoni and M. G. A. Paris, Physical Review A **82** (2010).

[62] A. S. Coelho, L. S. Constanzo, A. Zavatta, C. Hughes, M. S. Kim, and M. Bellini, arXiv:1407.664 (2014).

[63] C. Hughes, M. G. Genoni, T. Tufarelli, M. G. A. Paris, and M. S. Kim, Physical Review A **90** (2014).

[64] U. L. Andersen, G. Leuchs, and C. Silberhorn, Laser & Photonics Reviews **4**, 337 (2010).

[65] W. P. Schleich, *Quantum Optics in Phase Space* (Wiley-VCH, 2001).

[66] S. J. van Enk, Physical Review A **60** (1999).

[67] E. Wigner, Physical Review **40**, 749 (1932).

[68] H. Weyl, *Space, Time, Matter* (Methuen & Co. Ltd., 1952).

[69] P. Aniello, arXiv:1411.1304 [math-ph] (2014).

[70] M. S. Kim, Journal of Physics B: Atomic, Molecular and Optical Physics **41** (2008).

[71] K. Husimi, Proceedings of the Physical Society of Japan **22** (1940).

[72] N. Lütkenhaus and S. M. Barnett, Physical Review A **51** (1995).

[73] R. L. Hudson, Reports on Mathematical Physics **6** (1974).

[74] M. J. Lighthill, *An introduction to Fourier analysis and generalised functions* (Cambridge University Press, 1958).

[75] S. Olivares, The European Physical Journal Special Topics **203** (2012).

[76] B. L. Schumaker, Physics Reports **135** (1986).

[77] G. Adesso, Ph.D. thesis, Universitá degli Studi di Salerno (2006).

[78] L. Mandel and E. Wolf, *Optical Coherence and Quantum Optics* (Cambridge University Press, 1995).

[79] D. N. Klyshko, *Photons and Nonlinear Optics* (Gordon and Breach Science Publishers, 1988).

[80] S. Pirandola, S. Mancini, D. Vitali, and P. Tombesi, Physical Review A **68** (2003).

[81] S.-H. Xiang, W. Wen, Z.-G. Shi, and K.-H. Song, Physical Review A **81** (2010).

[82] M. J. Woolley, G. J. Milburn, and C. M. Caves, New Journal of Physics **10** (2008).

[83] P. Meystre, *Atom Optics* (Springer Verlag, 2001).

[84] N. Piovella, M. Cola, and R. Bonifacio, Physical Review A **67** (2003).

[85] M. G. A. Paris, M. Cola, N. Piovella, and R. Bonifacio, Optics Communications **227**, 349 (2003).

[86] M. Cola, M. G. A. Paris, N. Piovella, and R. Bonifacio, Journal of Physics B: Atomic, Molecular and Optical Physics **37**, S187 (2004).

[87] M. Cola, M. G. A. Paris, and N. Piovella, Physical Review A **70** (2004).

[88] L.-M. Kuang, A.-H. Zeng, and Z.-H. Kuang, Physics Letters A **319**, 24 (2003).

[89] A. Ferraro, S. Olivares, and M. G. A. Paris, *Gaussian states in continuous variable quantum information* (Bibliopolis, Napoli, 2005).

[90] M. A. Marchiolli and D. Galetti, Physica Scripta **78** (2008).

[91] W. H. Louisell, A. Yariv, and A. E. Siegman, Physical Review **124** (1961).

[92] E. Knill, R. Laflamme, and G. J. Milburn, Nature **409**, 46 (2001).

[93] S. D. Bartlett, B. C. Sanders, S. L. Braunstein, and K. Nemoto, Physical Review Letters **88** (2002).

[94] S. D. Bartlett and B. C. Sanders, Physical Review A **65** (2002).

[95] A. Einstein, B. Podolsky, and N. Rosen, Physical Review **47**, 777 (1935).

[96] J. S. Bell, Physics **1**, 195 (1964).

[97] J. F. Clauser, M. A. Horne, A. Shimony, and R. A. Holt, Physical Review Letters **23** (1969).

[98] N. Gisin, Physics Letters A **154** (1991).

[99] E. Schmidt, Mathematische Annalen **63** (1907).

[100] J. V. Neumann, *Mathematical Foundation of Quantum Mechanics* (Princeton University Press, 1955).

[101] S. Popescu and D. Rohrlich, Physical Review A **56** (1997).

[102] G. Vidal, Journal of Modern Optics **47** (2000).

[103] A. Peres, Physical Review Letters **77** (1996).

[104] M. Horodecki, P. Horodecki, and R. Horodecki, Physics Letters A (1996).

[105] M. Lewenstein, B. Kraus, J. I. Cirac, and P. Horodecki, Physical Review A (2000).

[106] O. Gühne and N. Lütkenhaus, Physical Review Letters **96** (2006).

[107] P. Hyllus and J. Eisert, New Journal of Physics **8**, 51 (2006).

[108] M. Barbieri, F. D. Martini, G. D. Nepi, P. Mataloni, G. M. D'Ariano, and C. Macchiavello, Physical Review Letters **91** (2003).

[109] M. Bourennane, M. Eibl, C. Kurtsiefer, S. Gaertner, H. Weinfurter, O. Gühne, P. Hyllus, D. Bruß, M. Lewenstein, and A. Sanpera, Physical Review Letters **92** (2004).

[110] H. H. *et al*, Nature **438**, 643 (2005).

[111] C.-Y. L. *et al*, Nature Physics **3**, 91 (2007).

[112] M. B. Plenio and S. Virmani, Quantum Information and Computation **7** (2007).

[113] M. Christandl, Ph.D. thesis, University of Cambridge (2006).

[114] V. Vedral, M. B. Plenio, K. Jacobs, and P. L. Knight, Physical Review A **56** (1997).

[115] K. Życzkowski, P. Horodecki, A. Sanpera, and M. Lewenstein, Physical Review A **58** (1998).

[116] J. Eisert, Ph.D. thesis, University of Potsdam (2001).

[117] M. Christandl and A. Winter, Journal of Mathematical Physics **45** (2004).

[118] C. H. Bennett, G. Brassard, C. Crépeau, R. Jozsa, A. Peres, and W. K. Wootters, Physical Review Letters **70** (1993).

[119] L. Davidovich, N. Zagury, M. Brune, J. M. Raimond, and S. Haroche, Physical Review A **50** (1994).

[120] J. I. Cirac and A. S. Parkins, Physical Review A **50** (1994).

[121] T. Sleator and H. Weinfurter, Annals of the New York Academy of Sciences **755** (1995).

[122] S. L. Braunstein and A. Mann, Physical Review A **51** (1994).

[123] D. Boschi, S. Branca, F. D. Martini, L. Hardy, and S. Popescu, Physical Review Letters **80** (1998).

[124] D. Bouwmeester, J.-W. Pan, K. Mattle, M. Eibl, H. Weinfurter, and A. Zeilinger, Nature **390**, 575 (1997).

[125] S. L. Braunstein and H. J. Kimble, Physical Review Letters **80** (1998).

[126] A. Furusawa, J. L. Sørensen, S. L. Braunstein, C. A. Fuchs, H. J. Kimble, and E. S. Polzik, Science **282 706-709** (1998).

[127] S. L. Braunstein, Nature **394**, 47 (1998).

[128] S. L. Braunstein and H. J. Kimble, Physical Review A **61** (2000).

[129] S. L. Braunstein, C. A. Fuchs, and H. J. Kimble, Journal of Modern Optics **47** (2000).

[130] C. H. Bennett, G. Brassard, S. Popescu, B. Schumacher, J. A. Smolin, and W. K. Wootters, Physical Review Letters **76** (1996).

[131] M. Horodecki, P. Horodecki, and R. Horodecki, Physical Review Letters **78** (1997).

[132] D. Deutsch, A. Ekert, R. Jozsa, C. Macchiavello, S. Popescu, and A. Sanpera, Physical Review Letters **77** (1996).

[133] P. T. Cochrane, T. C. Ralph, and G. J. Milburn, Physical Review A **65** (2002).

[134] S. Olivares, M. G. A. Paris, and R. Bonifacio, Physical Review A **67** (2003).

[135] D. Gross, S. T. Flammia, and J. Eisert, Physical Review Letters **102** (2009).

[136] W. K. Wootters and W. H. Zurek, Nature **299**, 802 (1982).

[137] H. Barnum, C. M. Caves, C. A. Fuchs, R. Jozsa, and B. Schumacher, Physical Review Letters **76** (1996).

[138] V. Scarani, S. Iblisdir, N. Gisin, and A. Acín, Reviews of Modern Physics **77** (2005).

[139] P. T. Cochrane, T. C. Ralph, and A. Dolińska, Physical Review A **69** (2004).

[140] U. L. Andersen, V. Josse, and G. Leuchs, Physical Review Letters **94** (2005).

[141] N. J. Cerf, O. Krüger, P. Navez, R. F. Werner, and M. M. Wolf, Physical Review Letters **95** (2005).

[142] M. Ban, Journal of Optics B: Quantum and Semiclassical Optics **1**, L9 (1999).

[143] X. Li, Q. Pan, J. Jing, J. Zhang, C. Xie, and K. Peng, Physical Review Letters **88** (2002).

[144] F. Casagrande, A. Lulli, and M. G. A. Paris, Physical Review A **75** (2007).

[145] T. C. Ralph, A. Gilchrist, G. J. Milburn, W. J. Munro, and S. Glancy, Physical Review A **68** (2003).

[146] A. P. Lund, T. C. Ralph, and H. L. Haselgrove, Physical Review Letters **100** (2008).

[147] M. Vasilyev, S.-K. Choi, P. Kumar, and G. M. D'Ariano, Physical Review Letters **84**, 2354 (2000).

[148] A. Ourjoumtsev, R. Tualle-Brouri, and P. Grangier, Physical Review Letters **96** (2006).

[149] J. Wenger, R. Tualle-Brouri, and P. Grangier, Physical Review Letters **92** (2004).

[150] N. Gisin and S. Popescu, Physical Review Letters **83** (1999).

[151] S. Massar, Physical Review A **62** (2000).

[152] N. J. Cerf and S. Iblisdir, Physical Review A **64** (2001).

[153] N. J. Cerf and S. Iblisdir, Physical Review Letters **87** (2001).

[154] J. Fiurášek, S. Iblisdir, S. Massar, and N. J. Cerf, Physical Review A **65** (2002).

[155] J. Fiurášek and N. J. Cerf, Physical Review A **77** (2008).

[156] W.-H. Zhang, L.-B. Yu, Z.-L. Cao, and L. Ye, Physical Review A **86** (2012).

[157] F. D. Martini, V. Bužek, F. Sciarrino, and C. Sias, Nature **419**, 815 (2002).

[158] H. Bechmann-Pasquinucci and N. Gisin, Physical Review A **59** (1999).

[159] V. Bužek, M. Hillery, and R. F. Werner, Physical Review A **60** (1999).

[160] S. M. Barnett and P. M. Radmore, *Methods in Theoretical Quantum Optics* (Clarendon Press, 1997).

[161] M. R. Vanner, M. Aspelmeyer, and M. S. Kim, Physical Review Letters **110** (2013).

[162] M. G. Raymer and M. Beck, Lecture Notes in Physics **649**, 235 (2004).

[163] A. Zavatta, S. Viciani, and M. Bellini, Laser Physics Letters **3** (2006).

[164] A. I. Lvovsky and M. G. Raymer, Reviews of Modern Physics **81**, 299 (2009).

[165] S. P. *et al*, IEEE Journal of Selected Topics in Quantum Electronics **42** (2006).

[166] W. H. Zurek, Physical Review A **76** (2007).

[167] C. M. Caves, Physical Review D **26** (1982).

[168] M. Ježek, M. Mičuda, I. Straka, M. Miková, M. Dušek, and J. Fiurášek, Physical Review A **89** (2014).

[169] E. Bimbard, N. Jain, A. MacRae, and A. I. Lvovsky, Nature Photonics **4**, 243 (2010).

[170] M. Arndt and K. Hornberger, Nature Physics **10**, 271 (2014).

[171] N. C. Menicucci, P. van Loock, M. Gu, C. Weedbrook, T. C. Ralph, and M. A. Nielsen, Physical Review Letters **97** (2006).

[172] M. Dykman, *Fluctuating Nonlinear Oscillators* (Oxford University Press, 2012).

[173] S. Haroche and J.-M. Raimond, *Exploring the Quantum* (Oxford University Press, 2006).

[174] D. Leibfried, R. Blatt, C. Monroe, and D. Wineland, Reviews of Modern Physics **75**, 281 (2003).

[175] D. Gottesman, A. Kitaev, and J. Preskill, Physical Review A **64** (2001).

[176] P. Marek, R. Filip, and A. Furusawa, Physical Review A **84** (2011).

[177] S. Deléglise, I. Dotsenko, C. Sayrin, J. Bernu, M. Brune, J.-M. Raimond, and S. Haroche, Nature **455**, 510 (2008).

[178] S. Ghose and B. C. Sanders, Journal of Modern Optics **54**, 855 (2007).

[179] N. C. Menicucci, X. Ma, and T. C. Ralph, Physical Review Letters **104** (2010).

[180] A. J. Roncaglia, L. Aolita, A. Ferraro, and A. Acín, Physical Review A **83** (2011).

[181] M. Gu, C. Weedbrook, N. C. Menicucci, T. C. Ralph, and P. van Loock, Physical Review A **79** (2009).

[182] S. Sefi and P. van Loock, Physical Review Letters **107** (2011).

[183] K. Marshall, R. Pooser, G. Siopsis, and C. Weedbrook, Physical Review A **91** (2015).

[184] M. Yukawa, K. Miyata, H. Yonezawa, P. Marek, R. Filip, and A. Furusawa, Physical Review A **88** (2013).

[185] V. B. Braginsky, Y. I. Vorontsov, and K. S. Thorne, Science **209** (1980).

[186] J.-F. Roch, K. Vigneron, P. Grelu, A. Sinatra, J.-P. Poizat, and P. Grangier, Physical Review Letters **78** (1997).

[187] B. C. Buchler, P. K. Lam, H. A. Bachor, U. L. Andersen, and T. C. Ralph, Physical Review A **65** (2001).

[188] P. Lougovski, H. Walther, and E. Solano, European Physics Journal D **38**, 423 (2006).

[189] T. C. Ralph, S. D. Bartlett, J. L. O'Brien, G. J. Pryde, and H. M. Wiseman, Physical Review A **73** (2006).

[190] A. Kitagawa, M. Takeoka, M. Sasaki, and A. Chefles, Physical Review A **73** (2006).

[191] L. Pezze and A. Smerzi, Physical Review Letters **102** (2009).

[192] R. M. Gomes, A. Salles, F. Toscano, P. H. S. Ribeiro, and S. P. Walborn, Proceedings of the National Academy of Sciences **106**, 21517 (2009).

[193] M. K. Olsen and J. F. Corney, Physical Review A **87** (2013).

[194] T. J. Bartley and I. A. Walmsley, New Journal of Physics **17** (2015).

[195] Y. Kurochkin, A. S. Prasad, and A. I. Lvovsky, Physical Review Letters **112** (2014).

[196] C. T. Lee, Physical Review A **44** (1991).

[197] C. T. Lee, Physical Review A **45** (1992).

[198] Arvind, N. Mukunda, and R. Simon, Physical Review A **56** (1997).

[199] Arvind, N. Mukunda, and R. Simon, Journal of Physics A: Mathematical and General **31**, 565 (1998).

[200] M. A. Marchiolli, V. S. Bagnato, Y. G. aes, and B. Baseia, Physics Letters A **279**, 294 (2001).

[201] M. G. A. Paris, Physics Letters A **289**, 167 (2001).

[202] V. V. Dodonov, Journal of Optics B: Quantum and Semiclassical Optics **4**, R1 (2002).

[203] A. Kenfack and K. Życzkowski, Journal of Optics B: Quantum and Semiclassical Optics **6**, 396 (2004).

[204] J. Paavola, M. J. W. Hall, M. G. A. Paris, and S. Maniscalco, Physical Review A **84** (2011).

[205] W. Vogel, Physical Review Letters **100** (2008).

[206] R. Simon, Physical Review Letters **84** (2000).

[207] L.-M. Duan, G. Giedke, J. I. Cirac, and P. Zoller, Physical Review Letters **84** (2000).

[208] P. Giorda and M. G. A. Paris, Physical Review Letters **105** (2010).

[209] G. Adesso and A. Datta, Physical Review Letters **105** (2010).

[210] F. Ferraro and M. G. A. Paris, Physical Review Letters **108** (2012).

[211] C. Gehrke, J. Sperling, and W. Vogel, Physical Review A **86** (2012).

[212] D. Buono, G. Nocerino, V. D'Auria, A. Porzio, S. Olivares, and M. G. A. Paris, Journal of the Optical Society of America B **27** (2010).

[213] D. Buono, G. Nocerino, A. Porzio, and S. Solimeno, Physical Review A **86** (2012).

[214] T. Bröcker and R. F. Werner, Journal of Mathematica Physics **36** (1995).

[215] A. Mandilara, E. Karpov, and N. J. Cerf, Physical Review A **79** (2009).

[216] A. Mari and J. Eisert, Physical Review Letters **109** (2012).

[217] V. Veitch, N. Weibe, C. Ferrie, and J. Emerson, New Journal of Physics **15** (2013).

[218] M. G. Genoni, M. G. A. Paris, and K. Banaszek, Physical Review A **76** (2007).

[219] A. Allevi, A. Andreoni, M. Bondani, M. G. Genoni, and M. G. A. Paris, Physical Review A **82** (2010).

[220] M. G. Genoni, M. L. Palma, T. Tufarelli, S. Olivares, M. S. Kim, and M. G. A. Paris, Physical Review A **87** (2013).

[221] M. Ježek, I. Straka, M. Mičuda, M. Dušek, J. Fiurášek, and R. Filip, Physical Review Letters **107** (2011).

[222] M. Ježek, A. Tipsmark, R. Dong, J. Fiurášek, J. L. Mišta, R. Filip, and U. L. Andersen, Physical Review A **86** (2012).

[223] A. Predojević, M. Ježek, T. Huber, H. Jayakumar, T. Kauten, G. S. Solomon, R. Filip, and G. Weihs, Optics Express **22** (2014).

[224] V. S. Shul'man, Encyclopedia of Mathematics (2015), URL `http://www.encyclopediaofmath.org/index.php?title=Spectrum_of_an_operator&oldid=11393`.

[225] K. E. Cahill and R. J. Glauber, Physical Review **177** (1969).

[226] C. Gerry and P. Knight, *Introductory Quantum Optics* (Cambridge University Press, 2005).

[227] A. Biswas and G. S. Agarwal, Physical Review A **75** (2007).

[228] G. M. D'Ariano, M. G. A. Paris, and M. F. Sacchi, Advances in Imaging and Electron Physics **128**, 205 (2003).

[229] M. G. A. Paris, A. V. Chizhov, and O. Steuernagel, Optics Communications **134**, 117 (1997).

Appendices

Appendix A

QNG Witnesses

The work presented in the following sections forms the supplementary material provided with Ref. [63]. This is original work.

A.1 General properties of the bounds

In this section we prove that if the minimum of Φ on $\mathcal{G}_n$ is not achieved by a pure Gaussian state, then it must be achieved by a Rank-2 mixture of pure Gaussian states. Before proving this, it is useful to introduce an auxiliary lemma.

Lemma 1 The function

$$B(n) \equiv \min_{\varrho_G \in \mathcal{G}_n} \Phi[\varrho_G]. \tag{A.1}$$

is convex.

Proof Let $\rho_1 \in \mathcal{G}_{n_1}$ and $\rho_2 \in \mathcal{G}_{n_2}$ be such that $B(n_1) = \Phi[\rho_1]$ and $B(n_2) = \Phi[\rho_2]$, and take $0 \leq p \leq 1$. Then

$$\begin{aligned} pB(n_1) + (1-p)B(n_2) &= p\Phi[\rho_1] + (1-p)\Phi[\rho_2] \\ &= \Phi[p\rho_1 + (1-p)\rho_2] \geq B(pn_1 + (1-p)n_2), \end{aligned} \tag{A.2}$$

where we have used the linearity of Φ and the fact that $p\rho_1 + (1-p)\rho_2 \in \mathcal{G}_{pn_1+(1-p)n_2}$ might not be the state which minimises Φ in that set.

Theorem 1 Given n, either there exists a pure Gaussian state $|\psi_n\rangle$ of $\mathcal{G}_n$ such that $B(n) = \Phi[|\psi_n\rangle\langle\psi_n|]$, or $B(n) = \Phi[\rho_n]$, where $\rho_n \in \mathcal{G}_n$ is a rank-2 state of the form $\rho_n = p|\psi_1\rangle\langle\psi_1| + (1-p)|\psi_2\rangle\langle\psi_2|$, $|\psi_1\rangle, |\psi_2\rangle$ being pure Gaussian states.

Proof It is sufficient to consider mixtures comprising a finite number of pure Gaussian states. Infinite sums and integrals [such as that appearing in the definition Eq.(4.1)] are included in the discussion via a limiting procedure, thanks to the continuity of Φ. Suppose $B(n) = \Phi(\rho_n)$, $\rho_n = \sum_j p_j|\psi_j\rangle\langle\psi_j|$ and the states $|\psi_j\rangle$ are pure Gaussian states of average photon number n_j, such that $\bar{n} \equiv \sum p_j n_j \leq n$. From Eq.(4.3) and the fact that $\mathcal{G}_n \subset \mathcal{G}_m$ for $m > n$, it follows that $B(n)$ is a non-increasing function of n (that is, the minimum is in general lower on a larger set). Then,

$$\begin{aligned} B(\bar{n}) \geq B(n) = \Phi[\rho_n] = \Phi[\sum_j p_j|\psi_j\rangle\langle\psi_j|] \\ = \sum_j p_j \Phi[|\psi_j\rangle\langle\psi_j|] \geq \sum_j p_j B(n_j) \geq B(\bar{n}), \end{aligned} \tag{A.3}$$

where the first inequality follows from the non-increasing behaviour of B, the second inequality follows from the fact that $|\psi_j\rangle \in \mathcal{G}_{n_j}$ may not be the state minimising Φ on $\mathcal{G}_{n_j}$, and the third from the convexity of B proven in Lemma 1. To avoid contradiction, only the equal signs are possible in Eq. (A.3). This also implies that for all pure states $|\psi_j\rangle$ involved in the sum it must be

$$\Phi[|\psi_j\rangle\langle\psi_j|] = B(n_j). \tag{A.4}$$

If $n_J = n$ for some J, then $B(n) = \Phi[|\psi_J\rangle\langle\psi_J|]$.

Otherwise, there must be at least two values j_1 and j_2 in the sum such that $n_{j_1} < \bar{n} < n_{j_2}$, thus one can find $0<q<1$ yielding $qn_{j_1} + (1-q)n_{j_2} = \bar{n}$. For r sufficiently small (and

positive), it is possible to decompose

$$\begin{aligned}\sum p_j|\psi_j\rangle\langle\psi_j| = r[q|\psi_{j_1}\rangle\langle\psi_{j_1}|+(1-q)|\psi_{j_2}\rangle\langle\psi_{j_2}|] \\ + (1-r)\sum \tilde{p}_j|\psi_j\rangle\langle\psi_j|\end{aligned} \tag{A.5}$$

where $\{\tilde{p}_j\}$ is a probability distribution such that $\sum \tilde{p}_j n_j = \bar{n}$. Correspondingly, Eq. (A.3) implies

$$\begin{aligned}B(\bar{n}) &= r\left(q\Phi[|\psi_{j_1}\rangle\langle\psi_{j_1}|]+(1-q)\Phi[|\psi_{j_2}\rangle\langle\psi_{j_2}|]\right) \\ &+ (1-r)\sum \tilde{p}_j\Phi[|\psi_j\rangle\langle\psi_j|] \\ &= r[qB(n_{j_1})+(1-q)B(n_{j_2})] + (1-r)\sum \tilde{p}_j B(n_j) \\ &\geq rB(\bar{n}) + (1-r)B(\bar{n}) = B(\bar{n}),\end{aligned} \tag{A.6}$$

where we have exploited Eq. (A.4) and the convexity of B. This implies that it must be $qB(n_{j_1})+(1-q)B(n_{j_2}) = B(\bar{n})$. Moreover, we had $B(n) = B(\bar{n})$. Therefore

$$B(n) = q\Phi[|\psi_{j_1}\rangle\langle\psi_{j_1}|]+(1-q)\Phi[|\psi_{j_2}\rangle\langle\psi_{j_2}|]. \tag{A.7}$$

We have thus proven that $B(n)$ is either achieved by a pure Gaussian state or by a Rank-2 mixture of pure Gaussian states.

A.2 Properties of the quasiprobability bounds

For a single-mode pure Gaussian quantum state $|\psi_G\rangle = D(\alpha)S(\xi)|0\rangle$, with $\alpha = |\alpha|e^{i\theta}, \xi = re^{i\phi}$ the value of the s-parametrised quasiprobability distribution in the origin can be written as

$$Q_s[|\psi_G\rangle\langle\psi_G|](0) = \frac{2e^{-\frac{2(n-m)(1+2m-2\sqrt{m(1+m)}\cos(2\theta-\phi)-s)}{1+s(s-2-4m)}}}{\pi\sqrt{1+s(s-2-4m)}} \tag{A.8}$$

where $n = |\alpha|^2 + \sinh^2 r$ is the average number of photons and $m = \sinh^2 r \leq n$ is the squeezing fraction. The condition $s < 0$ ensures that the expression in Eq. (A.8) is real. From this expression, we can prove some general properties of the functions $B_s(n)$. Firstly, we notice that $B_s(n) > 0$ for any $n \geq 0$. Also, since the only state in $\mathcal{G}_0$ is the vacuum $|0\rangle$, we have

$$B_s(0) = \frac{2}{\pi\sqrt{1+s(s-2)}}. \tag{A.9}$$

One can also see that $\lim_{n\to\infty} B_s(n) = 0$ for any $s < 0$. Then, it is easy to show that $B_s(n)$ is strictly decreasing: suppose that $\widetilde{n} > n$ but $B_s(\widetilde{n}) = B_s(n)$. Since B_s tends to zero for large n, it is possible to find $N > \widetilde{n} > n$ such that $B_s(N) < B_s(\widetilde{n})$, and $q \in (0,1)$ such that $qn+(1-q)N = \widetilde{n}$. Then one would obtain $qB_s(n)+(1-q)B_s(N) \geq B_s(\widetilde{n}) = B_s(n)$, on the other hand $qB_s(n) + (1-q)B_s(N) < qB_s(n) + (1-q)B_s(\widetilde{n}) = B_s(n)$ thus reaching a contradiction.

Finally, we show that the bound $B_s(n)$ is achieved by a state with n average photons, that is $B_s(n) = Q_s[\rho_n](0)$ and $\mathsf{Tr}[\rho_n a^\dagger a] = n$ (for brevity, in what follows we shall omit the phase space argument of Q_s, assuming it to be always "(0)"). Assuming that this is not the case, we write $B_s(n) = Q_s[\rho_{\widetilde{n}}]$, s.t. $\mathsf{Tr}[\rho_{\widetilde{n}} a^\dagger a] = \widetilde{n} < n$. However, one has $\rho_{\widetilde{n}} \in \mathcal{G}_{\widetilde{n}} \subset \mathcal{G}_n$, and as a consequence we reach the conclusion $B_s(n) = Q_s[\rho_{\widetilde{n}}] \geq B_s(\widetilde{n})$, which is in contradiction with the strict monotonicity of B_s.

We remark that all the properties derived in this section hold for any linear functional whose bound satisfies the properties: (i) $B(0) > 0$ and (ii) $\lim_{n\to\infty} B(n) = 0$.

A.3 Near-Optimality of pure states

We note that in general it must be $B_s^P(n) \geq B_s(n)$, since we can not exclude that the minimum may be reached by a Rank-2 state. We then adopt the same reasoning as in Ref. [220], which considers the bound for a convex mixture of Gaussian states and

shows that it is the same as the bound on pure states provided the pure states are convex in the variable n. As a result, $B_s^P(n) = B_s(n)$. While we have the conjecture that this is the case for any $s \leq 0$, the functional form of B_s^P is in general too cumbersome to verify its convexity analytically. Adopting a numerical approach that is part of the original work presented in this thesis, we have verified that, for the values $s = \{-1/4, -1/2, -1, -2, -3\}$, the function $B_s^P(n)$ is convex for $n \leq n_{\mathsf{max}} \simeq 10^{15}$ (that is, its second derivative is positive). We note that when $n \geq 3 \cdot 10^{15}$, our numerics become unstable and no conclusive results have been obtained.

Then, using the results of Appendix A.1 we note that the only possibility to have $B_s^P(n) \neq B_s(n)$ is when $B_s(n) = (1-p)B_s^P(n_1) + pB_s^P(n_2)$, with the average photon numbers of the two pure Gaussian states and the probability p verifying respectively $n_1 < n$, $n_2 > n_{\mathsf{max}}$, and $p < n/n_{\mathsf{max}}$. Thus, we have

$$\begin{aligned} 0 \leq B_s^P(n) - B_s(n) &= B_s^P(n) - B_s^P(n_1) \\ &+ p\left[B_s^P(n_1) - B_s^P(n_2)\right] \leq pB_s^P(n_1) \\ &< \frac{2}{\pi\sqrt{1+s(s-2)}}\frac{n}{n_{\mathsf{max}}} \sim 10^{-15}n, \end{aligned} \tag{A.10}$$

where we have used $B_s^P(n) - B_s^P(n_1) \leq 0$, which follows from $n_1 < n$ and $B_s^P(n)$ being monotonically decreasing in n [this can be seen easily from the abstract definition in Eq.(4.28), or more directly from Eq. (A.11)].

A.4 Pure state bounds

Our goal is now to minimise the function in Eq. (A.8) over all pure Gaussian states with average photon number n. We first notice that setting $2\theta - \phi = \pi$ yields the inequality

$$Q_s[|\psi_G\rangle\langle\psi_G|](0) \geq \frac{2e^{-\frac{2(n-m)(1+2m+2\sqrt{m(1+m)}-s)}{1+s(s-2-4m)}}}{\pi\sqrt{1+s(s-2-4m)}}. \tag{A.11}$$

Finally, one has to minimise the above expression with respect to the squeezing fraction m, under the constraint $m \leq n$. The optimising value of m for a given s is denoted $m_s(n)$. As an example, we here consider the case $s = -1$, where the function Q_{-1} is the so-called Husimi Q-function

$$Q_{-1}[\varrho](\alpha) = \frac{\langle\alpha|\varrho|\alpha\rangle}{\pi}. \tag{A.12}$$

Here $|\alpha\rangle = D(\alpha)|0\rangle$ denotes a coherent state, showing that the Husimi Q-function corresponds to the heterodyne probability distribution of the quantum state ϱ. For a generic state $\varrho \in \mathcal{G}$, the value of the squeezed photon number for which the Husimi Q-function in the origin is minimised is:

$$m_{-1}(n) = \frac{1}{6}\left(2(n-1) + \sqrt{3}\ \mathrm{Im}[g(n)] - \mathrm{Re}[g(n)]\right), \tag{A.13}$$

$$\text{where } g(n) = (-17 - 21n + 3n^2 + 8n^3 + 3i(1+n)\sqrt{6 + 3n(24 + n(37 + 16n))})^{1/3}. \tag{A.14}$$

The bound $B^P_{-1}(n)$ can be then obtained by substituting this function into the form of Eq. (A.11) where $s = -1$:

$$Q_{-1}[|\psi_G\rangle\langle\psi_G|](0) \geq \frac{2e^{-\frac{2(n-m_{-1}(n))(1+2m_{-1}(n)+2\sqrt{m_{-1}(n)(1+m_{-1}(n))}+1)}{1+(3+4m_{-1}(n))}}}{\pi\sqrt{1+(3+4m_{-1}(n))}}. \tag{A.15}$$

Where the final result is too cumbersome to be reported here. Identical approaches can be effectively pursued for other values of $s < 0$.